Chromobodies to Quantify Endogenous Proteins in Living Cells

Dissertation

der Mathematisch-Naturwissenschaftlichen Fakultät

der Eberhard Karls Universität Tübingen

zur Erlangung des Grades eines

Doktors der Naturwissenschaften

(Dr. rer. nat.)

vorgelegt von

Bettina-Maria Keller

aus Temeschburg (Rumänien)

Tübingen

2019

Gedruckt mit Genehmigung der Mathematisch-Naturwissenschaftlichen Fakultät der Eberhard Karls Universität Tübingen.

Tag der mündlichen Qualifikation:	13. September 2019
Dekan:	Professor Dr. Wolfgang Rosenstiel
1. Berichterstatter:	Professor Dr. Ulrich Rothbauer
2. Berichterstatter:	Professor Dr. Stefan Laufer

"Zwei Dinge sind zu unserer Arbeit nötig. Unermüdliche Ausdauer und die Bereitschaft, etwas, in das man viel Zeit und Arbeit gesteckt hat, wieder wegzuwerfen."

Albert Einstein

CONTENT

FIGURES

ABBREVATIONS

AAVS1	adeno-associated virus integration site 1
AB	antibody
AMCBS	antigen-mediated CB stabilization
BIO	6-bromoindirubin-3-oxime
BSA	bovine serum albumin
CA	capsid p24
CB	chromobody
CCC-CB	cell cycle chromobody
CCND1	cyclin D1
cDNA	complementary DNA
CDR	complementary determining region
C_H	contant domain of heavy chain
CHIR	CHIR99021
CHYSEL	*cis*-acting hydrolase element
C_L	contant domain of light chain
CMV	cytomegalovirus
CRC	colorectal cancer
CRISPR	clustered regularly interspaced short palindromic repeats
CTNNB1	β-catenin
dam methylation	deoxyadenosine methylase
DAPI	4′,6-diamidino-2-phenylindole
DARPin	designed ankyrin repeat proteins
dcm methylation	DNA cytosine methyltransferase
DMSO	dimethyl sulfoxide
DNA	deoxyribonucleic acid
dNTP	desoxynucleotide triphosphate
EDTA	ethylenediaminetetraacetic acid
EF1-α	elongation factor 1 alpha
eGFP	enhanced green fluorescent protein
ELISA	enzyme-linked immunosorbent assay
FBS	fetal bovine serum
Fc	fragment crystallizable region
FN3	fibronectin type III domain
FP	fluorescent protein
FR	framework region
FRAP	fluorescence recovery after photobleaching
GAPDH	glycerinaldehyde 3-phophate dehydrogenase
GAPDH	glyceraldehyde 3-phosphate dehydrogenase
GFP	green fluorescent protein
GPCR	G protein-coupled receptors
HA-L/R	homology arms left / right
hcAb	heavy-chain antibody
HDR	homology-directed repair
HIV	human immunodeficiency virus 1
h-βact	human β-actin
IC-IP	intracellular-immunoprecipitation
IF	immunofluorescence

Ig	immunoglobulin
iTRAQ	isobaric tags for relative and absolute quantification
KLD	kinase, ligase and DpnI
LOV	Light-oxygen-voltage (flavin-based fluorescent proteins)
MFI	mean fluorescence intensity
mRNA	messenger RNA
MS	mass spectrometry
MW	molecular weight
MYC	c-myc
NB	nanobody
PAM	protospacer adjacent motif
PBS	phosphate-buffered saline
PCNA	proliferating cell nuclear antigen
PCR	polymerase chain reaction
PEI	polyethylenimine
PEST	proline (P), glutamic acid (E), serine (S) and threonine (T)
POI	protein of interest
PPP1R12C	phosphatase 1 regulatory subunit 12C
PQR	protein quantitation rationing
PSD-95	postsynaptic density protein 9
PTM	posttranslational modification
qRT-PCR	quantitative real-time PCR
RFP	red fluorescent protein
RNA	deoxyribonucleic acid
RNAi	RNA interference
ROI	region of interest
S.D.	standard deviation
S.E.M.	standard error of mean
SA	splice acceptor
scFv	single-chain variable fragment
SDM	site-directed mutagenesis
SDS-PAGE	sodium dodecyl sulfate polyacrylamide gel electrophoresis
SELEX	systematic evolution of ligands by exponential enrichment
SILAC	stable isotope labeling by amino acids in cell culture
siRNA	small interfering RNA
SPR	surface plasmon resonance
T2A	self-cleaving peptide sequence
TBST	Tris-buffered saline with Tween20
TEMED	N′-tetramethylethylenediamine
TGF	transforming growth factor
Ub	ubiquitin
UPS	ubiquitin proteasome system
v/v	volume per volume
VEGF	vascular endothelial growth factor
V_H	variable domain of heavy chain
VHH	variable domain of heavy-chain-only antibody

VIM	vimentin
V_L	variable domain of light chain
w/v	weight per volume

1 ZUSAMMENFASSUNG

Die komplexe räumliche und zeitliche Regulation von zellulären Prozessen ist ein elementares Prinzip in Zellen und lebenden Organismen. Für ein tiefergehendes Verständnis dieser Prozesse werden Verfahren benötigt, die es ermöglichen dynamische Mengenveränderungen einzelner Proteine beobachten und quantifizieren zu können. Gemäß dem Credo „Seeing is believing“ ist die Fluoreszenzmikroskopie eines der wichtigsten Verfahren zur Entschlüsselung dieser grundlegenden Mechanismen. Diese Aufgabe wird bis dato hauptsächlich mit Hilfe von experimentellen *in vitro* Methoden bewältigt. Dabei beschränken sich die Analysen jedoch auf einzelne Momentaufnahmen und lösen sich vom nativen zellulären Kontext hin zu einer artifiziellen Umgebung.

Um endogene Proteine in lebenden Zellen mit Hilfe der Fluoreszenzmikroskopie zu visualisieren, haben sich Chromobodies als molekulare *in vivo* Sonden etabliert. CBs sind Fusionsproteine, bestehend aus der variablen Domäne eines Einzeldomänenantikörpers und einem fluoreszierenden Protein, die als Intrabody von lebenden Zellen gebildet werden. Im Rahmen dieser Dissertation wurde gezeigt, dass die CB-Technologie nicht nur die Visualisierung der dynamischen Verteilung endogener Proteine, sondern auch eine Quantifizierung der Mengenveränderung eines Antigens in lebenden Zellen erlaubt. In dieser Arbeit wurde eine Abhängigkeit der Menge an intrazellulärem CB von der Proteinkonzentration des zugehörigen Antigens nachgewiesen und demonstriert, dass sich Mengenveränderungen an endogenem Antigen über die Fluoreszenzintensitäten des CBs auslesen lassen. Grundlage bildet ein bisher nicht systematisch untersuchtes Phänomen, das „**A**ntigen-vermittelte (engl. **M**ediated) **CB S**tabilisierung“ (AMCBS) genannt wurde. Die Stabilisierung von CBs in Anwesenheit bzw. Depletion des entsprechenden Antigens wurde für vier etablierte CBs, die unterschiedlichste zelluläre Antigene binden, demonstriert. In Folge wurde durch gezielte Modifikation der CBs der dynamische Messbereich von AMCBS-basierten Quantifizierungen erweitert. Um den proteolytischen Abbau von nicht Antigen-gebundenem CB zu beschleunigen, wurden ausgewählte CBs unter Anwendung der „N-End Rule“ gentechnisch modifiziert, die erfolgreiche Optimierung im direkten Vergleich zwischen einem modifizierten und einem unmodifizierten β-Catenin bindenden CB gezeigt, und die Aktivität und Kinetik von β-Catenin modifizierenden Wirkstoffen mittels des AMCBS-Mechanismus quantitativ bestimmt. Abschließend wurde unter Verwendung der CRISPR/Cas9-Technologie ein Protokoll zur zielgerichteten Integration der genetischen Information AMCBS-optimierter CBs in das Genom von potentiellen Screening-Zelllinien

entwickelt und validiert. Zusammenfassend zeigt diese Arbeit, dass sich mit hochspezifischen und optimierten CBs dynamische Mengenveränderungen von endogenen Proteinen in lebenden Zellen über das AMCBS Phänomen bildbasiert quantifizieren lassen. Damit werden neue Einblicke in die Dynamik endogener Proteine z.B. nach Wirkstoffbehandlung möglich. Dieses Verfahren ist in der biomedizinischen Forschung breit einsetzbar, einfach zu implementieren und benötigt neben einem Fluoreszenzmikroskop keine aufwendige Ausrüstung.

2 ABSTRACT

As key cellular processes are dynamic in nature and underlie sophisticated spatial and temporal orchestration within living cells and whole organisms "*seeing is believing*" has turned into a main principle in cell biology. By employing live-cell fluorescence imaging, these important mechanisms can be deciphered. Importantly, an in-depth understanding of cellular processes requires the determination of dynamic changes in the concentration of endogenous proteins. However, today this task is mainly fulfilled by *in vitro* end point assays, which contradicts the requirement of assessing dynamic protein changes under native conditions within living cells.

During the last years fluorescently labeled nanobodies (chromobodies, CBs), implemented as intracellular molecular probes, have emerged as valuable tools to visualize the spatial and temporal localization of endogenous proteins in living cells. In this dissertation, a novel aspect of CBs was observed and illuminated: The intracellular CB amount directly depends on the concentration of its cognate antigen, which was termed "**A**ntigen-**M**ediated **CB S**tabilization" (AMCBS). Employing this phenomenon allows an expansion of the CB technology from the visualization of the spatiotemporal distribution of the antigen towards a relative quantification of time-resolved changes in endogenous protein concentration by simply determining the CB fluorescence. This idea was confirmed by analyzing four previously generated CBs, targeting β-catenin, proliferating cell nuclear antigen (PCNA), vimentin and HIV capsid protein p24, in their performance to monitor dynamic up- and downregulation of their respective antigens. To improve the accuracy and dynamic range of AMCBS, turnover-accelerated versions of these CBs were generated by utilizing the concept of the N-end rule and comparative analysis revealed that fast and reversible changes can be assessed more precisely by quantitative live-cell imaging applying the novel generated turnover-accelerated CBs. To illustrate a possible application, the turnover-accelerated β-catenin-specific CB was employed to monitor drug action and kinetics in living cells through AMCBS. Lastly, a protocol to generate stable cell lines expressing turnover-accelerated CBs was established by site-directed genetic integration into the adeno-associated virus integration site 1 (AAVS1) safe harbor locus of human cell lines using CRISPR/Cas9.

In summary, AMCBS-based protein quantification in combination with highly specific and functional CBs allow an imaging-based quantification of endogenous proteins in living cells, thereby enabling unprecedented insights into protein dynamics. For the future, this method

is broadly applicable in biomedical research as it is straight-forward to implement and the only technical requirement is a fluorescence microscope.

3 INTRODUCTION

3.1 Proteins - the key players in life

Proteins are highly complex macromolecules orchestrating key processes in cells and whole organisms. Essential physiological processes such as proliferation, migration but also decisions whether a cell is allowed to survive or has to undergo the programmed cell death are controlled and decided by these important molecules. Besides being the chief executor within a cell, proteins themselves need to be highly regulated in order to correctly fulfill their duties and during the last years and decades a broad range of sophisticated regulatory mechanisms of protein function have been identified.

The earliest observations of mechanisms regulating endogenous protein concentrations were obtained within the context of enzyme kinetics (Michaelis et al, 2011; Cornish-Bowden, 2013). For the first time, scientists noticed and described regulatory mechanisms as the inhibitory function of a product onto an enzyme reaction. To date, it is verified that binding of small molecules to an enzyme can induce conformational changes, thereby modifying the architecture of the active center, an observation, which was termed allosteric regulation (Cooper, 2000). Besides binding of small molecules, also the direct interaction of a specific protein with other proteins has the potential to activate or inactivate a specific protein function, which often is accompanied by the formation of a multi-protein complex. In addition to this non-covalent interactions, a huge variety of covalent regulatory protein modifications have also been described in the past (reviewed in (Knorre et al, 2009)). Probably the most prominent example of these so-called post-translational modifications (PTMs) is the phosphorylation of serine and tyrosine residues, which can function as a molecular switch. Consequently, this site-directed addition of a small residue to a protein has the power to regulate the activation state of whole pathways within a living cell and is a key regulatory mechanism in cellular physiology.

Finally, the abundance of a specific protein itself has a regulatory function under some circumstances and altering the amount of a specific protein can evoke a cellular response. A prominent example for a regulatory function orchestrated by protein abundance was described for the cell cycle, which is guided by changing levels of the cyclins. In this instance the cell cycle progression is achieved by recurring oscillations in the amount of the different members of the cyclin family (Morgan, op. 2007). Another illustrative example for a regulatory function depending on the respective protein amount represents the

transcriptional co-activator β-catenin (CTNNB1) mediating the expression of WNT-responsive elements (Behrens et al, 1996; Korinek, 1997). In WNT-off condition, the intracellular level of CTNNB1 is strictly controlled by the destruction complex, resulting in continuous degradation of CTNNB1 (Aberle et al, 1997; Orford et al, 1997; Kimelman & Xu, 2006). In case of WNT activation, CTNNB1 accumulates within the cytosol and translocates into the nucleus, where it mediates gene expression of various genes involved in proliferation or differentiation (reviewed in (Clevers & Nusse, 2012)).

In summary, cyclins and CTNNB1 are two well established examples how protein abundance and dynamic alterations in protein amount possess a crucial regulatory function. Based on this important role, it is not surprising that dysregulated protein amounts contribute to the development and progression of various diseases. Deciphering dynamic changes of endogenous proteins is therefore crucial to achieve an in-depth understanding of a protein's functionality and the orchestrated cellular processes.

3.2 Current methods to analyze and quantify endogenous proteins

In the past, a broad spectrum of methods has been developed in order to detect changes in the concentration of endogenous proteins. Although the intention is to study protein dynamics within a cellular system, the analyses are mainly performed by *in vitro* endpoint assays. The most common methods to quantify a specific protein amount can be structured into two approaches: (i) mass spectrometry (MS)-based analyses and (ii) antibody-based techniques (**Figure 1**).

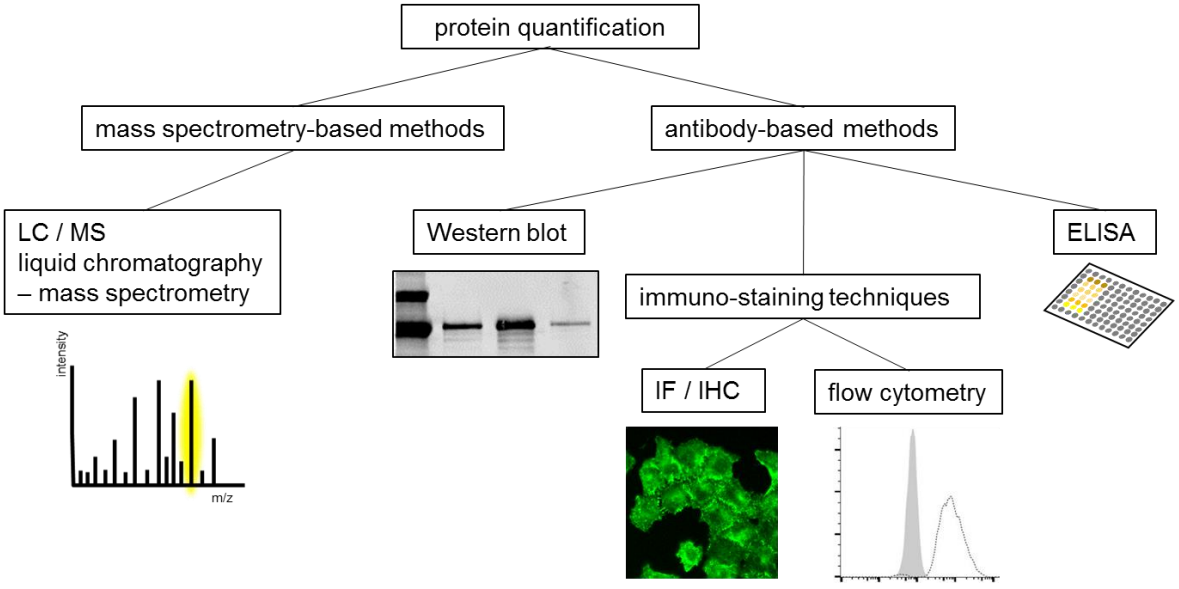

Figure 1 Illustration of methods used for quantification of specific endogenous proteins.

The mainly applied approaches for protein quantification are either mass spectrometry (MS)- or antibody-based. Among the antibody-based methods western blot, enzyme-linked immunosorbent assay (ELISA) and immunostaining techniques like immunofluorescence (IF) or flow cytometry are widely used to analyze specific proteins.

Mass spectrometry-based proteomic analyses have become an important tool in the field of biology, allowing precise relative and absolute protein quantification (Lindemann et al, 2017). By applying this technique in combination with bioinformatics, scientists nowadays are able to quantify thousands of proteins derived from complex samples. For a comparative proteome analysis, this method requires differential stable isotope labeling to create a specific mass tag, which provides the basis for quantification. Isotope incorporation into proteins and peptides can be accomplished by metabolic, chemical or enzymatical labeling (reviewed in (Bantscheff et al, 2007)). Stable isotope labeling by amino acids in cell culture (SILAC) depends on cellular protein synthesis to incorporate stable isotope-containing amino acids (e.g. $^{13}C_6$ arginine or $^{13}C_6$ lysine) into the proteome (Ong et al, 2002; Ong & Mann, 2006). For this purpose, cells are cultivated in growth media containing amino acids with heavy isotopes over five passages, which leads to the incorporation of these heavy amino acids into the endogenous proteins. In the following, cell populations containing heavy and normal (light) amino acids can be mixed and remain distinguishable by MS, thereby allowing accurate relative quantification (Ong & Mann, 2006). As metabolic labeling is restricted to cell culture systems, chemical labeling strategies like isotope-coded affinity tag (ICAT) further expand the possibilities of MS-based analyses to e.g. tissues (Gygi et al, 1999). By applying isobaric tags for relative and absolute quantification (iTRAQ) the sampling number could be expanded to up to eight samples by this approach (Choe et al, 2007; Wiese et al, 2007).

Undoubtedly, MS strongly contributed to a comprehensive knowledge of protein functionality in the past and was further the main driver of the new field of systems biology (Sabidó et al, 2012). However, a drawback of this method is the requirement of expensive equipment and trained personnel. Therefore, this technology is mainly applied for large-scale analyses rather than to study dynamic changes of only one specific protein within a complex sample.

The number of antibodies for scientific research has increased tremendously in the last decades, resulting in more than four million commercially available antibodies in March 2019, as listed in the largest antibody search machine (citeab.com). Among the antibody-based techniques, western blot and enzyme-linked immunosorbent assay (ELISA) are

probably the most commonly used methods to quantify endogenous proteins and these methods were further developed into sophisticated systems such as multiplex assays or single molecule arrays in the last few years. Although these techniques have an undoubted impact in research, some scientific questions might remain unaddressed by applying one of the mentioned approaches to quantify an endogenous protein of interest (POI). Firstly, cells have to be lysed prior to the analysis by western blot, what leads to the loss of the intercellular resolution and thus only average protein amounts can be quantified. Secondly, tracing changes in protein concentration over time is laborious and time-consuming, thereby limiting the number of analytes.

Immunofluorescence (IF) can overcome these limitations, as this *in situ* method allows to assess the subcellular localization as well as the relative concentration of POIs on single cell level. Moreover, the recent advances in imaging technology contributed to the success of this analysis method. Nowadays, a high number of images can be acquired in a short time frame and further smart software solutions allow automated analysis of these images (Mattiazzi Usaj et al, 2016). However, due to cell fixation and permeabilization dynamic changes of endogenous proteins cannot be analyzed in real-time. Moreover, it is essential that fixation and permeabilization have been tested and verified carefully, since both procedures obtain variabilities, which can introduce artifacts interfering with the analysis and might therefore not correctly reflect the *in vivo* situation (Stadler et al, 2010; Schnell et al, 2012).

All mentioned antibody-based techniques have in common that the success of the method mainly is defined by the quality and specificity of the applied antibodies. For decades polyclonal antibodies derived from immunized animals have been applied in scientific research. But some shortcomings limit and endanger the reproducibility of polyclonal antibody applied in research. Firstly, post immunization only a small porportion of the antibodies in a polyclonal reagent bind to their intended target and secondly, the immunization of an animal never results in the same mix of antibodies (Bradbury & Plückthun, 2015). The hybridoma technology opened the door for high-yield production of monoclonal antibodies in continuous cell culture with high reproducibility (Köhler & Milstein, 1975). Although this technique was a clear progress towards standardization and reproducibility, a study from 2008 revealed that only ~50 % of 6,120 tested commercial antibodies within the Human Protein Atlas research project specifically recognized their target (Berglund et al, 2008). Commonly occurring problems caused by commercial

antibodies are non-specific binding, background and noise, or batch-to-batch variability (Voskuil, 2014). These shortcomings of antibodies lead further to the assumption of antibodies being the major driver of the present 'reproducibility crisis' in biomedical research (Baker, 2015).

Nevertheless, given the predominant role of antibodies in research and diagnostics, it is not surprising that these methods have been extensively used during the last years and decades. In addition, methods like western blot or IF do not require expensive equipment and are easy to implement, both factors that mainly contributed to the high popularity of antibody-based techniques in research.

3.3 Monitoring and quantification of endogenous proteins in living cells

Considering that most cellular processes are dynamic in nature and rely on the spatiotemporal orchestration under native conditions, the assessment of time-dependent changes of endogenous protein level within the physiological context is highly preferred.

One popular approach to analyze dynamic processes within living cells is realized by ectopic expression of a reporter-tagged transgene, wherein fluorescent proteins (FPs) applied as reporter are commonly used. Although this method does not allow the assessment of an endogenous protein, it is frequently used to study protein dynamics. But it has to be considered that ectopic expression in cells results in high protein levels, which might change the dynamics and functionality of a POI (Moriya, 2015). A possible approach to circumvent this drawback is to aim for a cell line displaying a stable and low expression of the respective fusion protein. Recently, this approach was used to study subcellular dynamics of CTNNB1 in individual cells (Kafri et al, 2016). In this study, YFP-CTNNB1 was stably expressed in HEK293 cells, which was achieved by applying selection pressure post transfection to facilitate a random integration of the transgene. In the following, YFP-CTNNB1 low-expressing cells were screened and collected by FACS. Thus, this approach enabled the visualization of YFP-CTNNB1 distribution and dynamics in response to Wnt3a within these cells. But it has to be considered that the absolute number of CTNNB1 molecules is not accurately represented by this method since only the ectopically introduced protein can be visualized by fluorescence imaging and the intracellular protein amount of CTNNB1 was altered within this generated cell line.

With increasing popularity and the progressing simplicity in application, the insertion of a FP transgene to the native genomic locus by gene editing techniques like CRISPR/Cas9, provides a straightforward approach to optically monitor and quantify the relative amount of an endogenous POI. Tagging an endogenous gene with a FP provides multiple information about a POI, such as localization, translocation, dynamic changes in protein concentration, as well as protein half-life. Besides all these advantages some issues need to be addressed when aiming for this method. Firstly, a low abundant protein could be hard to detect by using this technique, as the fluorescent signals might be below the detection limit. Secondly, the cell line utilized for a CRISPR/Cas9-mediated FP-tag knock-in has to possess a certain efficiency for homology-directed repair (HDR), which varies among different cell lines (Miyaoka et al, 2016). Furthermore, CRISPR/Cas9 requires a protospacer adjacent motif (PAM-motif) to effectively target the Cas9 nuclease (Mojica, F J M et al, 2009). Based on statistics, PAM-motifs are frequent and using an alternative nuclease provides additional diversity in the sequence to utilize, but some target sites might lack a suitable PAM-motif, thereby excluding this method. Lastly, considering that a FP is composed of ~280 amino acids (~27 kDa), FP tagging of an endogenous protein might interfere with the proteins characteristics and functionality such as turnover, localization, transport and the participation in multiprotein-complexes (Snapp, 2009; Skube et al, 2010; Stadler et al, 2013; Virant et al, 2018). Especially for proteins described to have a broad range of different interaction partners like CTNNB1 (reviewed in (Valenta et al, 2012)), fluorescent tagging of the endogenous protein should be carefully evaluated. Notably, from a technical point of view it is possible to tag endogenous CTNNB1 with a C-terminal FP, thereby generating an endogenous fusion protein (Zhang et al, 2017). However, analysis of ectopically expressed CTNNB1 comprising a C-terminal FP tag revealed an interference with its transcriptional activity (Cong et al, 2003).

A promising approach to reduce the functional interference of covalently fused fluorescent reporters represents the use of a reporter with a smaller size. Recently, flavin-based fluorescent proteins (LOV-based FPs) have been established for cellular fluorescence imaging (Mukherjee & Schroeder, 2015). Comprising a molecular weight of only 12.1 kDa the derivate iLOV represents the smallest protein within this class and was reported to outperform GFP as real-time reporter of viral infection dynamics in plants (Buckley et al, 2015).

Another possibility for real-time visualization and quantification of proteins in living cells is provided by using so-called self-labeling proteins like the SNAP- or CLIP-tag, which catalyze an auto-attachment of a fluorophore within a living cell (Thorn, 2017). In a recent study, the SNAP-tag was applied to estimate protein half-lives in living cells, whereby the protein degradation rates have been directly determined by monitoring the decay of fluorescence signal over time. This was achieved by washing out the unbound dye, leading to the effect that newly synthesized proteins cannot be labeled and therefore the protein degradation rate can be directly monitored (Mandic et al, 2017). The application of self-labeling tags provides several advantages like enhanced photo-stability for fluorescence imaging as well as a high variety of commercially available fluorescent dyes, but some limitations need to be considered. The size of the SNAP- and CLIP-tag with approximately 20 kDa is comparable to the size of a FP and has the same drawbacks as already mentioned for the FPs. Additionally, their usage is quite extensive in handling and costs since an addition of the fluorescent dye is required for each experiment.

For optical monitoring of an endogenous protein without affecting its native state, a technique was recently described that is based on the co-translational separation of the POI and the fused FP. By applying CRISPR/Cas9 the endogenous locus of a POI is fused to a FP reporter and transcribed as bicistronic expression construct, followed by a co-translational separation, which is facilitated by a *cis*-acting hydrolase element (CHYSEL). This co-translational separation of POI and FP results in an equimolar ratio, therefore the fluorescence within the cell can be directly utilized as readout parameter for the concentration of the POI. Thus, protein quantitation rationing (PQR) provides a simple and efficient tool to quantify the steady-state protein level within a cell, without endangering the functionality of the POI (Lo et al, 2015). However, the genome-engineered stable cell lines require critical validation, since probably only one allele was addressed by genome editing and possible off-target genomic integrations of the fluorescent reporter need to be excluded. Moreover, it has to be considered that not every protein is accompanied and regulated by concordant changes in the expression of corresponding mRNAs (Schwanhäusser et al, 2011; Lu et al, 2009). Consequently, this approach is not applicable for proteins such as CTNNB1, whose intracellular concentration is not primarily regulated by transcription.

3.4 Intrabodies to monitor and quantify proteins in living cells

In the last decade the application of intracellular binding molecules to study specific endogenous proteins in living cells has become highly attractive in the field of biomedical research. The intracellular expression of affinity reagents (termed intrabodies) provides a versatile technique to examine cognate antigens within living cells. Intrabodies, expressed as FP fusions, serve as valuable tools to detect and continuously monitor spatiotemporal dynamics of a POI in real-time. Moreover, intrabodies can also be employed to actively modulate the respective target within a cell. In regards to visualization, the major benefit of this approach is that the endogenous POI remains in its native constitution and there is no further necessity to edit the endogenous gene locus of the POI. However, the impact of the molecular probe on the cognate antigen needs to be analyzed critically to exclude a possible interference with the functionality of the antigen.

For the generation of functional intracellular binding molecules various peptide-, protein- or nucleic acid-based binding molecules can be utilized. This great diversity of different nanoprobes is further expanded by a large selection of different reporters (e.g. FP, luciferase, fluorophores), which can be fused or coupled to the intrabody, thus allowing the detection of the binding molecule within the cell. Based on their structure, these binding molecules can be classified as non-immunoglobulin (Ig) scaffolds (**Figure 2**) and immunoglobulin G (IgG) scaffolds (**Figure 3**). The following chapters provide an overview of different intrabody formats currently used for live-cell imaging of endogenous proteins.

3.4.1 Visualization of intracellular targets by non-immunoglobulin scaffolds in living cells

Although most affinity reagents are protein-based, also nucleic acids can adopt complex 3D structures, which allow specific binding to target structures. These ssDNA- or RNA-based binding molecules, referred to as aptamers, are generated by an *in vitro* selection procedure termed systematic evolution of ligands by exponential enrichment (SELEX) (Stoltenburg et al, 2007; Dunn et al, 2017). Recently, aptamers have been applied as fluorophore-marked nanobiosensor for real-time monitoring of transcription and translation of vascular endothelial growth factor (VEGF) in living cells. In this study, the nanoprobes have been chemically generated, which was followed by binding to gold nanorods to facilitate their cellular internalization (Wang et al, 2018). The use of aptamers as tool for imaging of

intracellular targets in living cells is limited to a few studies, which mostly are applied in the visualization of RNA dynamics (Autour et al, 2018; Sato et al, 2018).

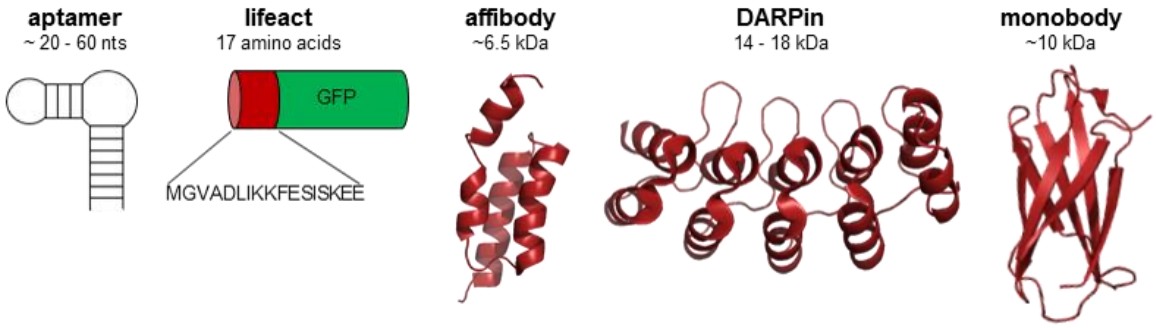

Figure 2 Overview of non-immunoglobulin scaffolds applied as intracellular affinity binder.
Illustrated are structures and molecular weights of selected non-Ig scaffolds applied as intrabodies. Aptamer and lifeact are schematically displayed. Crystal structures of the protein-based non-Ig scaffolds are shown: affibody (PDB ID: 2KZI), DARPin (PDB ID: 5LW2), monobody (PDB ID: 3RZW). The images of the structures have been generated with PyMOL Molecular Graphics System, Version 2.0 Schrödinger, LCC.

The majority of non-Ig scaffolds employed for molecular imaging are peptide- or protein-based. The smallest affinity reagent currently applied for live-cell imaging is based on a 17 amino acid peptide derived from the actin-binding protein (Adp140) of *Saccharomyces cerevisiae*, which was utilized to visualize F-actin in living cells. For the visualization of actin cytoskeleton dynamics by fluorescent microscopy, this small peptide is genetically fused to a N-terminal GFP (lifeact) and intracellularly expressed (Riedl et al, 2008; Riedl et al, 2010).

Representing a new class of affinity reagents, affibodies were originally derived from the B-domain within the immunoglobulin binding region of staphylococcal protein A. In this approach, specific binding is facilitated by a short cysteine-free peptide containing 58 amino acids (6.5 kDa) that folds into a three-helical bundle structure (Löfblom et al, 2010). Although affibodies have been mainly applied to stain and trace the internalization of cell surface receptors (Lyakhov et al, 2010), they have furthermore been applied as intracellularly expressed affinity reagents for the retention of the epidermal growth factor receptor in the secretory pathway (Vernet et al, 2009). Given this example, an application as intracellular molecular probes to visualize endogenous proteins would be conceivable.

Another protein binding scaffold is represented by so-called repeat proteins, comprising “designed ankyrin repeat proteins” (DARPins). Due to their compact size (14 - 18 kDa) and the lack of cysteines, DARPins can be functionally expressed inside the cell, fused to a reporter of choice (Plückthun, 2015). Recently, DARPin-based intracellular binding

molecules recognizing different fluorescent proteins have been identified, thus allowing tracing and manipulation of FP-labeled target proteins like H2A-YFP or mTFP-Rab5c within this model system (Brauchle et al, 2014; Vigano et al, 2018).

Lastly, naturally occurring protein scaffolds can be utilized in order to generate affinity reagents. One prominent example resulting in a wide range of affinity reagents is derived from the fibronectin type III domain (FN3) and led to the generation of so-called monobodies. Their small size, lack of disulfide-bonds and the formation of three loop structures that are comparable and modifiable like complementary determining regions (CDRs) of IgGs lead to a desirable intracellular application (Koide et al, 2012). In the field of neurological research, FP-fused monobodies enabled labeling and tracing of endogenous postsynaptic density protein 95 (PSD-95) and gephryin in living neurons, without affecting the morphology or functionality of neurons (Gross et al, 2013).

3.4.2 IgG-based scaffolds to visualize endogenous targets in living cells

As mentioned in chapter 3.2 conventional antibodies (IgGs) are indispensable tools for the detection and quantification of endogenous proteins in the field of biomedical research. However, because of their complex structure and size (~150 kDa), the use of full-length IgGs as intracellularly expressed affinity reagents is very limited. IgG molecules are composed of two different kinds of polypeptide chains: the heavy (H) chain with ~50 kDa and the 25 kDa light (L) chain. Each IgG molecule consists of two identical heavy and two identical light chains, thereby forming a heterotetrameric structure mediated by four disulfide bonds and resulting in two identical antigen-binding sites, which can bind simultaneously (**Figure 3**). Both chains can be divided into a constant domain (C_H and C_L respectively) and the amino-terminal variable domain (V_H or V_L respectively), which confers the ability of specific antigen binding (Janeway, 2005).

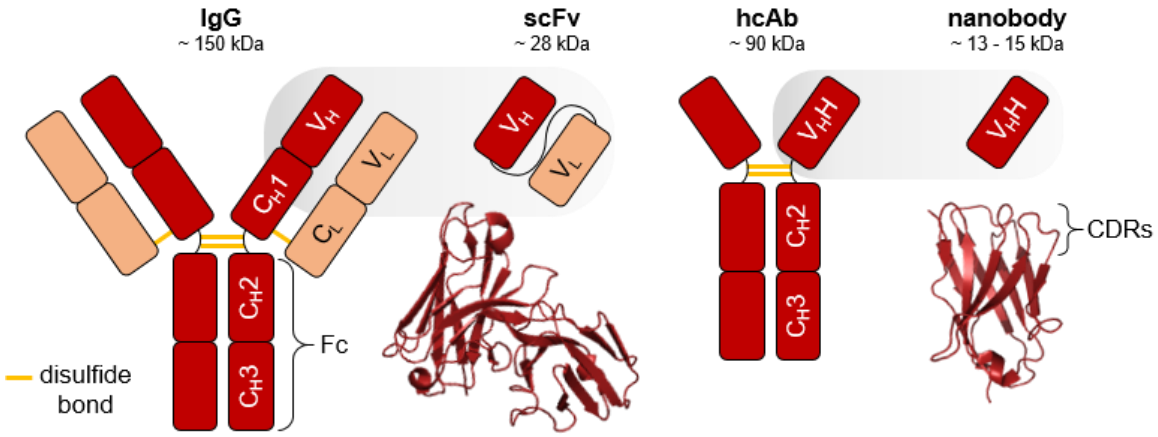

Figure 3 Illustration of immunoglobulin scaffold-based intracellular affinity binder.
Conventional IgG antibodies consist of two identical heavy (red, domains V_H and C_H1 - C_H3) and two identical light (orange, domains V_L and C_L) chains, interconnected via disulfide bonds (yellow). The single chain variable fragment (scFv) is a synthetic fusion comprising the V_H and V_L domain of a conventional antibody, connected by a linking peptide, structure of a scFv (PDB ID: 4P49). Heavy-chain antibodies derived from camelids consist of only two disulfide-linked identical heavy chains comprising the domains C_H2 - C_H3 and V_HH. The V_HH fragment (nanobody) can be utilized as intrabody. Structure of an anti-GFP nanobody (PDB ID: 3OGO) with indicated complementarity determining regions (CDRs). The images of the structures have been generated with PyMOL Molecular Graphics System, Version 2.0 Schrödinger, LCC.

The prerequisite for specific antigen binding is correct folding and disulfide bridge formation, thus the utilization of full-length IgGs as intrabodies is prevented by (i) the reducing environment of the cytosolic compartment and (ii) the size of ~150 kDa. Overcoming this natural restriction, recombinant antibody technology allows the fusion of the V_H and V_L domain by addition of a flexible peptide linker, commonly a $(Gly_4Ser)_3$ decapentapeptide, resulting in a single-chain fragment variable (scFv) with a molecular weight of ~28 kDa (**Figure 3**) (Bird et al, 1988; Maynard & Georgiou, 2000). However, the reduction of an IgG to a scFv molecule does not necessarily result in a functional intracellularly expressible affinity molecule. The obligatory removal of the constant domain for an expression as scFv results in the exposition of hydrophobic amino acids located at the interface between the variable and the constant domain to the aqueous environment. Additionally, antibody variable domains contain a conserved interchain disulfide bridge linking the two β-sheets of the immunoglobulin domains. Therefore, a direct adoption of IgG-based sequences for the expression of scFv-based intrabodies is limited as the reducing conditions *in vitro* lead to denaturation and aggregation (Glockshuber et al, 1992; Cattaneo & Biocca, 1999). Interestingly, some naturally occurring antibodies lacking these cysteine residues still display functionality and specificity (Rudikoff & Pumphrey, 1986), thus leading to the assumption of disulfide bridge formation not being mandatory for functional folding of Ig domains. An understanding of these limitations gave rise to the targeted

engineering of scFvs as the utilization of the huge pool of available antibodies as ectopically expressed intrabodies would be highly desirable. Applications for live-cell imaging of a few scFv-based intrabodies have been described, in which they target different antigens involved in DNA replication like PCNA (Freund et al, 2014), modification-specific intracellular antibodies (mintbodies) recognizing epigenetic histone modifications (Sato et al, 2013; Sato et al, 2016), or studying dynamics of scaffold proteins like tubulin (Cassimeris et al, 2013) or gephyrin (Varley et al, 2011).

In summary, the impact of scFv-based intrabodies for cellular imaging approaches was continuously expanded over the last few years. This development can mainly be explained by an extensive understanding of structure and binding mechanisms, which gave rise to the targeted engineering of scFv in order to adapt these molecules to the requirements of an intracellular expression and application.

3.4.3 Nanobodies - naturally occurring single domain antibodies

3.4.3.1 Heavy-chain only antibodies

The modular composition and structure of antibody molecules in general is remarkably conserved among mammals. However, about 25 years ago a second type termed heavy-chain only antibodies (hcAbs) have been identified alongside conventional antibodies circulating in the blood of camelids (Old World camelids including *Camelus dromedaries* and *Camelus bactrianus* and New World camilds including *Lama glama*, *Lama pacos*, *Lama guanicoe* and *Lama vicugna*), contributing to the immune response in these animals (Hamers-Casterman et al, 1993; Vincke & Muyldermans, 2012). In general, hcAbs represent 50 - 75 % of total circulating antibodies within camelids and in comparison to conventional hetero-tetrameric IgGs these molecules are devoid of light chains and only composed of two identical heavy-chains resulting in a molecular weight of ~90 kDa (**Figure 3**). A lack of the C_H1 domain is another characteristic of hcAbs compared to conventional IgGs (Hamers-Casterman et al, 1993). The lack of the C_H1 domain is explained by a specific genomic transition (G to A) in the splice signal at the 3' site of the C_H1 exon, causing the complete loss of the camelid C_H1 exon during mRNA processing (Khong Nguyen et al, 1999). As the C_H1 domain is crucial for the interaction between the light and the heavy chain in IgG molecules, correct IgG-like assembly is impossible in hcAbs. Consequently, the framework region 4 (FR4) of the variable domain is directly followed by the hinge region in hcAbs and antigen recognition is mediated by a single domain (V_HH or nanobody), which is the smallest

(13 - 15 kDa) naturally occurring antigen binding format (Hamers-Casterman et al, 1993). Contrary to expectations, loss of the light chain did neither impair the diversity of the antigen-binding repertoire nor the antigen-reactivity resulting in a broad spectrum of highly affine hcAbs, which recognize various antigens (Flajnik et al, 2011).

Although, V_HHs and V_Hs share about 80 % identity in amino acid sequence, several important adaptions were acquired in order to compensate the absence of the light-chain variable domain. The amino acids mediating the typical antiparallel beta strand structure of the immunoglobulin fold are preserved between V_H and V_HH. Both domains contain four framework regions (FR1-4), which are interspersed by three complementary determining regions (CDR1-3), wherein scaffold stabilization is achieved by an intradomain disulfide bond (Cys22 and Cys92, according to Kabat numbering, (Kabat et al, 1992)). However, the hydrophobic amino acids constituting the V_H-V_L interface in FR2 of V_Hs are substituted in V_HHs ((Val37Phe (or Tyr), Gly44Glu (or Gln), Leu45Arg (or Cys) and Trp47Gly (or Ser, Leu, Phe), Kabat numbering), resulting in an enhanced hydrophilicity (Desmyter et al, 1996; Muyldermans, 2001). These specific substitutions are referred to as hallmarks to distinguish between V_Hs and V_HHs (Vu et al, 1997).

Additionally to the adaptions at the V_H-V_L interface in hcAbs, the CDRs themselves within V_HHs differ from those in V_Hs since antigen binding is mediated by only three CDRs in V_HHs, whereas antigen recognition by conventional antibodies is achieved by six CDRs. Based on this major difference in V_HHs, new mechanisms had to be adopted for retaining antigen binding diversity and specificity. The hypervariable domain of CDR1 is extended towards the N-terminus, thereby spreading into the loop between to β-strands, which in turn results in a higher variability. Probably the main compensatory mechanisms is accomplished by an elongated CDR3 resulting in an enhancement of the surface area available for antigen interaction. An additional stabilization of elongated CDR3s can be obtained by inter-CDR disulfide bonds, which frequently appear in camelid CDR3 loops, preferentially in the long ones (Vu et al, 1997; Muyldermans et al, 2001). Based on the illustrated structure, V_HHs form a convex paratope, thereby expanding the spectrum of addressable epitopes, as V_HHs can recognize epitopes that are not accessible for conventional antibodies (e.g. clefts) (Genst et al, 2006). Interestingly, immunization experiments of camelids revealed an antigen-type dependency regarding a conventional or heavy-chain IgG immune response, which underlines the hypothesis that hcAbs expand the accessible antigen repertoire (van der Linden et al, 2000).

Based on the unique characteristics of V_HHs, including small size (13 - 15 kDa, ~2 x 4 nm), stability and tolerance of high salt concentrations, pH and temperature fluctuations as well as their solubility (van der Linden et al, 1999; Rothbauer et al, 2008), nanobodies have emerged as valuable tools ranging from biomedical research and diagnostics to clinical trials (Hassanzadeh-Ghassabeh et al, 2013; van Audenhove & Gettemans, 2016; Steeland et al, 2016; Traenkle & Rothbauer, 2017). Moreover, high production yields can be achieved in different expression systems, including bacteria, fungi, mammalian cell lines, plants or insect cells (Meyer et al, 2014). An additional advantage is provided by the straight-forward approach in nanobody selection procedure as naïve, immunized or synthetic libraries can be employed to identify affinity binders by phage display (Romao et al, 2016).

3.4.3.2 Monitoring of endogenous antigens by chromobodies

The aforementioned properties in V_HH structure and molecular composition substantially contributed to their successful utilization as intrabodies during the last years. A thermodynamically stable Ig-fold is required for ectopic expression of NBs in the reducing environment of the cytosol as the intradomain disulfide formation is blocked by this circumstance (Tanaka & Rabbitts, 2008). However, NBs containing an interdomain disulfide bond cannot be adapted as intracellularly expressed affinity reagents, since compensation of the lack in disulfide formation might interfere with the antigen binding capacity (Traenkle & Rothbauer, 2017). Consequently, different strategies (e.g. fluorescent-two-hybrid assay) for the identification of intracellularly functional binding molecules have been established (Zolghadr et al, 2008; Kaiser et al, 2014). Combining the advantages based on V_HH nature with improved display and screening techniques, it is not surprising that until now various NBs have been implemented to trace or manipulate different endogenous proteins (Kaiser et al, 2014; Schumacher et al, 2018).

With the development of the chromobody (CB) technology, comprising the chimeric genetic fusion of a nanobody and a FP followed by ectopic expression of the construct in mammalian cells, V_HHs turned into indispensable tools for live-cell visualization of endogenous proteins. The breakthrough of the CB technology was initiated by a proof-of-concept study, wherein a RFP-fused GFP binding NB (GBP-RFP) was demonstrated to specifically label co-expressed GFP-fusion proteins in different cellular compartments (Rothbauer et al, 2006). In the last years various specific CBs have been established to decipher the spatiotemporal dynamics of endogenous proteins. One group is classified by CBs tracing the reorganization of cytoskeleton components over time, such as lamin, F-actin or vimentin (Zolghadr et al,

2012; Panza et al, 2015; Maier et al, 2015). Furthermore, CBs tracing different endogenous nuclear components have been established. The cell cycle CB (CCC-CB) specifically targets the proliferating cell nuclear antigen (PCNA) resulting in the real-time assessment of cell cycle progression, which further enables a high-content approach to identify cell cycle modulating compounds (Schorpp et al, 2016). By implementing a poly(ADP-ribose) polymerase 1 (PARP1)-specific CB, PARP1 recruitment to compound-induced DNA damage sites can be monitored (Buchfellner et al, 2016). Furthermore, the chromatibody has been used to elucidate chromatin dynamics (Jullien et al, 2016). Illustrating the great potential of CBs, a binder specifically recognizing an activated version of G protein-coupled receptor (GPCR) β2-adrenoreceptor was established to visualize receptor trafficking after an activation-induced conformational change (Irannejad et al, 2013). Additionally, CBs targeting different virus components of HIV-1 or influenza A virus allow a functional analysis of virus morphogenesis (Helma et al, 2012; Ashour et al, 2015).

Taken together, CBs are emerging tools to monitor spatiotemporal dynamics of endogenous proteins in living cells without affecting the endogenous antigen. These benefits resulted in the establishment of a broad range of CBs targeting different kinds of antigens to monitor endogenous antigens in living cells. Notably, several CBs have been already applied *in vivo* to monitor endogenous proteins in whole organisms without an interference in antigen functionality (Panza et al, 2015; Jullien et al, 2016).

3.4.3.3 Chromobodies as tools to quantify changes in endogenous protein concentration

As illustrated (chapter 3.1 - 3.3), monitoring the dynamic behavior of intracellular proteins such as endogenous CTNNB1 is highly desirable but also very challenging. For CTNNB1 this can mainly be explained by the numerous interacting proteins and the strictly controlled intracellular level of CTNNB1 (reviewed in (Valenta et al, 2012)). Recently, a CB (BC1-CB) was described, which specifically binds to soluble hypo-phosphorylated CTNNB1 (Traenkle et al, 2015). The BC1-CB was stably introduced into HeLa cells (HeLa_BC1-CB) and the cells were treated with different compounds known to elevate the level of endogenous CTNNB1. Beside monitoring a nuclear translocation of CTNNB1 with the BC1-CB (Figure 9 of Traenkle et al, 2015), a global elevation in CB fluorescence upon induction of CTNNB1 was observed (**Figure 4**). Subsequent immunoblot analysis (Figure 11 of Traenkle et al, 2015) confirmed a correlation of compound-induced increase in CTNNB1

accompanied by elevated BC1-CB protein amounts. As the transcriptional level of the CB was not altered through compound treatment, it was speculated that the elevation of CTNNB1 led to a concomitant stabilization of the CB on protein level. This hypothesized novel mechanism of "**A**ntigen-**M**ediated **CB S**tabilization" (AMCBS) might provide a new approach to quantify changes in endogenous protein concentration within living cells by simply following the CB fluorescence signal. Interestingly, another study reported an analogous observation of antigen-mediated V_HH stabilization in mammalian cells, by analyzing the amount of bacterially injected V_HHs in presence or absence of the cognate antigen (Blanco-Toribio et al, 2010).

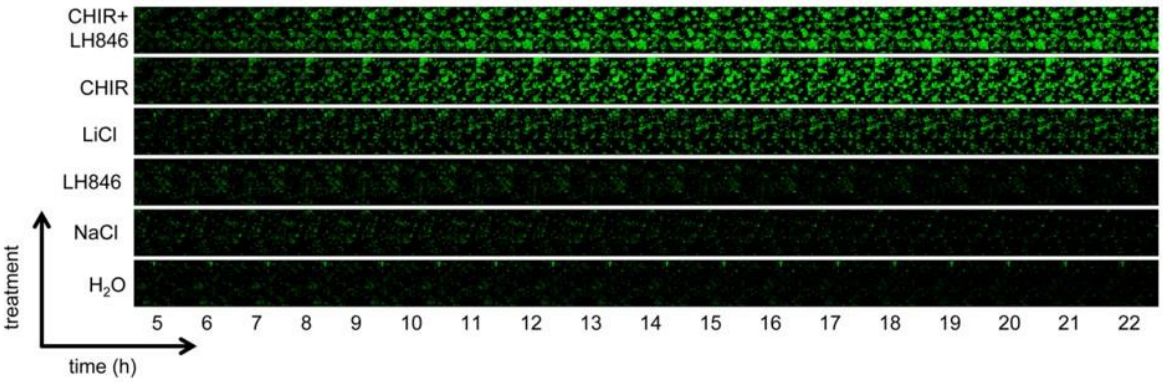

Figure 4 Time-lapse microscopy of compound-treated HeLa_BC1-CB cells.
HeLa_BC1-CB cells were treated with the indicated compounds or the respective controls followed by time-lapse imaging starting 5 h after compound treatment (Traenkle et al, 2015).

3.5 Aims and objectives

Elucidating the dynamics of endogenous proteins in real-time substantially contributes to a better understanding of physiological processes and disease generation, which consequently might promote drug discovery research. To date this task is mainly fulfilled by application of *in vitro* endpoint assays such as MS- or antibody-based techniques like quantitative western blotting, ELISA or immunofluorescence staining. However, the endpoint assay nature of these methods does not allow real-time assessment of dynamic changes and probing samples over time can be time consuming and labor-intensive.

Overcoming these limitations, chromobodies allow to monitor spatiotemporal dynamics of endogenous proteins in living cells under native conditions. The observation that an increase in CTNNB1 antigen level was accomplished by an increase in BC1-CB fluorescence led to the suggestion of a mechanism termed "**A**ntigen-**M**ediated **C**hromo**B**ody **S**tabilization" (AMCBS).

Within this dissertation, the first task was to analyze whether AMCBS is also evident for other CB-antigen combinations, which would suggest AMCBS as a general characteristic of CBs. Next, the respondency of CBs to monitor rapid and reversible changes of endogenous antigens was addressed. For this purpose three different strategies to generate destabilized or turnover-accelerated CBs were tested. Post testing of CB improvements in transient cellular systems, the next task was to generate and characterize cell lines stably expressing an optimized BC1-CB. A newly generated HeLa cell line was therefore compared to the originally described HeLa_BC1-CB cell line (Traenkle et al, 2015) regarding the CB respondency and dynamic range for image-based quantification of CTNNB1. The last task was to establish a protocol, which allows site-directed integration of optimized CBs into the AAVS1 safe harbor locus of a host cell by applying the CRISPR/Cas9 gene editing technology.

4 MATERIAL AND METHODS

4.1 Material

4.1.1 Chemicals and solutions

Chemical / solution	Manufacturer
10x RIPA buffer	ChromoTek, Martinsried, Germany
10x T4 DNA-Ligase reaction buffer	New England Biolabs, Frankfurt, Germany
2-Propanol	Carl Roth GmbH & Co. KG, Karlsruhe, Germany
5x Phusion GC-Buffer	New England Biolabs, Frankfurt, Germany
5x Phusion HF-Buffer	New England Biolabs, Frankfurt, Germany
6x DNA Loading Dye	ThermoFisher Scientific, Schwerte, Germany
Acrylamide Bisacrylamide	Carl Roth GmbH & Co. KG, Karlsruhe, Germany
Agarose, molecular biology grade	Carl Roth GmbH & Co. KG, Karlsruhe, Germany
Ammonium persulfate (APS)	Carl Roth GmbH & Co. KG, Karlsruhe, Germany
Ampicillin	Applichem GmbH, Darmstadt, Germany
Antibleaching live cell visualization medium DMEMgfp-2	Evrogen, Moscow, Russia
Bovine Serum Albumin (BSA, lyophilized powder)	Sigma-Aldrich Chemie GmbH, Munich, Germany
DAPI (4,6-diamiddino-2-phenylindole)	Roche Diagnostics GmbH, Mannheim, Germany
DMEM, high glucose, with phenolred	ThermoFisher Scientific, Schwerte, Germany
DMSO ≥99 %	Carl Roth GmbH & Co. KG, Karlsruhe, Germany
DNAse I	Applichem GmbH, Darmstadt, Germany
dNTP Solution Mix	New England Biolabs, Frankfurt, Germany
Ethanol, absolute grade	Sigma-Aldrich Chemie GmbH, Munich, Germany
Ethanol, denatured	Carl Roth GmbH & Co. KG, Karlsruhe, Germany
Ethidiumbromide solution (0.025%)	Carl Roth GmbH & Co. KG, Karlsruhe, Germany
Ethylenediaminetetraacetic acid (EDTA)	Applichem GmbH, Darmstadt, Germany
Fetal Bovine Serum (FBS)	ThermoFisher Scientific, Schwerte, Germany
Formaldeyde (37 %)	Applichem GmbH, Darmstadt, Germany
G418	ThermoFisher Scientific, Schwerte, Germany
GeneRuler 1kB plus DNA Ladder	ThermoFisher Scientific, Schwerte, Germany
Gibson Assembly® Master Mix	New England Biolabs GmbH, Frankfurt, Germany
Glycine	Carl Roth GmbH & Co. KG, Karlsruhe, Germany
Hoechst33258	ThermoFisher Scientific, Schwerte, Germany
Kanamycin	Carl Roth GmbH & Co. KG, Karlsruhe, Germany
L-Glutamine	ThermoFisher Scientific, Schwerte, Germany
Lipofectamine 2000	ThermoFisher Scientific, Schwerte, Germany
Lipofectamine LTX	ThermoFisher Scientific, Schwerte, Germany
Luria Broth (LB) Medium	Carl Roth GmbH & Co. KG, Karlsruhe, Germany
Magnesium chloride	Sigma-Aldrich Chemie Gmbh, Munich, Germany
Methanol, min. 99 %	Sigma-Aldrich Chemie GmbH, Munich, Germany
Midiprep System PureYield Plasmid	Promega GmbH, Mannheim, Germny
Midiprep System PureYield Plasmid	Qiagen N.V., Venlo, Netherlands
Milkpowder, Blotting Grade	Carl Roth GmbH & Co. KG, Karlsruhe, Germany
N′-tetramethylethylenediamine (TEMED)	Carl Roth GmbH & Co. KG, Karlsruhe, Germany
NEB-Buffer 1-4, Cut Smart	New England Biolabs, Frankfurt, Germany
NP-40	Carl Roth GmbH & Co. KG, Karlsruhe, Germany
NucleoSpin Gel and PCR Clean-up Kit	Macherey-Nagel, Düren Germany
NucleoSpin Plasmid Kit	Macherey-Nagel, Düren Germany
Opti-MEM, reduced serum media	ThermoFisher Scientific, Schwerte, Germany
PageRuler™ Prestained Protein Ladder Plus	Fermentas GmbH, St.Leon-Rot, Germany
Penicillin Streptomycin	ThermoFisher Scientific, Schwerte, Germany
Phenylmethanesulfonylfluoride (PMSF)	SERVA Electrophoresis GmbH, Heidelberg, Germany
Phosphate Buffered Saline (PBS), 1x	ThermoFisher Scientific, Schwerte, Germany
Phusion™ High-Fidelity DNA Polymerase	New England Biolabs, Frankfurt, Germany
Polyethyleneimine	Sigma-Aldrich Chemie GmbH, Munich, Germany
Ponceau S	Sigma-Aldrich Chemie Gmbh, Munich, Germany
Potassium chloride	Sigma-Aldrich Chemie Gmbh, Munich, Germany

Protease Inhibitor Mix M	SERVA Electrophoresis GmbH, Heidelberg, Germany
Puromycin	Sigma-Aldrich Chemie Gmbh, Munich, Germany
Q5®Site-Directed Mutagenesis Kit	New England Biolabs GmbH, Frankfurt, Germany
Red Mastermix (2x) Taq Matermix	Genaxxon bioscience GmbH, Ulm, Germany
Restrictionenzymes	New England Biolabs GmbH, Frankfurt, Germany
Sodium dodecyl sulfate (SDS)	Carl Roth GmbH & Co. KG, Karlsruhe, Germany
T4 Ligation Kit	New England Biolabs GmbH, Frankfurt, Germany
Triton X-100	Carl Roth GmbH & Co. KG, Karlsruhe, Germany
Trypsin-EDTA (0.25 %), phenol red	ThermoFisher Scientific, Schwerte, Germany
Tween20	Carl Roth GmbH & Co. KG, Karlsruhe, Germany
β-Mercaptoethanol	Carl Roth GmbH & Co. KG, Karlsruhe, Germany

4.1.2 Devices

Device	Manufacturer
Autoclave VX-95	Systec GmbH, Wettenberg, Germany
CASY TT Cell Counter System	OLS OMNI Life Science GmbH & Co. KG, Bremen, Germany
Cell Observer SD	Zeiss AG, Oberkochen, Germany
Centrifuge 5415R	Eppendorf AG, Hamburg, Germany
Centrifuge 5424	Eppendorf AG, Hamburg, Germany
Centrifuge 5810R	Eppendorf AG, Hamburg, Germany
Centrifuge Universal 2S	Hettich GmbH & Co KG, Tuttlingen, Germany
CO_2-Incubator CB150	Binder GmbH, Tuttlingen, Germany
Elektrophoresis Chamber	Bio-Rad Laboratories GmbH, München, Germany
GFL water bath 1002	GFL Gesellschaft für Labortechnik mbH, Burgwedel, Germany
GFL water bath 1083	GFL Gesellschaft für Labortechnik mbH, Burgwedel, Germany
High-content microscope MetaXpressXL system	Molecular Devices, Biberach, Germany
Incubator shaker C25	New Brunswick Scientific, Nürtingen, Germany
INTAS UV documentation system	INTAS, Goettingen, Germany
Light microscope TMS-F	Nikon, Duesseldorf, Germany
Magnet stirrer RCTbasic	IKA-Werke GmbH, Staufen, Germany
Microscope Axiovert 200M	Zeiss AG, Oberkochen, Germany
Multipipet plus	Eppendorf AG, Hamburg, Germany
Mupid One electrophoresis unit	NIPPON Genetics EUROPE GmbH, Dueren, Germany
Neubauer chamber	Brand, Wertheim, Germany
Overhead rotator	Bachofer, Reutlingen, Germany
PCR device Primus 96 plus	MWG Biotech AG, Ebersberg, Germany
pH meter	Mettler-Toledo GmbH, Giessen, Germany
PHERAstar plate reader	BMG Labtech, Offenburg, Germany
Pipet HandyStep	Brand GmbH & Co KG, Wertheim, Germany
Pipettes 10 µl, 20 µl, 100 µl, 200 µl, 1000 µl	Brand GmbH & Co KG, Wertheim, Germany
Pipettboy	Integra BioSciences, Fernwald, Germany
Pipette, 8-Kanal, 0.5 µl - 1200 µl	Eppendorf AG, Hamburg, Germany
Power supply gel elektrophoresis MP-300V	Major Science, USA
PowerPac Basic Power Supply	Bio-Rad Laboratories GmbH, München, Germany
Semi-Dry transfer cell	Bio-Rad Laboratories GmbH, München, Germany
Spectrometer NanoDrop 2000	ThermoFisher Scientific, Schwerte, Germany
StepOne™ Plus Real-Time PCR System	ThermoFisher Scientific, Schwerte, Germany
Steril hood	BDK GmbH, Sonnenbühl-Genkingen, Germany
Thermomixer comfort	Eppendorf AG, Hamburg, Germany
Typhoon TRIO	GE Healthcare Life Sciences

4.1.3 Consumables

Consumable	Manufacturer
µClear 96-well microplate	Greiner Bio-One, Frickenhausen, Germany

Blotting Paper Grade 703	Bio-Rad Laboratories GmbH, Munich, Germany
Cell Culture Flasks T-25, T-75, T-125	Corning GmbH, Wiesbaden, Germany
100 mm cell culture dish	Corning GmbH, Wiesbaden, Germany
Falcon Tubes (15 and 50 ml)	Sarstedt AG & Co., Nümbrecht, Germany
Falcon-Tubes 15ml und 50ml	Greiner Bio-One, Frickenhausen, Germany
GFP-Trap	ChromoTek GmbH, Martinsried, Germany
Parafilm	Brand GmbH & Co. KG, Wertheim, Germany
PCR-Reaction tube, 200 µl	Sarstedt AG & Co., Nümbrecht, Germany
Petridish, 92 x 16 mm	Sarstedt AG & Co., Nümbrecht, Germany
pH Indicatorstrips, pH 0-14	Merck KGaA, Darmstadt, Germany
Pipettes (2, 5, 10 und 25 ml)	Sarstedt AG & Co., Nümbrecht, Germany
Amersham Protan 0,45 µm Nitrocellulose	GE Healthcare, Uppsala, Sweden
Pipettetips (10, 20, 200, 1000, 1250 µl)	Starlab GmbH, Hamburg, Germany
Multiwell plate: 6, 12, 24, 48, 96 well	Corning GmbH, Wiesbaden, Germany
Reaction tube 1.5 ml / 2 ml	Sarstedt AG & Co., Nümbrecht, Germany
Cryotubes, 1.8 ml	Greiner Bio-One, Frickenhausen, Germany

4.1.4 Antibodies

Antibody	Dilutionfactor	Company
Primary		
anti-CTNNB1 (mouse, mAb)	1000	BD Biosciences, Heidelberg, Germany
anti-GAPDH FL335 (rabbit, pAb)	1000	Santa Cruz, Dallas, USA
anti-GFP 3H9 (rat, mAb)	1000	ChromoTek GmbH, Munich, Germany
anti-PCNA 16D10	1000	ChromoTek GmbH, Munich, Germany
anti-RFP 6G6 (mouse, mAb)	5000	ChromoTek GmbH, Munich, Germany
anti-TagRFP AB233 (rabbit, mAb)	1000	Evrogen, Moscow, Russia
Secondary		
anti-mouse (goat) Alexa 488/546/647 conjugates	2000	ThermoFisher Scientific, Schwerte, Germany
anti-rabbit (goat) Alexa 488/546/647 conjugates	2000	ThermoFisher Scientific, Schwerte, Germany
anti-rat (goat) Alexa 488/546/647 conjugates	2000	ThermoFisher Scientific, Schwerte, Germany

4.1.5 Oligonucleotides

4.1.5.1 Primer for DNA amplification

Primer name	Primer sequence, 5' - 3'
4GS-linker-oligo1	CAG GTC ACC GTC TCC TCC GGA GGC GGG GGA AGC GGA GGC GGG GGA AGC GGA GGC GGG GGA TCC ATG AGC GGG GGC GAG G
4GS-linker-oligo2	CCT CGC CCC CGC TCA TGG ATC CCC CGC CTC CGC TTC CCC CGC CTC CGC TTC CCC CGC CTC CGG AGG AGA CGG TGA CCT G
AAVS1-CB-donor-fragment-2-for	TAG AGG CGG CAA TTG TTC A
AAVS1-CB-donor-fragment-2-rev	TGT TGT TAA CTT GTT TAT TGC AGC
BC1-2GS-rev	GGA GAC GGT GAC CTG GGT CC
BC1-for	ATG GCT CAG GTG CAG CTG CAG
BC1-NB-C92Y-for	CCG TGT ATT ACT ATA ACG CTC TAT C
BC1-NB-C92Y-rev	CCG TGT CCT CAG GTT TC
BC1-NB-S113F-for	CCG TCT CCT TCA GAA GCT TCG
BC1-NB-S113F-rev	TGA CCT GGG TCC CCT G
BC1-NB-S70R-for	GGG CCG GTT CAC CAT CCG CAG AGA CAA AGC C
BC1-NB-S70R-rev	TTC ACG GAG TCT TGA TAG TTT GTG
BC1-rev	GCT TCC CCC GCC TCC GCT TCC CCC GCC TCC GGA GGA GAC GGT GAC CTG GGT C
BC1-TagGFP2-PEST-for	TAT ATA TCT AGA TCA TGG CTT CCC GCC GGA GGT GGA GGA GCA GGA TGA TGG CAC GCT GCC CAT GTC TTG TGC CCA GGA GAG CGG GAT GGA CC
BC1-TagGFP2-PEST-rev	TAT ATA CAA TTG CTA GGT CCA TCC CGC TCT CCT GG
BspEI-ins-for	TCC GGA ACC GCG GGC CCG GGA TCC

BspEI-ins-rev	ACC GTC GAC TGC AGA ATT CGA AGC
eGFP-for	ATA TAT GGA TCC ATG GTG AGC AAG GGC GAG G
eGFP-rev	ATA TAT TCT AGA TCA CTT GTA CAG CTC GTC CAT
genPCR-AAVS1-int-for	TCG ACT TCC CTT CTT CCG ATG
genPCR-AAVS1-int-rev	CTC AGA TTC TGG GAG AGG GTA
mCherry-CTNNB1-for	GGA GGT ACC GCT ACT CAA GCT GAT TTG
mCherry-CTNNB1-rev	CTT GGA TCC TCA CAG GTC AGT ATC AAA C
mCherry-for	CCA GGA CGG CGA GTT CAT C
mCherry-rev	ATA TAT TCT AGA TCA CTT GTA CAG CTC GTC CAT
mCherry-silent-mut-for	CCA GGA CTC CTC CCT CCA GGA CGG CGA G
mCherry-silent-mut-rev	GTC ACG GTC ACC ACG CCG CCG TC
NB-N-term-A-mut-for	CGT CTC AGA GGT GGG GCG GCT CAG GTG CAG CTG
NB-N-term-C-mut-for	CGT CTC AGA GGT GGG TGC GCT CAG GTG CAG CTG
NB-N-term-D-mut-for	CGT CTC AGA GGT GGG GAC GCT CAG GTG CAG CTG
NB-N-term-E-mut-for	CGT CTC AGA GGT GGG GAG GCT CAG GTG CAG CTG
NB-N-term-F-mut-for	CGT CTC AGA GGT GGG TTC GCT CAG GTG CAG CTG
NB-N-term-G-mut-for	CGT CTC AGA GGT GGG GGG GCT CAG GTG CAG CTG
NB-N-term-H-mut-for	CGT CTC AGA GGT GGG CAC GCT CAG GTG CAG CTG
NB-N-term-I-mut-for	CGT CTC AGA GGT GGG ATC GCT CAG GTG CAG CTG
NB-N-term-K-mut-for	CGT CTC AGA GGT GGG AAG GCT CAG GTG CAG CTG
NB-N-term-L-mut-for	CGT CTC AGA GGT GGG CTG GCT CAG GTG CAG CTG
NB-N-term-N-mut-for	CGT CTC AGA GGT GGG AAC GCT CAG GTG CAG CTG
NB-N-term-P-mut-for	CGT CTC AGA GGT GGG CCG GCT CAG GTG CAG CTG
NB-N-term-Q-mut-for	CGT CTC AGA GGT GGG CAG GCT CAG GTG CAG CTG
NB-N-Term-rev	GAG TAC CAG GTG CAG GGT GG
NB-N-term-R-mut-for	CGT CTC AGA GGT GGG AGG GCT CAG GTG CAG CTG
NB-N-term-S-mut-for	CGT CTC AGA GGT GGG AGC GCT CAG GTG CAG CTG
NB-N-term-T-mut-for	CGT CTC AGA GGT GGG ACC GCT CAG GTG CAG CTG
NB-N-term-V-mut-for	CGT CTC AGA GGT GGG GTG GCT CAG GTG CAG CTG
NB-N-term-W-mut-for	CGT CTC AGA GGT GGG TGG GCT CAG GTG CAG CTG
NB-N-term-Y-mut-for	CGT CTC AGA GGT GGG TAC GCT CAG GTG CAG CTG
NB-uni-for	ATA TAT CTG CAG GAG TCT GGG GGA GGC TTG GTG CA
NB-uni-rev	ATA TAT TCC GGA GGA GAC GGT GAC CTG GGT CCC
Seq-AAVS1-CB-donor-1	TAT GGA AAA ACG CCA GCA AC
Seq-AAVS1-CB-donor-2	ATG TGG CTC TGG TTC TGG G
Seq-AAVS1-CB-donor-3	AGC GGC TCG GCT TCA C
Seq-AAVS1-CB-donor-4	CCT TAG ATG TTT TAC TAG CCA GAT
TagGFP2-2GS-for	GGA GGC GGG GGA TCC ATG AGC GGG G
TagGFP2-2GS-for	ATG AGC GGG GGC GAG GAG CTG
TagGFP2-for	GGA GGC GGG GGA AGC GGA GGC GGG GGA TCC ATG AGC GGG GGC GAG GAG C
TagGFP2-rev	GTG GTA TGG CTG ATT ATG ATC TAG ATC ACC TGT ACA GCT CGT CCA TGC C
TagRFP-for	ATA TAT GGA TCC ATG GTG TCT AAG GGC GAA G
TagRFP-rev	ATA TAT TCT AGA TCA ATT AAG TTT GTG CCC CAG TTT G
Ub-G76V-mut-rev	CAC ACC TCT GAG ACG GAG TAC C
ubiquitin-for	TTT AGT GAA CCG TCA GAT CCG CTA GCG CCA CCA TGC AGA TCT TCG TGA AGA CTC TG
ubiquitin-rev	CAG CTG CAC CTG AGC CAT CCC ACC TCT GAG ACG GAG TAC
αCA-mCherry -PEST-rev	TAT ATA TCT AGA CTA GGT CCA TCC CGC TCT CCT GG
αCA-mCherry-PEST-for	TAT ATA TGT ACA AGC ATG GCT TCC CGC CGG AGG TGG AGG AGC AGG ATG ATG GCA CGC TGC CCA TGT CTT GTG CCC AGG AGA GCG GGA TGG ACC
β-actin-promoter-for	GGA ATT AAT ACT GCC TGG CCA CTC CAT G
β-actin-promoter-mut-PstI-for	AGA GCT CCT TGT GCA GGA GCG
β-actin-promoter-rev	TCC GCT AGC TCG GCA AAG GCG AGG C
β-actin-promotoe-mut-PstI-rev	TGG AGG GCA TGG AGT GGC

4.1.5.2 gBlocks® gene fragments and synthesized plasmids

Sequence name	Primer sequence, 5' - 3'
EF1-α promoter gBlock® gene fragment	TTACCGCCATGCATTAGTTATTAATGGCTCCGGTGCCCGTCAGTGGGCAGAGCGCACAT CGCCCACAGTCCCCGAGAAGTTGGGGGGAGGGGTCGGCATTTGAACCGGTGCCTAGAGA AGGTGGCGCGGGGTAAACTGGGAAAGTGATGTCGTGTACTGGCTCCGCCTTTTTCCCGA GGGTGGGGGAGAACCGTATATAAGTGCAGTAGTCGCCGTGAACGTTCTTTTTCGCAACG GGTTTGCCGCCAGAACACAGGTAAGTGCCGTGTGTGGTTCCCGCGGGCCTGGCCTCTTT ACGGGTTATGGCCCTTGCGTGCCTTGAATTACTTCCACCTGGCTCCAGTACGTGATTCT TGATCCCGAGCTTCGGGTTGGAAGTGGGTGGGAGAGTTCGAGGCCTTGCGCTTAAGGAG CCCCTTCGCCTCGTGCTTGAGTTGAGGCCTGGCCTGGGCGCTGGGGCCGCCGCGTGCGA ATCTGGTGGCACCTTCGCGCCTGTCTCGCTGCTTTCGATAAGTCTCTAGCCATTTAAAA TTTTTGATGACCTGCTGCGACGCTTTTTTTCTGGCAAGATAGTCTTGTAAATGCGGGCC AAGATCTGCACACTGGTATTTCGGTTTTTGGGGCCGCGGGCGGCGACGGGGCCCGTGCG TCCCAGCGCACTTGTTCGGCGAGGCGGGGCCTGCGAGCGCGGCCACCGAGAATCGGACG GGGGTAGTCTCAAGCTGGCCGGCCTGCTCTGGTGCCTGGTCTCGCGCCGCCGTGTATCG CCCCGCCCTGGGCGGCAAGGCTGGCCCGGTCGGCACCAGTTGCGTGAGCGGAAAGATGG CCGCTTCCCGGCCCTGCTCCAGGGAGCTCAAAATGGAGGACGCGGCGCTCGGGAGAGCG GGCGGGTGAGTCACCCACACAAAGGAAAAGGGCCTTTCCGTCCTCAGCCGTCGCTTCAT GTGACTCCACGGAGTACCGGGCGCCGTCCAGGCACCTCGATTAGTTCTCGAGCTTTTGG AGTACGTCGTCTTTAGGTTGGGGGGAGGGGTTTTATGCGATGGAGTTTCCCCACACTGA GTGGGTGGAGACTGAAGTTAGGCCAGCTTGGCACTTGATGTAATTCTCCTTGGAATTTG CCCTTTTTGAGTTTGGATCTTGGTTCATTCTCAAGCCTCAGACAGTGGTTCAAAGTTTT TTTCTTCCATTTCAGGTGTCGTGAGCTAGCGCCACCATGCAGATCTTCG
AAVS1-CB-donor fragment 1 gene synthesis, plasmid DNA	CCTTTTGCTGGCCTTTTGCTCACATGTTGCTTTCTCTGACCAGCATTCTCTCCCCTGGG CCTGTGCCGCTTTCTGTCTCCAGCTTGTGGCCTGGGTCACCTCTACGGCTGGCCCAGAT CCTTCCCTGCCGCCTCCTTCAGGTTCCGTCTTCCTCCACTCCCTCTTCCCCTTGCTCTC TGCTGTGTTGCTGCCCAAGGATGCTCTTTCCGCAGCACTTCCTTCTCGGCGCTGCACCA CGTGATGTCCTCTGAGCGCATCCTCCCCGTGTCTGGGTCCTCTCCGGGCATCTCTCCTC CCTCACCCAACCCCATGCCGTCTTCACTCGCTGGGTTCCCTTTTCCTTCTCCTTCTGGG GCCTGTGCCATCTCTCGTTTCTTAGGATGGCCTTCTCCGACGGATGTCTCCCTTGCGTC CCGCCTCCCCTTCTTGTAGGCCTGCATCATCACCGTTTTTCTGGACAACCCCAAAGTAC CCCGTCTCCCTGGCTTTAGCCACCTCTCCATCCTCTTGCTTTCTTTGCCTGGACACCCC GTTCTCCTGTGGATTCGGGTCACCTCTCACTCCTTTCATTTGGGCAGCTCCCCTACCCC CCTTACCTCTCTAGTCTGTGCAAGCTCTTCCAGCCCCCTGTCATGGCATCTTCCAGGGG TCCGAGAGCTCAGCTAGTCTTCTTCCTCCAACCCGGGCCCCTATGTCCACTTCAGGACA GCATGTTTGCTGCCTCCAGGCATCCTGTGTCCCCGAGCTGGGACCACCTTATATTCCCA GGGCCGGTTAATGTGGCTCTGGTTCTGGGTACTTTTATCTGTCCCCTCCACCCCACAGT GGGGCAAGCTTCTGACCTCTTCTCTTCCTCCCACAGGGCCTCGAGAGATCTGGCAGCGG AGAGGGCAGAGGAAGTCTTCTAACATGCGGTGACGTGGAGGAGAATCCCGGCCCTAGGC TCGAGATGACAGAATACAAACCCACGGTGCGGCTCGCGACTCGCGATGACGTGCCCCGA GCGGTGAGAACATTGGCAGCAGCGTTCGCAGACTATCCGGCTACGCGGCATACTGTCGA TCCTGATCGACATATTGAACGGGTCACCGAGTTGCAGGAGCTTTTCCTCACACGCGTTG GATTGGATATTGGCAAAGTATGGGTCGCGGACGACGGGGCAGCTGTCGCCGTGTGGACC ACCCCCGAGTCAGTGGAGGCTGGAGCGGTATTCGCTGAGATCGGCCCTCGGATGGCAGA ATTGAGCGGCTCCAGACTGGCGGCTCAACAGCAGATGGAAGGGCTCCTCGCCCCTCATA GACCTAAGGAACCTGCTTGGTTCCTCGCAACCGTGGGCGTCTCACCAGACCATCAGGGG AAGGGCCTTGGGTCTGCGGTGGTCTTGCCGGGGGTCGAGGCaGCAGAGAGAGCTGGGGT ACCCGCGTTTTTGGAAACAAGTGCGCCCCGAAACCTCCCGTTTTACGAACGGCTTGGCT TTACAGTCACAGCAGATGTTGAAGTACCGGAGGGACCAAGGACCTGGTGCATGACCCGC AAGCCGGGAGCTTGATCAAGAGGGCCCGTTTAAACCCGCTGATCAGCCTCGACTGTGCC TTCTAGTTGCCAGCCATCTGTTGTTTGCCCCTCCCCCGTGCCTTCCTTGACCCTGGAAG GTGCCACTCCCACTGTCCTTTCCTAATAAAATGAGGAAATTGCATCGCATTGTCTGAGT AGGTGTCATTCTATTCTGGGGGGTGGGGTGGGGCAGGACAGCAAGGGGGAGGATTGGGA AGACAATAGCAGGCATGCTGGGGATGCGGTGGGCTCTATGGACTAGTATTAATTAAATC TAGAGGCGGCAATTGTTCACTCCTCAGGTGCAGGC
AAVS1-CB-donor fragment 2	AAATCTAGAGGCGGCAATTGTTCACTCCTCAGGTGCAGGCTGCCTATCAGAAGGTGGTG GCTGGTGTGGCCAATGCCCTGGCTCACAAATACCACTGAGATCTTTTTCCCTCTGCCAA AAATTATGGGGACATCATGAAGCCCCTTGAGCATCTGACTTCTGGCTAATAAAGGAAAT TTATTTTCATTGCAATAGTGTGTTGGAATTTTTTGTGTCTCTCACTCGGAAGGACATAT GGGAGGGCAAATCATTTAAAACATCAGAATGAGTATTTGGTTTAGAGTTTGGCAACATA TGCCATATGCTGGCTGCCATGAACAAAGGTGGCTATAAAGAGGTCATCAGTATATGAAA CAGCCCCCTGCTGTCCATTCCTTATTCCATAGAAAAGCCTTGACTTGAGGTTAGATTTT TTTTATATTTTGTTTTGTGTTATTTTTTTCTTTAACATCCCTAAAATTTTCCTTAGATG TTTTACTAGCCAGATTTTTCCTCCTCTCCTGACTACTCCCAGTCATAGCTGTCCCTCTT CTCGTCGACAGTACTAAGCTTTGACAGAAAAGCCCCATCCTTAGGCCTCCTCCTTCCTA GTCTCCTGATATTGGGTCTAACCCCCACCTCCTGTTAGGCAGATTCCTTATCTGGTGAC ACACCCCCATTTCCTGGAGCCATCTCTCTCCTTGCCAGAACCTCTAAGGTTTGCTTACG ATGGAGCCAGAGAGCATCCTGGGAGGGAGAGCTTGGCAGGGGGTGGGAGGGAAGGGGGG GATGCGTGACCTGCCCGGTTCTCAGTGGCCACCCTGCGCTACCCTCTCCCAGAACCTGA GCTGCTCTGACGCGGCTGTCTGGTGCGTTTCACTGATCCTGGTGCTCCAGCTTCCTTAC ACTTCCCAAGAGGAGAAGCAGTTTGGAAAAACAAAATCAGAATAAGTTGGTCCTGAGTT CTAACTTTGGCTCTTCACCTTTCTAGTCCCCAATTTATATTGTTCCTCCGTGCGTCAGT TTTACCTGTGAGATAAGGCCAGTAGCCAGCCCCGTCCTGGCAGGGCTGTGGTGAGGAGG GGGGTGTCCGTGTGGAAAACTCCCTTTGTGAGAATGGTGCGTCCTAGGTGTTCACCAGG TCGTGGCCGCCTCTACTCCCTTTCTCTTTCTCCATCCTTCTTTCCTTAAAGAGTCCCCA GTGCTATCTGGGACATATTCCTCCGCCCAGAGCAGGGTCCCGCTTCCCTAAGGCCCTGC

	TCTGGGCTTCTGGGTTTGAGTCCTTGGCAAGCCCAGGAGAGGCGCTCAGGCTTCCCTGT CCCCCTTCCTCGTCCACCATCTCATGCCCCTGGCTCTCCTGCCCCTTCCCTACAGGGGT TCCTGGCTCTGCTCTCAATTGTTGTTGTTAACTTGTTTATTGCAGCTTATAATGG

4.1.6 Expression constructs

Expression construct	Origin
AAVS1_Ub-R-ActinNB-eGFP	this study
AAVS1_Ub-R-BC1-eGFP	this study
Actin-CB	(Panza et al, 2015), kindly provided by Chromotek
BC1-TagGFP2	(Traenkle et al, 2015)
BC1-TagGFP2-PEST	Master thesis Kathy-Ann Secker
BC1-TagGFP-PEST	Master thesis Kathy-Ann Secker
Cas9_AAVS1-gRNA	(Oceguera-Yanez et al, 2016)
CCC-TagRFP	(Burgess et al, 2012; Schorpp et al, 2016), kindly provided by Chromotek
EF1-α_Ub-R-BC1-eGFP	this study
GFP-CA	(Ivanchenko et al, 2009; Lampe et al, 2007)
LMN-CB	(Zolghadr et al, 2012)
mCherry	(Toulany et al, 2017)
mCherry-CTNNB1	this study
pEGFP-N1	Clonetech
Ub-A-BC1-eGFP	this study
Ub-A-BC1-mCherry	this study
Ub-A-BC1-TagGFP2	this study
Ub-A-BC1-TagRFP	this study
Ub-A-VB6-TagGFP2	this study
Ub-A-αCA-TagGFP2	this study
Ub-C-BC1-TagGFP2	this study
Ub-D-BC1-TagGFP2	this study
Ub-E-BC1-TagGFP2	this study
Ub-F-BC1-eGFP	this study
Ub-F-BC1-mCherry	this study
Ub-F-BC1-TagGFP2	this study
Ub-F-BC1-TagRFP	this study
Ub-F-VB6-TagGFP2	this study
Ub-F-αCA-TagGFP2	this study
Ub^{G76V}-M-BC1-TagGFP2	this study
Ub-G-BC1-TagGFP2	this study
Ub-H-BC1-TagGFP2	this study
Ub-I-BC1-TagGFP2	this study
Ub-K-BC1-TagGFP2	this study
Ub-L-BC1-TagGFP2	this study
Ub-M-BC1-$(G_4S)_2$-TagGFP2	this study
Ub-M-BC1-$(G_4S)_4$-TagGFP2	this study
Ub-M-BC1-eGFP	this study
Ub-M-BC1-mCherry	this study
Ub-M-BC1-TagGFP2	this study
Ub-M-BC1-TagRFP	this study
Ub-M-LMN-CB	this study
Ub-M-VB6-TagGFP2	this study
Ub-M-αCA-TagGFP2	this study
Ub-N-BC1-TagGFP2	this study
Ub-P-BC1-TagGFP2	this study
Ub-Q-BC1-TagGFP2	this study
Ub-R-BC1-eGFP	this study
Ub-R-BC1-mCherry	this study
Ub-R-BC1-TagGFP2	this study
Ub-R-BC1-TagRFP	this study
Ub-R-LMN-CB	this study

Ub-R-VB6-TagGFP2	this study
Ub-R-αCA-TagGFP2	this study
Ub-S-BC1-eGFP	this study
Ub-S-BC1-mCherry	this study
Ub-S-BC1-TagGFP2	this study
Ub-S-BC1-TagRFP	this study
Ub-S-VB6-TagGFP2	this study
Ub-S-αCA-TagGFP2 (	this study
Ub-T-BC1-TagGFP2	this study
Ub-V-BC1-TagGFP2	this study
Ub-W-BC1-TagGFP2	this study
Ub-Y-BC1-TagGFP2	this study
VB6-eGFP	(Maier et al, 2015)
VB6-TagRFP	(Maier et al, 2015)
αCA-mCherry	(Helma et al, 2012)
αCA-mCherry-PEST	Master thesis Kathy-Ann Secker
αCA-mCherry-PEST	Master thesis Kathy-Ann Secker
β-actin promoter	(Damdindorj et al, 2014), pAAV-hBACT-PIGA, a gift from Hiroyuki Konishi
β-actin_Ub-R-BC1-eGFP	this study

4.1.7 RNAi constructs

siRNA	Distributor	Sequence or order-ID
siCTR1	Dharmacon	ON-Target plus non-targeting siRNA #1 (D-001810-01)
siCTR2	Dharmacon	ON-Target plus non-targeting siRNA #1 (D-001810-02)
siPCNA1	ambion, life technologies	5'-CGUAUAUGCCGAGAUCUCAtt-3'
siPCNA2	ambion, life technologies	5'-GGAGUGAAAUUUUCUGCAAtt-3'
siPCNA3	ambion, life technologies	5'-GAAGAUAUCAUUACACUAAtt-3'
siVIM1	ambion, life technologies	5'-GGUUGAUACCCACUCAAAAtt-3'
siVIM2	ambion, life technologies	5'-GAGGGAAACUAAUCUGGAUtt-3'
siVIM3	ambion, life technologies	5'-GUCUUGACCUUGAACGCAAtt-3'

4.1.8 PrimeTime® qPCR assay primer

Gene name	Assay name	RefSeqNumber	Exon location
AXIN2	Hs.PT.58.39305692	NM_004655	3-4
CCND1	Hs.PT.56a.4930170	NM_053056	1-2
CTNNB1	Hs.PT.58.40551289	NM_00109821	10-11
GAPDH	Hs.PT.39a.22214836	NM_002046	2-3
MYC	Hs.PT.58.26770695	NM_002467	2-3

4.1.9 Cell lines

4.1.9.1 Parental cell lines

Cell line	Additional information	Obtained from
DLD-1	CCL-221 human colorectal adenocarcinoma	ATCC
HCT116	CCL-247 human colorectal carcinoma	ATCC
HEK293T	CRL-3216 human embryonic kidney	ATCC
HeLa Kyoto	Cellosaurus no. CVCL_1922 human cervix adenocarcinoma	Kyoto University, Japan
U2OS	HTB-96 human bone osteosarcoma	ATCC

4.1.9.2 Stably transfected cell lines

Cell line	Origin
A549_VB6-eGFP	(Maier et al, 2015)
A549_VB6-TagRFP	unpublished cell line generated by Dr. Julia Maier, University of Tuebingen
DLD-1_AAVS1_Ub-R-BC1-eGFP	this study
DLD-1_BC1-TagGFP2	unpublished cell line generated by Bettina-Maria Keller, University of Tuebingen
HCT116_AAVS1_Ub-R-BC1-eGFP	this study
HeLa_AAVS1_Ub-R-ACT-eGFP	this study
HeLa_ACT-eGFP	unpublished cell line generated by Dr. Björn Tränkle, University of Tuebingen
HeLa_BC1-TagGFP2	(Traenkle et al, 2015)
HeLa_CCC-TagRFP	(Panza et al, 2015)
HeLa_Ub-R-BC1-eGFP	this study
HeLa_αCA-mCherry	(Helma et al, 2012)
U2OS_Ub-R-BC1-eGFP	this study

4.2 Methods

4.2.1 Molecular biological methods

4.2.1.1 Polymerase chain reaction

To amplify DNA fragments and to introduce specific restriction sites, polymerase chain reaction (PCR) was performed. The standard PCR set-up contained the following components: (1) template DNA, (2) DNA primers (listed in oligonucleotides) complementary to 3'- ends of the sense and anti-sense strand, (3) thermostable DNA polymerase, (4) deoxynucleotide triphosphates (dNTPs) mix, (5) reaction buffer (**Table 1**). PCR was carried out according to the conditions shown in **Table 2**, wherein the annealing temperature was adjusted to the nucleotide composition of the DNA primers and the extension time to the length of the amplicon.

Table 1 Standard PCR reaction setup

Component	Volume	Final concentration
5X Phusion HF or Buffer	10 µl	1X
10 mM dNTP mix	1 µl	200 µM
10 µM forward primer	2.5 µl	0.5 µM
10 µM reverse primer	2.5 µl	0.5 µM
Template DNA (10 ng/µl)	1 µl	10 ng
Phusion DNA Polymerase	0.5 µl	1.0 units/50 µl PCR
ddH_2O	32.5 µl	-

Table 2 Standard PCR cycling conditions

Step	Temperature	Time	Number of cycles
Initial denaturation	98 °C	30 s	1
Denaturation Annealing Extension	98 °C 53 – 62 °C 72 °C	10 s 15 s 15 s per kb	30x
Final extension	72 °C	10 min	1
Hold	4 °C	∞	

4.2.1.2 Restriction analysis

Enzymatic digestion of amplified DNA fragments and plasmids was performed using restriction enzymes from New England Biolabs according to the manufacturer's instruction. For analytical purposes, 500 – 1000 ng DNA and for plasmid preparation 10 µg DNA were digested by restriction enzymes.

4.2.1.3 Agarose gel electrophoresis

Agarose gel electrophoresis was used for size separation, analysis and purification of DNA samples from enzymatic restriction and / or PCR reaction. The separation was carried out on 0.8 - 1.5 % agarose dissolved in 1X Tris-acetate-EDTA buffer containing 0.025 µg/ml ethidium bromide to allow detection of DNA under UV exposure. DNA samples were mixed with 6X DNA loading dye and loaded on the gel for size separation. As standard Generuler 1 kb Plus DNA Ladder was used. Ethidium bromide-stained DNA was detected with an Intas UV system (Intas Science Imaging). In case of a preparative gel respective DNA bands were cut out from the gel and purified using the NucleoSpin Gel and PCR clean-up Kit (Macherey-Nagel) according to the manufacturer's instructions.

4.2.1.4 Colony PCR

To determine the presence or absence of an insert within DNA plasmid constructs, colony PCR was performed. Therefore individual transformants were directly picked from the agar plate and transferred into a PCR tube containing Genaxxon Red Mastermix (2X), 0.25 µM of the respective forward and reverse primer, and ddH_2O. After running a PCR program as described in **Table 2** PCR amplicons were analyzed by agarose gel electrophoresis.

4.2.1.5 Site-directed mutagenesis

Using site-directed mutagenesis (SDM) targeted mutations were introduced in plasmid DNA. First, primers containing the desired mutation were designed by the NEBase Changer online software (version 1.2.8). In the next step, these primers carrying the desired mutation were used in a PCR (**Table 3**), resulting in the amplification of the whole plasmid.

Table 3 Standard PCR reaction setup for SDM

Component	25 µl reaction	Final concentration
Q5 Hot Start High-fidelity 2X Master Mix	12.5 µl	1X
10 µM forward primer	1.25 µl	0.5 µM
10 µM reverse primer	1.25 µl	0.5 µM
Template DNA (10 ng/µl)	1 µl	10 ng

Nuclease-free water	9 µl	

PCR was carried out according to the conditions shown in **Table 4**, wherein the annealing temperature was adjusted to the nucleotide composition of the DNA primers and the extension time to the length of the amplicon.

Table 4 PCR thermocycling conditions for SDM

Step	Temperature	Time	Number of cycles
Initial denaturation	98 °C	30 s	1
Denaturation Annealing Extension	98 °C 50– 72 °C 72 °C	10 s 20 s 20 s per kb	25X
Final extension	72 °C	2 min	1
Hold	4 °C	∞	-

Following the PCR, the kinase, ligase and DpnI (KLD) treatment was carried out (**Table 5**) for ligation and template removal by using a methylation-dependent endonuclease.

Table 5 Kinase, ligase and DpnI (KLD) treatment

Component	25 µl reaction	Final concentration
PCR product	1 µl	
2X KLD reaction buffer	5 µl	1X
10X KLD enzyme mix	1 µl	1X
Nuclease-free water	3 µl	

KLD reaction mixture was incubated at room temperature for 5 min and subsequently 5 µl of the mixture was transformed in chemically competent *E. coli*.

4.2.1.6 Gibson assembly

For the generation of plasmids consisting of multiple DNA fragments Gibson assembly (Gibson et al, 2009) was performed. Cloning strategy and amplification primers were designed using the NEBuilder Assembly Tool online software (version 1.12.18). DNA insert fragments containing appropriate overlaps were amplified using standard PCR as previously described (**Table 1** and **Table 2**). The linearized vector backbone was generated by a restriction digest. All fragments were analyzed on an agarose gel and purified using the NucleoSpin Gel and PCR Clean-up kit (Macherey-Nagel) according to manufacturer's instruction. Concentrations of all DNA fragments were determined using the NanoDrop2000 spectrometer. Gibson Assembly reaction was set up as described in **Table 6** and incubated at 50 °C for 60 min. Subsequently, 5 µl of the reaction were transformed into chemically competent *E. coli*.

Table 6 Gibson assembly protocol

Component	2-3 fragment assembly	4-6 fragment assembly
Vector amount	50 ng	50 ng
Inserts amount	2-3 fold excess*	2-3 fold excess*
Total amount of fragments	0.02 – 0.5 pmol	0.2 – 1 pmol
Gibson Assembly Master Mix (2X)	10 µl	10 µl
Nuclease-free ddH_2O	10 µl – x µl	10 µl – x µl
Total volume	20 µl	20 µl

* 5 times more of insert if the size was less than 200 bps was applied.

4.2.1.7 DNA ligation

In order to construct a recombinant plasmid containing the DNA insert and the linearized vector backbone, DNA ligation was performed by the NEB T4 DNA ligase enzyme. The used molar ratios for ligation differed from 1:1 to 7:1 (insert to vector ratio). If the insert size was similar to the size of the digested vector backbone a ratio of 1:1 was chosen, whereas high molar ratios (7:1) were preferred for small DNA inserts. Ligation reactions (**Table 7**) were incubated at room temperature for 1 - 2 h or 16 °C for overnight and afterwards transformed into chemically competent *E. coli*. To determine the background due to undigested vector or vector re-circularization the digested backbone without insert was employed as ligation control.

Table 7 Standard ligation reaction

Component	20 µl reaction
T4 DNA Ligase Buffer	2 µl
Vector DNA	100 ng
Insert	1 – 7X excess
T4 DNA Ligase	2 µl
ddH_2O	up to 20 µl

4.2.1.8 Transformation of bacteria

Chemically competent *E. coli* XL1 blue or *E. coli* INV110 (*dam* and *dcm* methylation negative) were used for the transformation of plasmids into bacteria. Bacteria were thawed on ice and per transformation 50 µl of bacteria were transferred into a pre-chilled reaction tube. Subsequently ~10 ng of plasmid or 5 µl of the ligation reaction were added to the cells and mixed by flicking the reaction tube. Cells were continuously incubated on ice for 30 min followed by a heat shock at 42 °C for 30 s. Tubes were again placed on ice for 2 min followed by the addition of 250 µl SOC media to the bacteria. Tubes were placed at 37 °C for 60 min and shaken at 600 rpm. After the incubation cells were plated on agar plates with appropriate selection antibiotics and incubated overnight at 37 °C.

4.2.1.9 Plasmid isolation from E. coli (mini- and midipreps)

For small scale DNA preparation (miniprep) a single bacterial colony of transformed *E.coli* was inoculated in 5 ml of LB media containing appropriate selection antibiotics and grown over night at 37 °C under continuous shaking, whereas for high DNA amounts (midipreps) 50 ml LB medium containing selection antibiotics were inoculated. Bacteria were harvested by centrifugation (6,000 x g for 5 min at RT). Small scale DNA amounts were isolated with the NucleoSpin® Plasmid Kit (Macherey-Nagel) and large DNA amounts were purified using the QIAGEN Plasmid *Plus* Kit according to the manufacturer's protocol. Each plasmid concentration was determined using the NanoDrop2000 spectrometer. All generated expression constructs were confirmed by sequence analysis utilizing an appropriate sequencing primer by Eurofins Genomics.

4.2.1.10 Cloning procedure of expression constructs generated in this study

All plasmids generated in this dissertation were either generated by classical cloning, site-directed mutagenesis (SDM) or Gibson assembly. For simplicity the procedure for each construct containing template, insert, amplification primers and the cloning method is described in **Table 8**.

Table 8 Molecular cloning procedure of expression constructs generated in this dissertation.

generated expression construct	template / digested backbone	insert(s)	amplification primer	cloning method
BC1-TagGFP2-PEST	BC1-TagGFP	-	BC1-TagGFP2-PEST-for BC1-TagGFP2-PEST-rev	SDM
αCA-mCherry-PEST	αCA-mCherry-PEST	-	αCA-mCherry-PEST-for αCA-mCherry -PEST-rev	SDM
Ub-M-BC1-TagGFP2	pEGFP-N1 (NheI and XbaI digested)	(1) ubiquitin (2) BC1 (3) GS-linker (generated by hybridization of 4GS-linker-oligo1 4GS-linker-oligo2) (4) TagGFP2	ubiquitin-for ubiquitin-rev BC1-for BC1-rev TagGFP2-for TagGFP2-rev	Gibson assembly
Ub-D-BC1-TagGFP2	Ub-M-BC1-TagGFP2	-	NB-N-term-D-mut-for NB-N-Term-rev	SDM
Ub-E-BC1-TagGFP2	Ub-M-BC1-TagGFP2	-	NB-N-term-E-mut-for NB-N-Term-rev	SDM
Ub-F-BC1-TagGFP2	Ub-M-BC1-TagGFP2	-	NB-N-term-F-mut-for NB-N-Term-rev	SDM
Ub-G-BC1-TagGFP2	Ub-M-BC1-TagGFP2	-	NB-N-term-G-mut-for NB-N-Term-rev	SDM
Ub-A-BC1-TagGFP2	Ub-M-BC1-TagGFP2	-	NB-N-term-A-mut-for NB-N-Term-rev	SDM
Ub-C-BC1-TagGFP2	Ub-M-BC1-TagGFP2	-	NB-N-term-C-mut-for NB-N-Term-rev	SDM

Ub-L-BC1-TagGFP2	Ub-M-BC1-TagGFP2	-	NB-N-term-L-mut-for NB-N-Term-rev	SDM
Ub-N-BC1-TagGFP2	Ub-M-BC1-TagGFP2	-	NB-N-term-N-mut-for NB-N-Term-rev	SDM
Ub-H-BC1-TagGFP2	Ub-M-BC1-TagGFP2	-	NB-N-term-H-mut-for NB-N-Term-rev	SDM
Ub-I-BC1-TagGFP2	Ub-M-BC1-TagGFP2	-	NB-N-term-I-mut-for NB-N-Term-rev	SDM
Ub-K-BC1-TagGFP2	Ub-M-BC1-TagGFP2	-	NB-N-term-K-mut-for NB-N-Term-rev	SDM
Ub-T-BC1-TagGFP2	Ub-M-BC1-TagGFP2	-	NB-N-term-T-mut-for NB-N-Term-rev	SDM
Ub-W-BC1-TagGFP2	Ub-M-BC1-TagGFP2	-	NB-N-term-W-mut-for NB-N-Term-rev	SDM
Ub-V-BC1-TagGFP2	Ub-M-BC1-TagGFP2	-	NB-N-term-V-mut-for NB-N-Term-rev	SDM
Ub-Q-BC1-TagGFP2	Ub-M-BC1-TagGFP2	-	NB-N-term-Q-mut-for NB-N-Term-rev	SDM
Ub-P-BC1-TagGFP2	Ub-M-BC1-TagGFP2	-	NB-N-term-P-mut-for NB-N-Term-rev	SDM
Ub-S-BC1-TagGFP2	Ub-M-BC1-TagGFP2	-	NB-N-term-S-mut-for NB-N-Term-rev	SDM
Ub-R-BC1-TagGFP2	Ub-M-BC1-TagGFP2	-	NB-N-term-R-mut-for NB-N-Term-rev	SDM
Ub-Y-BC1-TagGFP2	Ub-M-BC1-TagGFP2	-	NB-N-term-Y-mut-for NB-N-Term-rev	SDM
UbG76V-M-BC1-	Ub-M-BC1-TagGFP2	-	BC1-for Ub-G76V-mut-rev	SDM
Ub-M-BC1-(G4S)2-TagGFP2	Ub-M-BC1-TagGFP2	(1) ubiquitin (2) BC1 (3) TagGFP2	ubiquitin-for ubiquitin-rev BC1-for BC1-2GS-rev TagGFP2-2GS-for TagGFP2-rev	Gibson assembly
Ub-M-BC1-(G4S)4-	Ub-M-BC1-TagGFP2 (NheI and XbaI digested)	(1) ubiquitin (2) BC1 (3) TagGFP2	ubiquitin-for ubiquitin-rev BC1-for BC1-4GS-rev TagGFP2-4GS-for TagGFP2-rev	Gibson assembly
Ub-M-BC1-eGFP	Ub-M-BC1-TagGFP2 (BamHI and XbaI digested)	eGFP	eGFP-for eGFP-rev	restriction enzyme cloning
Ub-F-BC1-eGFP	Ub-F-BC1-TagGFP2 (BamHI and XbaI digested)	eGFP	eGFP-for eGFP-rev	restriction enzyme cloning
Ub-A-BC1-eGFP	Ub-A-BC1-TagGFP2 (BamHI and XbaI digested)	eGFP	eGFP-for eGFP-rev	restriction enzyme cloning
Ub-R-BC1-eGFP	Ub-R-BC1-TagGFP2 (BamHI and XbaI digested)	eGFP	eGFP-for eGFP-rev	restriction enzyme cloning
Ub-S-BC1-eGFP	Ub-S-BC1-TagGFP2 (BamHI and XbaI digested)	eGFP	eGFP-for eGFP-rev	restriction enzyme cloning
Ub-M-BC1-mCherry	Ub-M-BC1-TagGFP2 (BamHI and XbaI digested)	mCherry	mCherry-for mCherry-rev	restriction enzyme cloning
Ub-F-BC1-mCherry	Ub-F-BC1-TagGFP2 (BamHI and XbaI digested)	mCherry	mCherry-for mCherry-rev	restriction enzyme cloning
Ub-A-BC1-mCherry	Ub-A-BC1-TagGFP2 (BamHI and XbaI digested)	mCherry	mCherry-for mCherry-rev	restriction enzyme cloning
Ub-R-BC1-mCherry	Ub-R-BC1-TagGFP2 (BamHI and XbaI digested)	mCherry	mCherry-for mCherry-rev	restriction enzyme cloning
Ub-S-BC1-mCherry	Ub-S-BC1-TagGFP2 (BamHI and XbaI digested)	mCherry	mCherry-for mCherry-rev	restriction enzyme cloning
Ub-M-BC1-TagRFP	Ub-M-BC1-TagGFP2 (BamHI and XbaI digested)	TagRFP	TagRFP-for TagRFP-rev	restriction enzyme cloning
Ub-F-BC1-TagRFP	Ub-F-BC1-TagGFP2 (BamHI and XbaI digested)	TagRFP	TagRFP-for TagRFP-rev	restriction enzyme cloning

Ub-A-BC1-TagRFP	Ub-A-BC1-TagGFP2 (BamHI and XbaI digested)	TagRFP	TagRFP-for TagRFP-rev	restriction enzyme cloning
Ub-R-BC1-TagRFP	Ub-R-BC1-TagGFP2 (BamHI and XbaI digested)	TagRFP	TagRFP-for TagRFP-rev	restriction enzyme cloning
Ub-S-BC1-TagRFP	Ub-S-BC1-TagGFP2 (BamHI and XbaI digested)	TagRFP	TagRFP-for TagRFP-rev	restriction enzyme cloning
Ub-M-αCA-TagGFP2	Ub-M-BC1-TagGFP2 (PstI and BspEI digested)	αCA	NB-uni-for NB-uni-rev	restriction enzyme cloning
Ub-F-αCA-TagGFP2	Ub-F-BC1-TagGFP2 (PstI and BspEI digested)	αCA	NB-uni-for NB-uni-rev	restriction enzyme cloning
Ub-A-αCA-TagGFP2	Ub-A-BC1-TagGFP2 (PstI and BspEI digested)	αCA	NB-uni-for NB-uni-rev	restriction enzyme cloning
Ub-R-αCA-TagGFP2	Ub-R-BC1-TagGFP2 (PstI and BspEI digested)	αCA	NB-uni-for NB-uni-rev	restriction enzyme cloning
Ub-S-αCA-TagGFP2	Ub-S-BC1-TagGFP2 (PstI and BspEI digested)	αCA	NB-uni-for NB-uni-rev	restriction enzyme cloning
Ub-M-VB6-TagGFP2	Ub-M-BC1-TagGFP2 (PstI and BspEI digested)	VB6	NB-uni-for NB-uni-rev	restriction enzyme cloning
Ub-F-VB6-TagGFP2	Ub-F-BC1-TagGFP2 (PstI and BspEI digested)	VB6	NB-uni-for NB-uni-rev	restriction enzyme cloning
Ub-A-VB6-TagGFP2	Ub-A-BC1-TagGFP2 (PstI and BspEI digested)	VB6	NB-uni-for NB-uni-rev	restriction enzyme cloning
Ub-R-VB6-TagGFP2	Ub-R-BC1-TagGFP2 (PstI and BspEI digested)	VB6	NB-uni-for NB-uni-rev	restriction enzyme cloning
Ub-S-VB6-TagGFP2	Ub-S-BC1-TagGFP2 (PstI and BspEI digested)	VB6	NB-uni-for NB-uni-rev	restriction enzyme cloning
mCherry-CTNNB1	pmCherry-C1 (KpnI and BamHI digested)	CTNNB1	mCherry-CTNNB1-for mCherry-CTNNB1-rev	restriction enzyme cloning
BC1-TagGFP-PEST (Master thesis Kathy-Ann Secker)	BC1-TagGFP2	-	BC1-TagGFP2-PEST-for BC1-TagGFP2-PEST-rev	SDM
αCA-mCherry-PEST (Master thesis Kathy-Ann Secker)	αCA-mCherry	-	αCA-mCherry-PEST-for αCA-mCherry-PEST-rev	SDM
EF1-α_Ub-R-BC1-eGFP	Ub-R-BC1-eGFP (AseI and NheI digested)	EF1-α promoter	EF1-α promoter (gBlock® gene fragment)	Gibson assembly
β-actinPstI_Ub-R-BC1-eGFP	Ub-R-BC1-eGFP (AseI and NheI digested)	β-actin promoter	β-actin-promoter-for β-actin-promoter-rev	restriction enzyme cloning
β-actin_Ub-R-BC1-eGFP	β-actinPstI_Ub-R-BC1-eGFP	-	β-actin-promoter-mutPstI-for β-actin-promoter-mutPstI-for	SDM
AAVS1-CB-donor plasmid - described separately in the following section	-	-	-	-

4.2.1.11 Molecular cloning of AAVS1-CB donor plasmid

For molecular cloning of the AAVS1-CB donor plasmid two gene fragments were produced by gene synthesis. At first, the synthesized plasmid AAVS1-CB-donor fragment 1 was digested using PciI and MfeI and directly ligated into pEGFP-N1 digested with the same

restriction enzymes. Secondly, the resulting plasmid was digested with MfeI and XbaI, which was then completed with AAVS1-CB-donor fragment 2 amplified with the primer set AAVS1-CB-donor-fragment-2-for and AAVS1-CB-donor-fragment-2-rev. Donor plasmid sequence was verified using the sequencing primers Seq-AAVS1-CB-donor-1 - 4. To generate an AAVS1-CB donor plasmid containing the (EF1α)-Ub-R-BC1-eGFP AseI and XbaI restriction sites were used within the donor plasmid. The BC1-NB within the plasmid was exchanged towards Actin-NB by utilizing PstI and BspEI restriction site.

4.2.1.12 Genomic DNA isolation from mammalian cells

To isolate genomic DNA from mammalian cells 3 x 10^6 cells were seeded into 100 mm cell culture dishes and were incubated for 24 h under standard conditions. Cells were washed 2 times with ice cold PBS, harvested by cell scraping and collected by centrifugation (500 x g, 5 min, 4 °C). Afterwards, genomic DNA was isolated using the QIAmp DNA Mini Kit (QIAGEN) according to the manufacturer's instructions. Concentration of genomic DNA was determined with the NanoDrop 2000 system.

4.2.1.13 RNA isolation and cDNA synthesis

Mammalian cells were seeded at a density of 2.5 x 10^5 cells per well into 6 well plates and incubated for 24 h under standard conditions. Cells were stimulated with 10 µM CHIR99021, harvested after 8 or 16 h of treatment by cell scraping and collected by centrifugation (500 x g, 5 min, 4 °C). Isolation of RNA was carried out using the NucleoSpin® RNA Kit (Macherey-Nagel) as described by the manufacturer. RNA concentration was determined with the NanoDrop2000 spectrometer. For synthesis of complementary DNA (cDNA) based on mRNA templates NEB First Strand cDNA Synthesis Kit was used. First, denaturation of template mRNA was performed by a 5 min incubation of the mRNA-primer mix at 65 °C (**Table 9**).

Table 9 Initial mRNA denaturation reaction

Component	Volume
mRNA	1 µg
Random Primer mix (60 µM)	1 µl
10 mM dNTPs	1 µl
Nuclease-free H_2O	up to 10 µl

After denaturation, the samples were put immediately on ice and the following components listed in **Table 10** were added:

Table 10 Standard cDNA synthesis reaction

Component	Volume
10x M-MuLV buffer	2 µl
M-MuLV Reverse Transcriptease (200 U/µl)	1 µl
RNase Inhibitor (40 U/µl)	0.2 µl
Nuclease-free H_2O	6.8 µl

cDNA synthesis reaction was incubated at 25 °C for 5 min followed by an incubation for 1 h at 42 °C. Subsequently enzymes were inactivated at 65 °C for 20 min. The cDNA products were stored at -20 °C prior use in qRT-PCR.

4.2.1.14 Quantitative real-time PCR (qRT-PCR)

Analysis of gene expression was achieved by qRT-PCR of specific target genes from mammalian cells. For this purpose, IDT PrimeTime® qPCR Probe Assays consisting of a specific primer pair and a 5' nuclease probe were selected. qRT-PCR was performed in 96-well format and a total volume of 25 µl (**Table 11**).

Table 11 qRT-PCR reaction mixture.

Component	Volume per 20 µl reaction
PrimeTime® Gene Expression Master Mix (2X)	10 µl
PrimeTime® qPCR Assay (20X)	1 µl
cDNA template	2 µl
Nuclease-free H_2O	7 µl

Preparation of qRT-PCR reaction mixture was carried out on ice, avoiding strong light exposure. PCR reaction (**Table 12**) and subsequent data analysis were both performed using the ThermoFisher StepOnePlus™ Real-Time PCR System. Quantification was carried out using the ΔΔCt method, using Ct-values obtained with GAPDH-specific primer as reference (ΔCt). Next, these values were normalized to the values obtained from non-treated control cells, leading to the illustration of a fold change in mRNA expression between non-treated and treated cells.

Table 12 qRT-PCR cycling protocol

Step	Temperature	Time	Number of cycles
Polymerase activation	95 °C	3 min	1
Denaturation Annealing/Extension	95 °C 60 °C	15 s 1 min	40x

4.2.2 Biochemical methods

4.2.2.1 Mammalian cell lysis

Depending on the aim of the experiment 7.5 x 10^5 – 3 x 10^6 cells were seeded in 100 mm cell culture dishes (Corning) and grown for 24 h under standard conditions. Hereafter, cells

were either treated with compounds or subjected to plasmid DNA transfection. Subsequently, cells were washed and harvested in PBS, snap-frozen in liquid nitrogen and stored at -20 °C. Cell pellets were homogenized in 100 µl NP40 lysis buffer by repeated pipetting and / or vortexing for 30 - 60 min on ice. Lysates were clarified by centrifugation for 15 min at 18,000 x g and 4 °C. Protein concentrations of the soluble supernatants were determined by Bradford Protein Assay (Biorad) and accordingly adjusted to equal concentrations.

4.2.2.2 SDS-PAGE and western blot

For size dependent separation of proteins denaturing polyacrylamide gel electrophoresis was performed using the BIO-RAD Mini-PROTEAN® Tetra Cell System (**Table 13** and **Table 14**). Protein samples were boiled in 2X reducing SDS sample buffer for 10 min at 95 °C. Denatured samples were loaded onto the acrylamide gel and separated at 120 – 200 V in SDS-PAGE running buffer. As standard PageRuler Plus prestained protein ladder was used.

Table 13 Resolving gel preparation

Component	Final concentration
Acrylamide	8-15 % (v/v)
Tris/HCl pH 8.8	375 mM
SDS	0.1 % (w/v)
APS	0.05 % (w/v)
TEMED	0.1 % (v/v)

Table 14 Stacking gel preparation

Component	Final concentration
Acrylamide	5 % (v/v)
Tris/HCl pH 6.8	60 mM
SDS	0.1 % (w/v)
APS	0.05 % (w/v)
TEMED	0.1 % (v/v)

By semi-dry western blotting (BIO-RAD Trans-Blot Semi-Dry Transfer Cell or BIO-RAD Trans-Blot Turbo Transfer System) the separated proteins were transferred from SDS-gel onto a nitrocellulose membrane (GE Healthcare). Protein transfer was carried out at 2.5 mA per cm^2 for 30 min – 2 h using Towbin blotting buffer. Membranes were incubated for 5 min with Ponceaus S solution to reversibly stain proteins immobilized on the membrane. Specific proteins were detected by incubation of the membranes with primary antibodies diluted in M-TBST over night at 4 °C. On the next day membranes were washed trice with TBST for 10 min followed by an incubation with fluorescently labeled species-specific secondary antibody diluted in M-TBST for 2 h at room temperature. Membranes were washed three times with TBST for 10 min and were allowed to dry at room temperature. Subsequently,

fluorescent signals were detected using a Typhoon-Trio laser scanning system (GE Healthcare) and analyzed with the GE Healthcare ImageQuantTL software (version 8.1).

4.2.2.3 Intracellular immunoprecipitation

Intracellular immunoprecipitation (IC-IP) of the CBs was performed using either transiently or stable CB expressing cells. For transient CB expression 3 x 10^6 HEK293T cells were transfected with equal amounts of expression vectors encoding for the respective CB constructs. Transfection efficiency was controlled by fluorescence microscopy and the cells were harvested and lysed 24 h after transfection as described (chapter 4.2.2.1). For IC-IP from stable cell lines 3 x 10^6 stable CB expressing cell lines were seeded onto 100 mm cell culture dishes and harvested after 48 h. Subsequently, GFP-CA, BC1-CB variants or eGFP were precipitated using the GFP-Trap (ChromoTek) according to the manufacturer's protocol. Input and bound fractions were subjected to SDS-PAGE followed by western blot analysis using appropriate antibodies.

4.2.3 Cell culture methods

4.2.3.1 Culturing of mammalian cell lines

All cell lines used in this study were grown according to standard procedures (**Table 15**). Cells were passaged using 0.05 % trypsin-EDTA (ThermoFisher Scientific) and incubated at 37 °C in a humidified chamber with a 5 % CO_2 atmosphere. All cell lines were tested negative for mycoplasma using the PCR mycoplasma kit Venor GeM Classic (Minerva Biolabs) and the Taq DNA polymerase (Minerva Biolabs). Since this study does not include cell line-specific analysis, all cell lines were used without additional authentication.

Table 15 Medium composition for growing mammalian cell lines

Cell line	Cell culture media	Supplements
HeLa Kyoto	DMEM, high glucose, pyruvate, GlutaMAX	10 % FCS 1 % Pen/Strep
HEK293T	DMEM, high glucose, pyruvate, GlutaMAX	10 % FCS 1 % Pen/Strep
U2OS	DMEM, high glucose, pyruvate, GlutaMAX	10 % FCS 1 % Pen/Strep
A549	DMEM/F-12, high glucose, pyruvate	10 % FCS 1 % Pen/Strep 1 % L-Glutamine
DLD-1	RPMI 1640	10 % FCS 1 % Pen/Strep
HCT116	DMEM, high glucose, pyruvate, GlutaMAX	10 % FCS 1 % Pen/Strep
HeLa_BC1_TagGFP2	DMEM, high glucose, pyruvate, GlutaMAX	10 % FCS 1 % Pen/Strep 3 µg/ml Blasticidine
A549_VB6-eGFP	DMEM/F-12, high glucose, pyruvate	10 % FCS 1 % Pen/Strep 1 % L-Glutamine

		80 µg/ml Hygromycin
A549_VB6-TagRFP	DMEM/F-12, high glucose, pyruvate	10 % FCS 1 % Pen/Strep 1 % L-Glutamine 1 µg/ml Puromycin
HeLa_CCC-TagRFP	DMEM, high glucose, pyruvate, GlutaMAX	10 % FCS 1 % Pen/Strep 0.5 mg/ml G418
HeLa_αCA-mCherry	DMEM, high glucose, pyruvate, GlutaMAX	10 % FCS 1 % Pen/Strep 0.5 mg/ml G418
HeLa_Ub-R-BC1-eGFP	DMEM, high glucose, pyruvate, GlutaMAX	10 % FCS 1 % Pen/Strep 0.5 mg/ml G418
U2OS_Ub-R-BC1-eGFP	DMEM, high glucose, pyruvate, GlutaMAX	10 % FCS 1 % Pen/Strep 0.5 mg/ml G418
HeLa_ACT-TagGFP2	DMEM, high glucose, pyruvate, GlutaMAX	10 % FCS 1 % Pen/Strep 3 µg/ml Blasticidine
HeLa_AAVS1_ Ub-R-ACT-eGFP	DMEM, high glucose, pyruvate, GlutaMAX	10 % FCS 1 % Pen/Strep
DLD-1_BC1-TagGFP2	DMEM, high glucose, pyruvate, GlutaMAX	10 % FCS 1 % Pen/Strep
DLD-1_AAVS1_ Ub-R-BC1-eGFP	DMEM, high glucose, pyruvate, GlutaMAX	10 % FCS 1 % Pen/Strep
HCT116_AAVS1_ Ub-R-BC1-eGFP	DMEM, high glucose, pyruvate, GlutaMAX	10 % FCS 1 % Pen/Strep

4.2.3.2 Cell seeding and treatment

For cell seeding all adherent cell lines were detached using 0.05 % trypsin-EDTA and cell number was determined by using the CASY Cell Counter system or the Neubauer chamber. For microscopical analyses 1,500 – 10,000 cells were seeded per well into µClear 96-well plates and were allowed to grow for 24 to 72 h under standard conditions. For time-lapse imaging cell culture media was replaced by Evrogen Antibleaching DMEM-gfp medium containing 2 µg/ml Hoechst33258 about 3 h before starting the time-lapse experiment. For biochemical analyses and isolation of genomic DNA 7.5 x 10^5 – 3 x 10^6 cells were seeded into 100 mm cell culture dishes and subjected to transient transfection and/or compound treatment. For RNA isolation 2.5 x 10^5 cells were seeded in 6 well plates and treated 24 h after seeding until the indicated time points.

4.2.3.3 Transfection

Plasmid DNA was transfected using the following transfection reagents: Lipofectamine 2000 (ThermoFisher Scientific) for U2OS cells, Lipofectamine LTX (ThermoFisher Scientific) for A549 cells, polyethylenimine (PEI, Sigma) for HeLa Kyoto and HEK293T cells and Mirus TransIT-X2 for HCT116 and DLD-1. Prior to transfection, cells were allowed to grow to ~70 % confluency. To generate DNA/PEI complexes for transfection in a 96-well plate format 100 - 200 ng DNA were mixed with 0.5 µg PEI in 20 µl serum-free

medium. Transfection mixture was incubated for 15 min at room temperature and subsequently was added to the adherent cells. Transfections using Lipofectamine 2000, Lipofectamine LTX or Mirus TransIT-X2 were carried out according to the manufacturer's protocol. RNA interference-mediated knockdown of PCNA and vimentin was accomplished using Lipofectamine RNAiMax (ThermoFisher Scientific) for all cell lines according to manufacturer's instructions. Analysis of a siRNA-mediated knockdown was performed 72 h post transfection via immunofluorescence staining.

4.2.3.4 Generation of stable cell lines via plasmid transfection and selection

Stable cell lines HeLa_Ub-R-BC1-eGFP and U2OS_Ub-R-BC1-eGFP were generated by plasmid transfection of the indicated chromobody construct using Lipofectamine 2000 (ThermoFisher Scientific) according to the manufacturer's protocol. 24 h post transfection cells were subjected to a three-week selection period using 0.5 mg/ml G418 (Roth) followed by single cell separation. Single clones were analyzed regarding Ub-R-BC1-eGFP expression and response to CTNNB1 elevating compounds.

4.2.3.5 Stable CB integration into AAVS1 locus using CRISPR/Cas9 technology

For site-directed integration of the CBs into the AAVS1 locus of host cell lines (DLD-1, HCT116 and HeLa), cells were co-transfected with equal amounts of plasmids coding for Cas9-AAVS1-gRNA (kindly provided by (Oceguera-Yanez et al, 2016)) and the AAVS1-CB-donor plasmid using standard transfection method for the respective cell lines (chapter 4.2.3.3). 24 h post transfection cells were subjected to a 48 h long selection using 0.6 µg/ml puromycin dihydrochloride (Sigma Aldrich). 48 h post transfection non-treated control cells were completely killed by the antibiotic. Puromycin-resistant cells were allowed to grow for one week before single cell clones were isolated and analyzed regarding the CB expression level. To verify site-directed integration of the CB-donor plasmid at the AAVS1-locus, genotyping was performed using a primer set (genPCR-AAVS1-int-for and genPCR-AAVS1-int-rev), which bind in the genomic part of AAVS1 and the transgene, resulting in an amplicon of ~1,400 bps.

4.2.3.6 Immunocytochemistry and fluorescence microscopy

Parental and stable CB expressing cells were seeded at 2,000 – 5,000 cells per well in µClear 96-well plates (Greiner) and grown for 24 - 48 h. For fixation, cells were washed twice with PBS and fixed with 4 % formaldehyde (v/v, PFA, Applichem) in PBS. Subsequently, cells were blocked and permeabilized using 5 % bovine serum albumin (w/v, BSA) and 0.3 % Triton X-100 (v/v) in PBS. Primary and fluorochrome-conjugated secondary antibodies were diluted in 1 % BSA and 0.3 % Triton X-100 in PBS and antibody staining was carried out according to standard procedures. Fluorescence images were acquired using MetaXpress Micro XL system (Molecular Devices) and 20X or 40X magnification.

4.2.3.7 Time-lapse imaging

For time-lapse imaging cells were seeded at a concentration of 1,500 – 5,000 cells cells per well in µClear 96-well plates (Greiner) and were allowed to adhere for 24 h to 48 h. Cells were either directly seeded into Evrogen antibleaching live cell visualization medium or media was exchanged ~4 h before starting the experiment in order to allow cells to equilibrate and adapt to imaging medium. Nuclei were stained with 2 µg/ml Hoechst33258. Depending on the aim of the experiment, cells were treated with the indicated compounds and directly subjected to time-lapse microscopy. Live-cell imaging was performed using the MetaXpress Micro XL system (Molecular Devices) and 20 X magnification at 37 °C in a humidified atmosphere containing 5 % CO_2. Fluorescence images were acquired for up to 48 h, in which the time interval of image acquisition was depending on the experimental setup.

4.2.3.8 Automated image segmentation and analysis

Fluorescence images acquired with the ImageXpress Micro XL system were analyzed by the MetaXpress software (64 bit, 5.1.0.41, Molecular Devices). To allow automated nuclei segmentation, nuclei of live cells were stained with 2 µg/ml Hoechst33258 and nuclei of fixed cells were stained with DAPI.

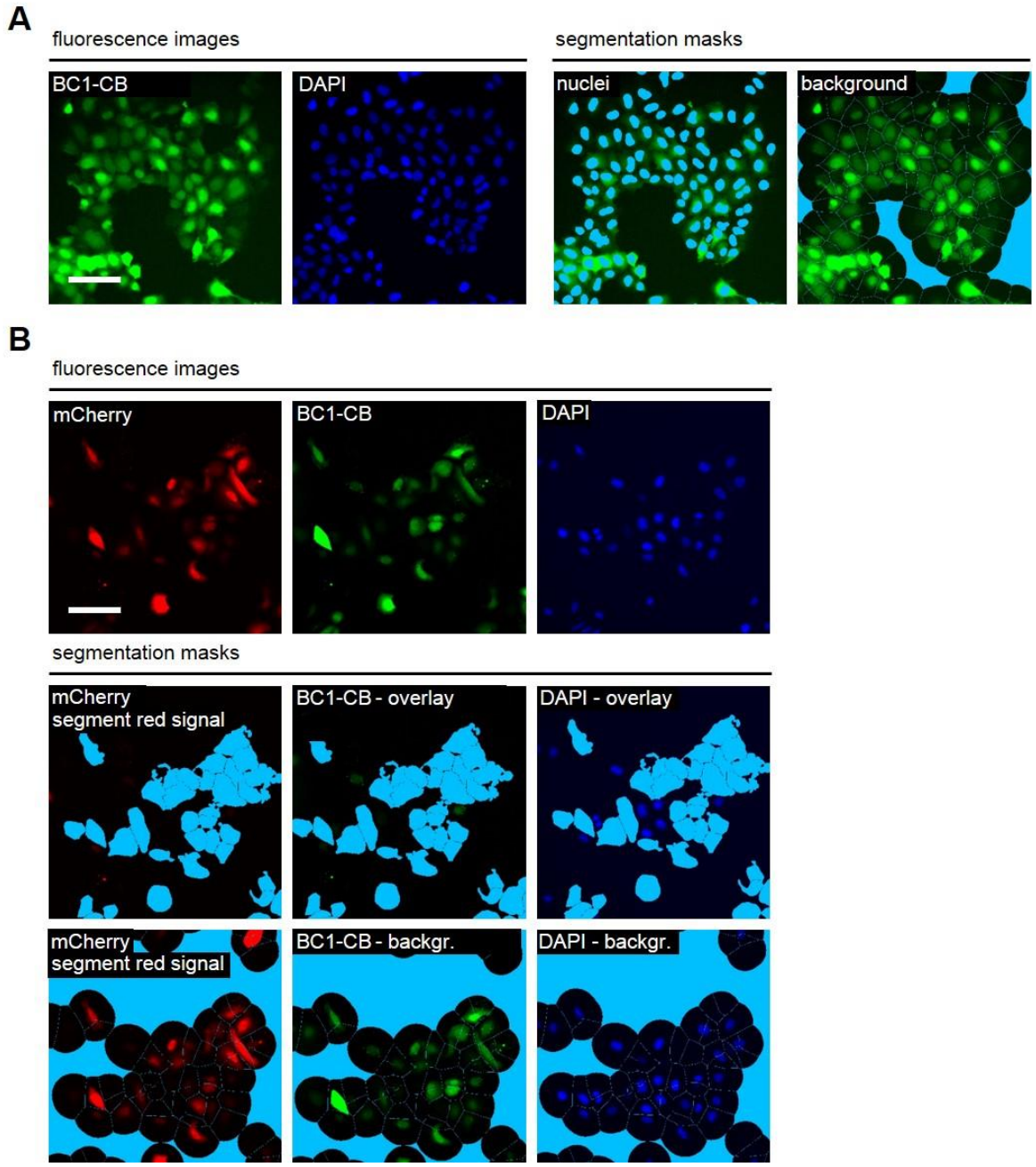

Figure 5 Schematic overview of automated analysis of fluorescence images.
*(**A**) Fluorescence images of HeLa_BC1-CB cells showing CB-signal (green, left image) and nuclei stained with DAPI (blue, right image), scale bar: 100 µm. On the right side segmentation masks (light blue) to determine average fluorescence intensity within the nuclei and the background are shown. (**B**) Representative image segmentation of transiently transfected cells. The first row displays HeLa cells co-transfected with mCherry (red) and the BC1-CB (green), nuclei of fixed cells were stained with DAPI (blue) (Hoechst was used for live-cell imaging only), scale bar: 100 µm. The second row shows utilization of the mCherry signal to generate a segmentation mask (light blue) within the fluorescence intensity of the co-transfected CB was measured. The determination of the background signal (light blue) was performed as showed in the third row.*

To determine the average fluorescence intensity within the nuclei region an algorithm determining the intensity above the local background for the DAPI channel was applied. The settings to identify the regions of interest (ROI) were: (i) an approximate minimum width of 10 µm, (ii) an approximate maximum width of 30 µm and (iii) a minimum intensity of

120 (AU) above the local background. From these identified ROIs a segmentation mask was generated and an overlay with the fluorescence image was generated to determine the average fluorescence intensity of CBs and/or immunofluorescence within the nuclei (**Figure 5A**). This algorithm was applied to images generated from stably CB-expressing cells and immunofluorescence stainings. For the determination of background fluorescence the signal of identified nuclei was enlarged to a size of 80 pixels and applied as a negative marker and the background signal was determined in the remaining region.

For the segmentation of transiently transfected cells, this algorithm could not be applied because it has to be considered, that a transfection efficiency is usually at around 30-70 % (depending on transfected plasmids and used cell line). Therefore it was essential to exclude the impact of non-transfected cells in the quantification and another segmentation strategy had to be applied. To segment the whole cell (nuclear and cytosolic compartment) the signal of the ectopic expressed antigen or its respective control (mCherry signal in **Figure 5B**) was utilized for the generation of the segmentation mask. The settings to identify the mCherry signal were: (i) an approximate minimum width of 13 µm, (ii) an approximate maximum width of 35 µm and (iii) a minimum intensity of 200 above the local background. Next, the same algorithm as explained above was used to ensure that only cells containing an intact nucleus were segmented. The generated segmentation mask was the applied to the fluorescence image in order to determine the fluorescence intensity within the whole cell. Background segmentation was performed with the same algorithm as described above.

For both segmentation strategies either the fluorescence intensity per cell (population-wide analysis) or the average fluorescence intensity for each image was subjected to automated image analysis, followed by subtraction of the background intensity. From the different images per condition, the average fluorescence intensity and standard deviation were calculated and for statistical analysis student’s t-test was used. In favor of a more comprehensible data presentation, the calculated fluorescence intensities were normalized to the respective control.

5 RESULTS

5.1 Quantitative image analysis of antigen-mediated stabilization of a CTNNB1- specific CB (BC1-CB)

As previously shown in Traenkle et al., CHIR-treatment of HeLa_BC1-CB cells not only led to an increase of endogenous CTNNB1 protein level but further this increase was accompanied by rising levels of the BC1-CB, which was demonstrated by fluorescence time-lapse imaging (**Figure 4**) and western blot analysis (Traenkle et al, 2015).

To verify these observations using an image-based readout, HeLa_BC1-CB (hereafter referred to as HeLa_BC1-TagGFP2) cells were treated with CHIR for 20 h and the levels of endogenous CTNNB1 and BC1-TagGFP2 were analyzed *in situ* by immunofluorescence staining using a CTNNB1-specific antibody and simultaneous detection of BC1-TagGFP2 fluorescence. The immunostaining revealed that CHIR treatment led to a strong increase in CTNNB1 protein amount in HeLa_BC1-TagGFP2 and parental HeLa cells. Detection of BC1-TagGFP2 fluorescence showed a corresponding increase in CB fluorescence (**Figure 6A**).

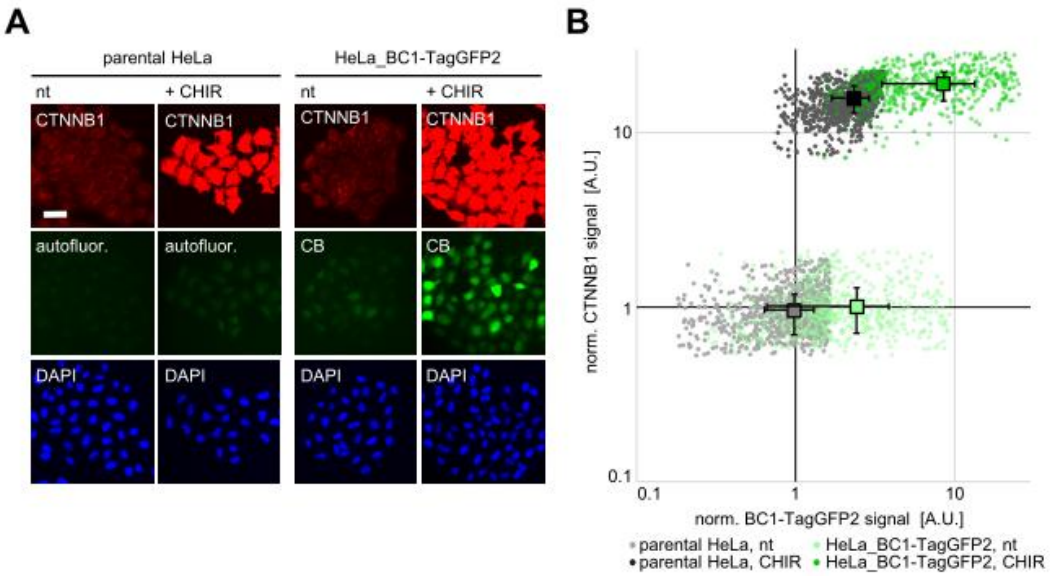

Figure 6 CTNNB1-mediated stabilization of the BC1-CB in HeLa_BC1-TagGFP2 cells.
*(**A**) Representative fluorescence images of parental HeLa cells and HeLa_BC1-TagGFP2 cells, which were either treated with 10 µM CHIR99021 for 20 h or left non-treated (nt). Cells were fixed and endogenous CTNNB1 was detected by antibody staining while the CB signal was directly detected via the TagGFP2 fluorescence. Nuclei were stained with DAPI, scale bar: 50 µm. (**B**) Population-wide comparison of CTNNB1 immunofluorescence staining and BC1-TagGFP2 signal intensity of HeLa_BC1-TagGFP2 cells and parental HeLa cells. CTNNB1 staining and CB signal were determined for each cell and fluorescence intensities of CHIR treatment were normalized to the non-treated control. Shown are the fluorescence values within the 5th*

to 95th percentile of analyzed cells. Number of cells within this interval were: HeLa_BC1-TagGFP2 - nt: n=591; +CHIR: n=504; parental HeLa - nt: n= 889; +CHIR: n=1077. Squares illustrate mean fluorescence intensity of the analyzed population. Error bars: standard deviation (S.D.).

To allow for a representative quantification of the fluorescence signals an automated image segmentation algorithm was established, wherein a population-wide quantitative analysis comprising hundreds of cells was performed (algorithm described in detail in section 4.2.3.8). By applying this algorithm, fluorescence signals derived from CTNNB1 antibody staining and BC1-TagGFP2 were determined for individual cells (**Figure 6B**). The quantification of the CTNNB1 signal in non-treated and CHIR-treated cells confirmed a strong increase of signal intensities in parental HeLa and HeLa_BC1-TagGFP2 cells, illustrated by a shift in the direction of the y-axis of the population-wide analysis. As the CHIR-induced increase of CTNNB1 in parental HeLa and HeLa_BC1-TagGFP2 cells was similar, this result suggests that the presence of the CB did not affect the endogenous level of CTNNB1. Notably, this analysis reveals an increase in BC1-TagGFP2 fluorescence in HeLa_BC1-TagGFP2 cells upon CHIR treatment as it was previously observed by quantitative western blot analysis (Traenkle et al, 2015).

In favor of a more comprehensible data representation, the entirety of individual cell fluorescence is depicted as a population-wide mean fluorescence. Applying this analysis, CHIR-treated HeLa_BC1-TagGFP2 cells displayed a 19-fold increase in CTNNB1 accompanied by a 4.6-fold increase in CB fluorescence (**Figure 7A, B**).

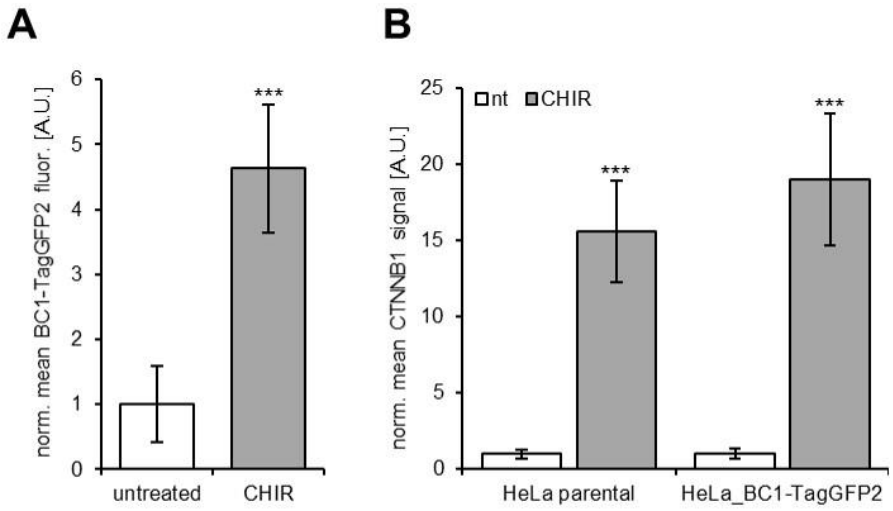

Figure 7 Population-wide mean fluorescence of the BC1-CB and CTNNB1 in HeLa_BC1-TagGFP2 cells. *(**A**) Bar chart of mean CB fluorescence of HeLa_BC1-TagGFP2 cells analyzed in Figure 6B, error bars: S.D. (**B**) Bar chart of mean CTNNB1 antibody staining of non-treated and CHIR-treated parental HeLa and HeLa_BC1-TagGFP2 cells from Figure 6B. Error bars: S.D., for statistical analysis student's t-test was performed, *** p < 0.001.*

To confirm antigen binding of the CB within HeLa_BC1-TagGFP2 cells, intracellular immunoprecipitation (IC-IP) was performed in non-treated and CHIR-treated cells. Western blot analysis after IC-IP proved an efficient binding of CTNNB1 by BC1-TagGFP2 (**Figure 8**).

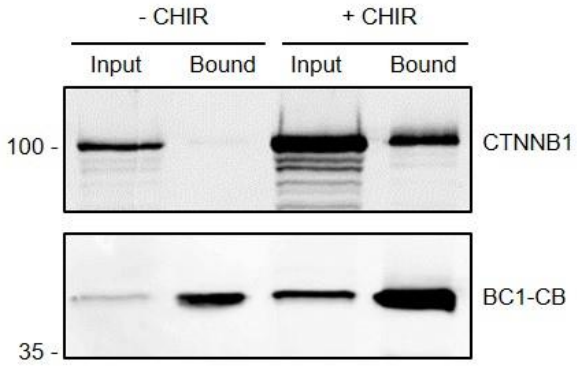

Figure 8 Endogenous CTNNB1 is precipitated by the BC1-CB in HeLa_BC1-TagGFP2 cells.
HeLa_BC1-TagGFP2 cells were either left non-treated or were treated with 10 µM CHIR for 20 h. Cells were lysed using NP40 lysis buffer and precipitation of the CBs from the soluble protein fractions was performed with the GFP-Trap. 1 % of input and 20 % of the bound fraction were subjected to SDS-PAGE followed by western blot analysis using CTNNB1- or GFP-specific antibodies.

Next, it was analyzed whether the BC1-CB can also be stabilized by ectopically expressed CTNNB1. By Traenkle et al. it was demonstrated that treatment with CHIR did not alter the CB transcription level in HeLa_BC1-TagGFP2 cells. Here, it was additionally tested whether a compound-independent approach to elevate the amount of CTNNB1 can induce an increase in CB signal according to AMCBS. For this purpose, parental HeLa cells were co-transfected with plasmids coding for BC1-TagGFP2 and mCherry-CTNNB1 or mCherry as control (**Figure 9A**). After transient transfection the expression levels of CB and antigen differed among individual cells, but on average a stabilization of the BC1-CB was observable. In mCherry-CTNNB1 expressing cells BC1-TagGFP2 fluorescence was increased 1.7-fold compared to CB fluorescence of mCherry-transfected cells (**Figure 9B**).

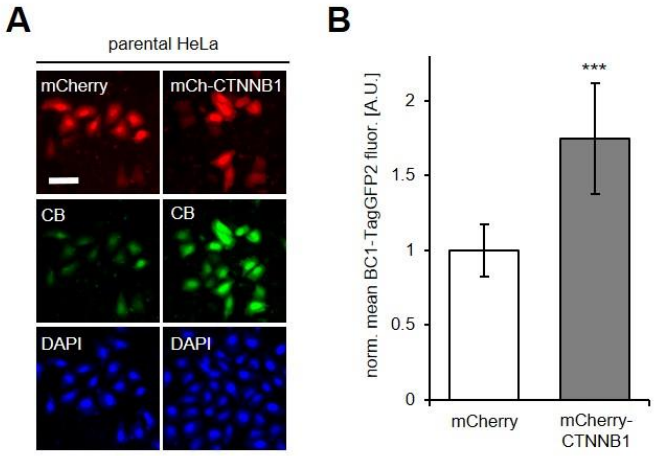

Figure 9 CTNNB1-mediated BC1-CB stabilization in transiently transfected HeLa cells.
*Parental HeLa cells were transiently co-transfected with plasmids coding for the BC1-TagGFP2 in combination with either mCherry or mCherry-CTNNB1. 24 h after transfection cells were PFA-fixed and nuclei were stained with DAPI. (**A**) Representative fluorescence images of parental HeLa cells transiently expressing BC1-TagGFP2 and mCherry or mCherry-CTNNB1, scale bar: 50 µM. (**B**) Bar chart of mean CB fluorescence intensity detected in mCherry- or mCherry-CTNNB1 expressing cells. CB fluorescence intensity was normalized to CB signal intensity detected in mCherry transfected cells. Mean fluorescence was calculated from three different samples (n=3), comprising >200 cells. Error bars: S.D., for statistical analysis student's t-test was performed, *** $p < 0.001$.*

The results of this section clearly support the idea of a CTNNB1-mediated stabilization of the BC1-CB as previously stated (Traenkle et al, 2015). Notably, increasing CB levels were detected upon CHIR treatment in stable HeLa_BC1-TagGFP2 as well as in parental HeLa cells after ectopic expression of the BC1-CB and CTNNB1.

5.2 Observation of antigen-mediated stabilization of chromobodies targeting further antigens

After demonstrating an antigen-mediated CB stabilization for the BC1-CB, the next question was whether this phenomenon is also evident for other CB-antigen combinations. For this purpose, a set of three previously described CBs was analyzed: (i) an HIV p24 capsid protein (CA)-specific CB (αCA-mCherry (Helma et al, 2012)), (ii) a proliferating cell nuclear antigen (PCNA)-specific CB (CCC-TagRFP (Schorpp et al, 2016)) and (iii) vimentin (VIM)-specific CBs (VB6-eGFP and VB6-TagRFP (Maier et al, 2015)). **Figure 10** shows a multiple sequence alignment of the binding moieties of these three CBs and the BC1-CB.

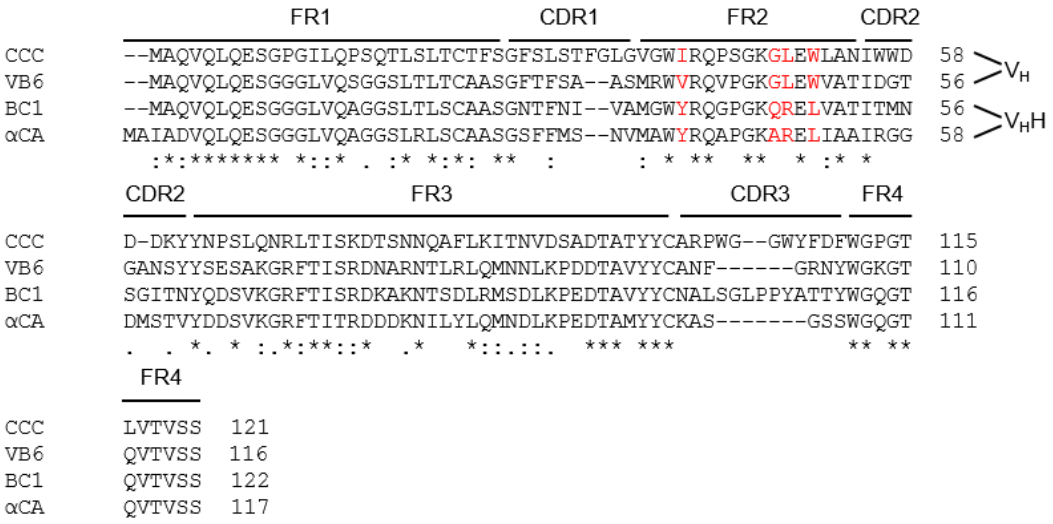

Figure 10 Multiple sequence alignment of BC1-, CCC-, VB6- and αCA-CB binding moiety.
Multiple sequence alignment was performed with Clustal Omega (version 1.2.4) provided by EMBL-EBI, (Goujon et al, 2010; Sievers et al, 2011). Framework regions (FR1-4) and complementary determining regions (CDR1-3) are indicated by headers. Hallmarks to distinguish between V_H and V_HH are highlighted in red.

This sequence analysis for the four binding moieties of the compared CBs illustrates a substantial sequence homology within the framework regions (~70 %, determined by multiple sequence alignment of the framework regions using GeneBee). Further, amino acid sequence of FR2 reveals that BC1 and αCA carry more hydrophilic amino acids (Gln/Ala, Arg) as compared to CCC and VB6, which instead comprise hydrophobic amino acids in this region (Ile/Val, Leu, Tyr). Previous studies have shown that this substitution towards hydrophilic amino acids in FR2 is typically for V_HH fragments, whereas the presence of hydrophobic amino acids is characteristic for V_H domains (Muyldermans, 2001; Li et al, 2016). These specific substitutions (Val37Phe/Tyr, Gly44Glu/Gln, Leu45Arg, Trp47Gly/Leu) are referred to as hallmarks to distinguish V_HH from V_H (Vu et al, 1997). A detailed description of these characteristics can be found in section 3.4.3.1.

Taken together, three more CBs were analyzed, carrying binding moieties derived from V_HH (αCA) as well as V_H (CCC and VB6), regarding a possible CB-stabilization mediated by the corresponding antigens.

5.2.1 HIV-capsid protein (CA)-specific CB (αCA-mCherry)

The first chromobody, which was tested regarding the AMCBS phenomenon was the HIV p24 capsid protein (CA)-specific chromobody αCA-mCherry (Helma et al, 2012). To address this question, a previously established stable CB expressing cell line HeLa_αCA-mCherry was used (Helma et al, 2012). All experiments described in this chapter were

performed and analyzed independently by the former Master student Kathy-Ann Secker (Secker, 2016).

At first, it was analyzed whether the stably expressed αCA-mCherry CB binds to the cognate antigen GFP-CA within the stable HeLa_αCA-mCherry cell line. Thus, HeLa_αCA-mCherry cells were transfected with the corresponding antigen GFP-CA or GFP as control followed by intracellular co-immunoprecipitation using the GFP-Trap. Western blot analysis revealed co-precipitation of αCA-mCherry, thereby demonstrating binding of the CB to its antigen in living cells (**Figure 11A**). Next, it was tested whether AMCBS is observable for this antigen-CB combination by fluorescence microscopy. HeLa_αCA-mCherry were transfected with either GFP-CA or GFP and fluorescence images were acquired (**Figure 11B**). The images illustrate that cells expressing GFP-CA displayed an increased αCA-mCherry signal compared to non-transfected cells (indicated by white arrows) and no difference in CB fluorescence was detected for GFP expressing cells. Moreover, in the absence of GFP-CA the CB was homogenously distributed between cytoplasm and nucleus, whereas in presence of the antigen the CB strongly co-localized with its target within the cytoplasm. Using software-assisted image segmentation, αCA-mCherry fluorescence was quantified in nuclear, cytoplasmic or whole-cell area of GFP- or GFP-CA expressing cells resulting in a 2.5-, 6.0-, or 4.3-fold increase, respectively (**Figure 11C**).

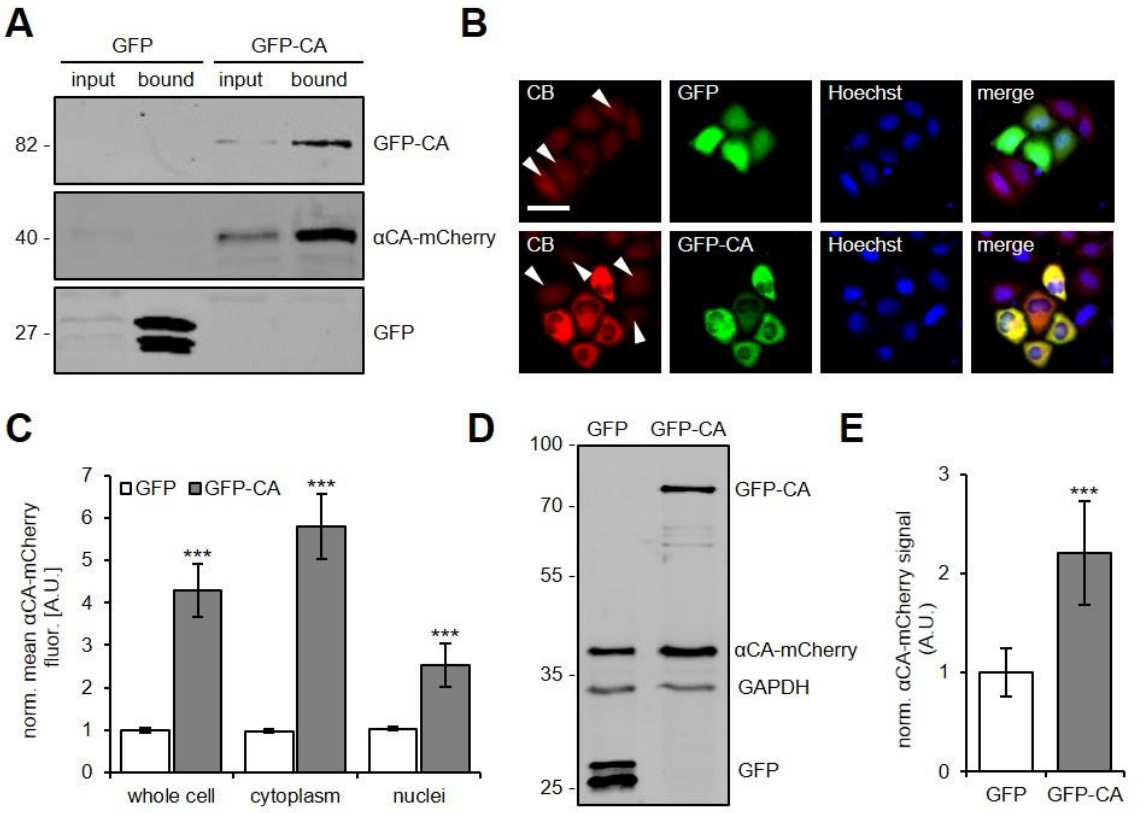

Figure 11 Antigen-mediated stabilization of an HIV CA-specific CB in stable HeLa-αCA-mCherry cells. *(Secker, 2016), (**A-E**) For the analysis of antigen-mediated CB stabilization of the αCA-CB stably expressing HeLa_αCA-mCherry cells were used. Cells were transiently transfected with the corresponding antigen GFP-gag-pol (GFP-CA) or GFP as control and analyzed 24 h post transfection. (**A**) αCA-mCherry binds its antigen within living cells. Transfected HeLa_αCA-mCherry cells were lysed using a 0.5 % NP-40 lysis buffer, followed by an intracellular immunoprecipitation of GFP and GFP-CA from the soluble lysate proportion using the GFP-Trap. 0.5 % of input and 20 % of the bound fraction were subjected to SDS-PAGE followed by western blot analysis. (**B**) Representative fluorescence images of living HeLa_αCA-mCherry cells transfected with GFP-CA or GFP as control. Non-transfected cells are indicated with white arrows. Nuclei were stained with Hoechst33258, scale bar: 50 µM. (**C**) Optical quantification of αCA-mCherry signal intensity in HeLa_αCA-mCherry cells after ectopic antigen expression. Mean αCA-mCherry fluorescence was detected in the cytoplasm, the nuclei and in the whole cellular area of GFP- or GFP-CA-expressing cells. Mean fluorescence was calculated from three samples (n=3; >200 cells). (**D**) Biochemical analysis of the HeLa_αCA-mCherry transfected with GFP or GFP-CA. Cells were lysed using 0.5 % NP40 lysis buffer and equal protein amounts of the soluble fraction were subjected to SDS-PAGE followed by western blot analysis. (**E**) Densiometric analysis of αCA-mCherry level in presence and absence of the corresponding antigen GFP-CA. Signal intensities were quantified from three biological replicates (N=3). (**C** and **E**) Error bars: S.D.; for statistical analysis student's t-test was performed.*

Finally, quantitative western blot analysis was performed to test if the antigen-mediated stabilization of αCA-mCherry can also be observed using a biochemical approach (**Figure 11D** and **E**). Post transfection of HeLa_αCA-mCherry with plasmids coding for GFP-CA or GFP, cells were lysed and equal amounts of soluble protein lysates were subjected to SDS-PAGE followed by western blot analysis. Compared to GFP-transfected cells an increase in αCA-mCherry band intensity could be observed and densiometric analysis of three biological replicates revealed a 2.2-fold enrichment of the CB in presence of the antigen.

Considering a transfection efficiency of ~50 % this biochemical result is comparable to the values determined by fluorescence microscopy.

5.2.2 Proliferating Cell Nuclear Antigen binding cell-cycle-CB (CCC-TagRFP)

The next CB analyzed within the context of AMCBS was CCC-TagRFP (Panza et al, 2015) recognizing endogenous PCNA, a key factor in DNA replication and cell cycle regulation (reviewed in (Strzalka & Ziemienowicz, 2011)). To test whether the fluorescence intensities of the CB also respond to antigen depletion, endogenous PCNA level were downregulated using small interfering RNAs (siRNAs) in HeLa cells stably expressing CCC-TagRFP (HeLa_CCC-TagRFP). 72 h post transfection of siRNAs targeting either PCNA or with non-targeting control siRNAs fluorescence images were acquired followed by quantification of CB signal intensity within the nuclear region (**Figure 12A, B**). Compared to control siRNAs, knockdown of PCNA led to a ~70 % reduction in CCC-TagRFP fluorescence, which was evident for all three PCNA targeting siRNAs. In addition, the results obtained from microscopic analysis were confirmed using a biochemical assay approach. Western blot analysis of HeLa_CCC-TagRFP 72 h after siRNA transfection illustrates that PCNA protein levels were efficiently downregulated by the respective siRNAs. Accordingly, immunoblot analysis revealed a strong reduction of CCC-TagRFP protein level (**Figure 12C**).

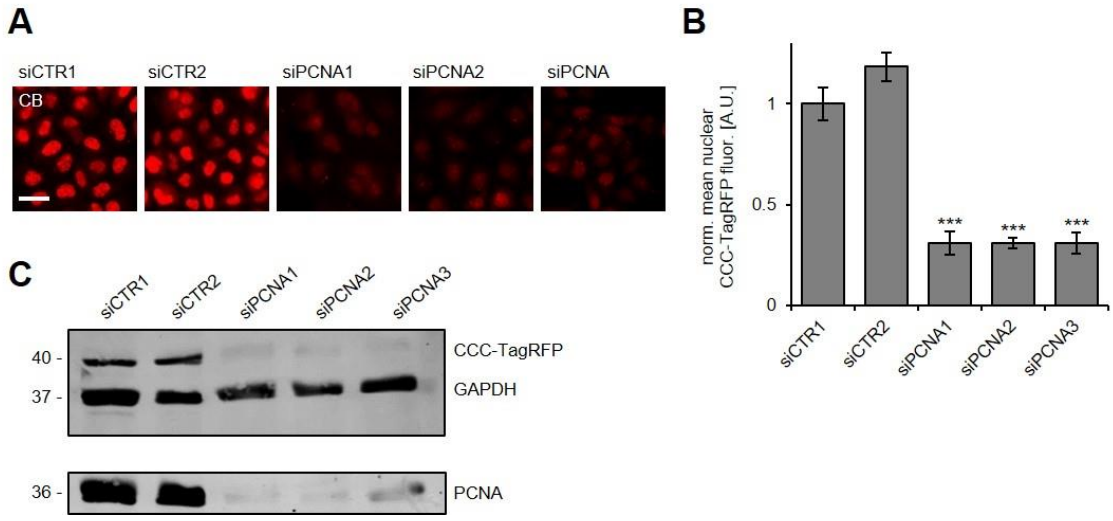

Figure 12 siRNA-mediated depletion of PCNA can be monitored by the CCC-TagRFP fluorescence.
*(**A**-**C**) HeLa_CCC-TagRFP cells were transfected with either two control siRNAs (siCTR1, siCTR2) or three different siRNAs (siPCNA1-3) mediating knockdown of endogenous PCNA. 72 h after transfection of the siRNAs the analyses were performed. (**A**) Representative fluorescence images of HeLa_CCC-TagRFP after siRNA transfection, scale bar: 50 µM. (**B**) Bar chart shows mean nuclear CCC-TagRFP fluorescence normalized to signal of cells transfected with siCTR1 of three different samples (n=3; >200 cells). Error bars: S.D., for statistical analysis student's t-test was used, *** p < 0.001. (**C**) Biochemical analysis of HeLa_CCC-*

TagRFP after siRNA-mediated PCNA depletion. 72 h post transfection cells were lysed and equal protein amounts of the soluble fraction were subjected to SDS-PAGE followed by western blot analysis using antibodies targeting TagRFP, PCNA and GAPDH as loading control.

5.2.3 Vimentin targeting VB6-CBs

Finally AMCBS was tested for a nanobody targeting the intermediate filament vimentin (VIM). VIM is ubiquitously expressed in mesenchymal cells, where it maintains cellular integrity. Furthermore, VIM is reported to be overexpressed in various epithelial cancers and has become an important marker for epithelial-mesenchymal transition (Satelli & Li, 2011). As ectopic VIM expression directly affects shape, adhesion and motility of the cells (Mendez et al, 2010), it is highly desirable to study endogenous VIM. Recently, VIM targeting CBs were developed and stably CB expressing cell lines (A549_VB6_eGFP and A546_VB6_TagRFP) were established (Maier et al, 2015). Using these cell lines, it was analyzed whether an induction of VIM by treatment with the transforming growth factor-β (TGF-β) or an siRNA-mediated depletion of VIM is accompanied by corresponding changes in CB fluorescence. Previously, it was shown by western blot analysis that both treatments were highly effective to raise or deplete the cellular levels of endogenous VIM in these cell models (Maier et al, 2015). The experiments reported in this chapter were performed by Dr. Julia Maier, whereas the data analysis was done independently by adapting the described segmentation strategy to the A549_VB6-eGFP and A549_VB6-TagRFP cell lines. A549_VB6-eGFP cells were treated with TGF-β for up to 72 h to induce expression of endogenous vimentin. Fluorescence images were acquired every 12 h revealing a continuous increase of the CB signal with a ~4-fold elevation after 72 h estimated by quantification of the CB fluorescence (**Figure 13A, B**).

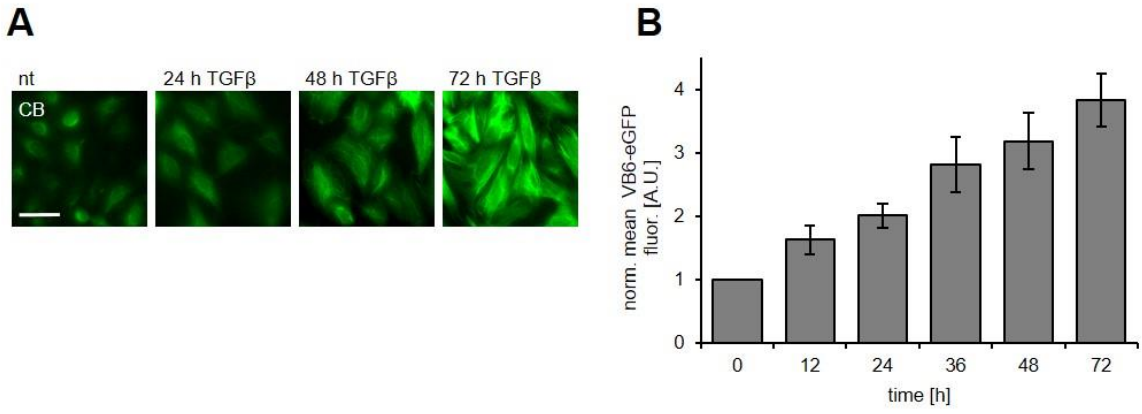

Figure 13 TGF-β-induced vimentin expression can be quantified by following the CB fluorescence intensity in A549 cells stably expressing the VB6-CB.
(A) *A549_VB6-eGFP cells were either stimulated with 5 ng/ml TGF-β or left non-treated. Fluorescence images were continuously acquired at indicated time points, scale bar: 50 µM.* ***(B)*** *Quantification of mean VB6-eGFP*

cellular fluorescence derived from time-lapse imaging after stimulation with 5 ng/ml TGF-β. Mean fluorescence intensities were normalized to the CB-signal intensity at 0 h, (N=3. > 200 cells each), error bars: S.D.

After showing that VIM induction can be monitored by visualizing the CB signal, siRNA-mediated depletion of VIM was performed in A549_VB6-TagRFP cells. The results showed that 72 h after siRNA treatment CB signal intensity was decreased to ~20 % compared to control siRNAs (**Figure 14A, B**).

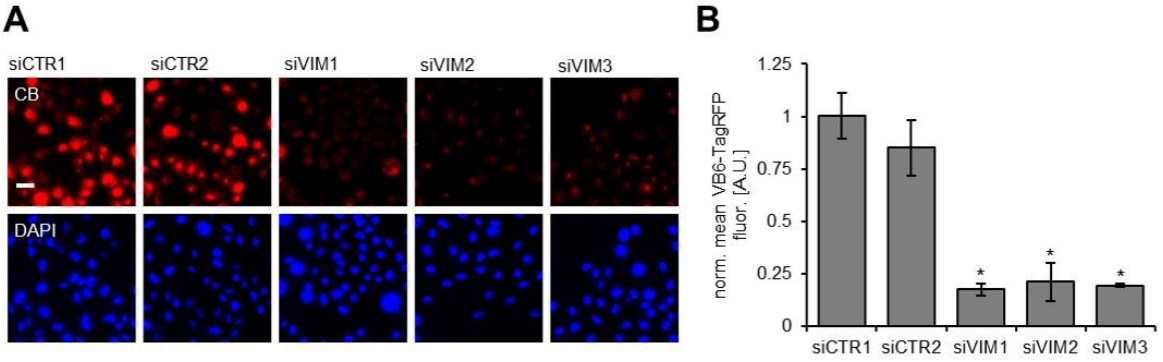

Figure 14 Visualization of siRNA-mediated VIM depletion by observing the VB6-TagRFP fluorescence. *(**A-B**) A549 cells stably expressing the VIM binding VB6-TagRFP (A549_VB6-TagRFP) were transfected with either two control siRNAs (siCTR1, siCTR2) or three different siRNAs (siVIM1-3) mediating knockdown of endogenous vimentin. 72 h post transfection of respective siRNAs the cells were analyzed by fluorescence microscopy. (**A**) Representative fluorescence images of A549_VB6-TagRFP after siRNA transfection, scale bar: 50 µM. (**B**) Bar chart shows mean VB6-TagRFP fluorescence intensity normalized to the signal of cells transfected with siCTR1 of three different samples (n=3; >200 cells). Error bars: S.D., for statistical analysis student's t-test was used, *** p < 0.001.*

5.2.4 AMCBS as general CB phenomenon

Taken together, the results obtained from experiments using CBs targeting different antigens such as CTNNB1, CA, PCNA and VIM strongly support the hypothesis that AMCBS is a general phenomenon. Notably, by utilizing the AMCBS phenomenon an increase in antigen concentration (CA, VIM) as well as depletion of the antigen (PCNA, VIM) could be monitored by simply following the CB signal over time. Furthermore, the results were obtained from different cell lines (HeLa and A549 cells) and the CBs stably integrated in these cell lines comprised different fluorescent moieties (TagGFP2, eGFP, mCherry and TagRFP). In addition, these results strongly suggest that AMCBS is a universal effect, which is observable for V_HH- but also for V_H-derived CBs.

5.3 Optimization of chromobody turnover

In most of current CB expression constructs, CB expression is driven from strong promotors such as the cytomegalovirus (CMV) promotor, which results in high yields of intracellularly available CB. If the protein level of the CB is higher than the amount of the antigen, the signal of antigen-bound CB might be masked due to elevated amounts of the unbound CB, thereby preventing the detection of small changes.

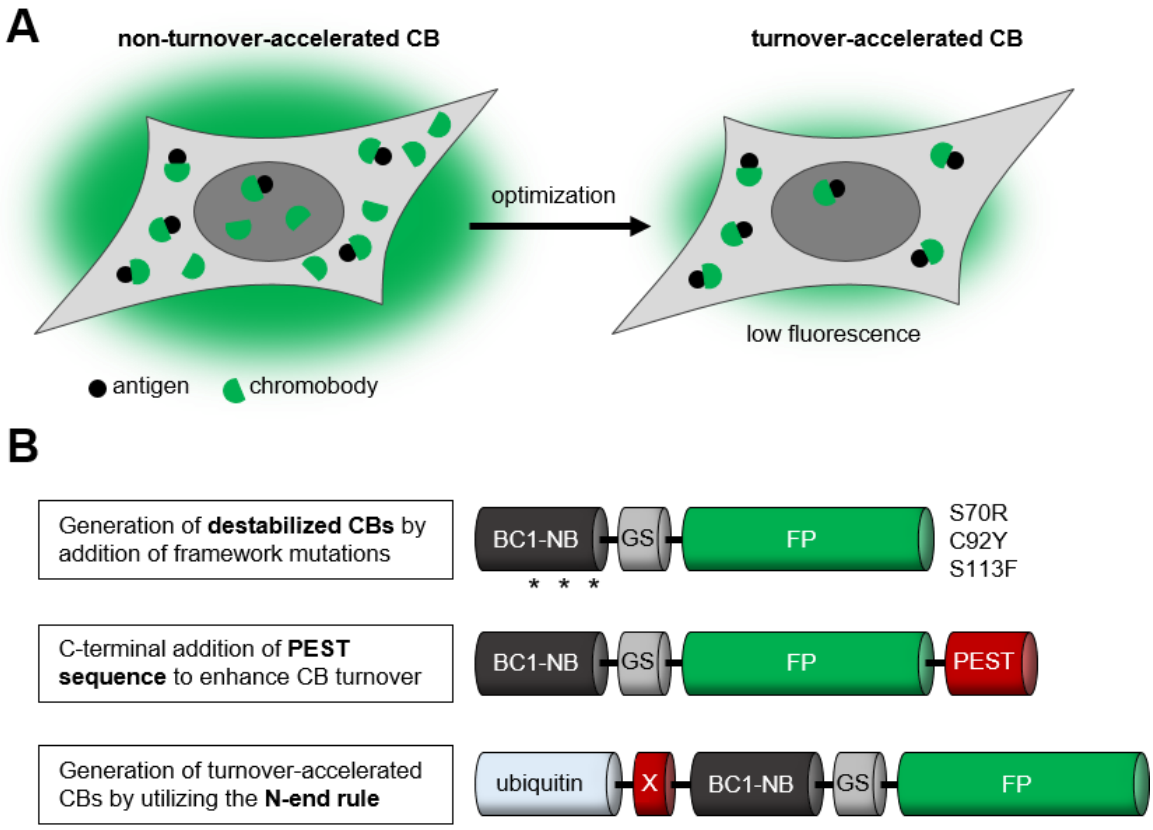

Figure 15 Strategies to reduce the basal amount of unbound CB within a cellular expression system.
*(**A**) Schematic illustration of CB fluorescence reduction by enhancing CB turnover. (**B**) Pursued strategies to enhance CB turnover in this study.*

As a low basal antigen-independent CB level is desirable, three different strategies to reduce the CB ground level were followed in this thesis (illustrated in **Figure 15**): (i) by addition of mutations into the framework region of the nanobody moiety destabilized BC1-CB variants were generated. Recently, these specific framework mutations have been described to rapidly create a conditional system, in which the stability of a NB depended on binding to its cognate antigen. Consequently, the antigen-independent NB fraction was degraded, resulting in a system suitable for the detection and quantification of endogenous antigens (Tang et al, 2016). (ii) a region containing proline (P), glutamic acid (E), serine (S) and threonine (T), a so-called PEST sequence, was C-terminally fused to the BC1- and αCA-CB.

This PEST sequence acts as a signal peptide for the proteasomal protein degradation, thereby resulting in a reduced half-life of the protein carrying this sequence (Rogers et al, 1986). And (iii) turnover-accelerated CBs were generated by utilizing the N-end rule, which is a key determinant of the half-life of a protein (Bachmair et al, 1986). To apply this method, the ubiquitin fusion technique was implemented, allowing the generation of CBs that only differ in their N-terminal amino acid (Varshavsky, 2005).

5.3.1 Destabilizing nanobody framework mutation to break down unbound CB

One recently described method to reduce the cellular amount of non-bound CB is the generation of conditionally stable nanobodies (Tang et al, 2016). To modify NBs that their amount strongly depends on antigen co-expression, the authors utilized a GFP-binding NB (GBP1) and generated a library encoding randomly mutagenized variants of GBP1-NB fused to TagBFP (GBP1-TagBFP). Next, the authors co-infected HEK293T cells with the generated library and the corresponding antigen (YFP) and analyzed the GPB1-TagBFP fluorescence. Interestingly, some GBP1-TagBFP mutants showed almost no fluorescence in antigen absence and a strong fluorescence in presence of the antigen YFP. Sequence analysis of these CBs led to the identification of three mutations, located in the framework region of the NB (S70R, C92Y and S113F, according to Kabat numbering (Kabat et al, 1992)), which strongly influenced the intracellular stability of the CB. As the NB framework regions are highly conserved, the authors hypothesized that these specific framework mutation could also be transferred to other NBs and applied these three mutations to other NBs resulting in similar observations. Based on these findings, this destabilizing framework were transferred to BC1-TagGFP2 (**Figure 16**).

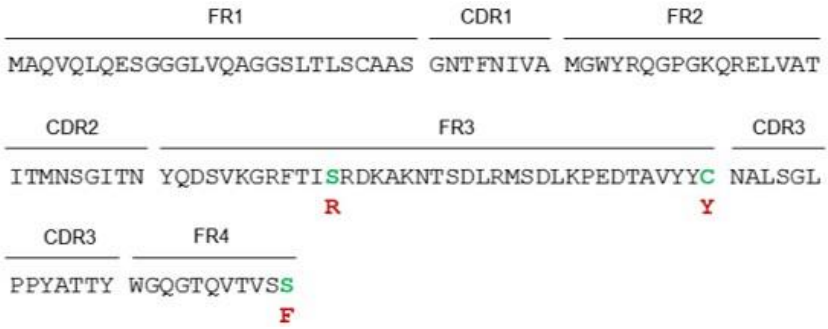

Figure 16 Illustration of destabilizing framework mutations in the BC1-TagGFP2.
Amino acid sequence of the BC1 nanobody binding moiety with labeled framework (FR1-4) and complementarity determining regions (CDR1-3). Highlighted in red are the previously described FR mutations (S70R, C92Y and S113F, Kabat numbering (Kabat et al, 1992)).

Expression constructs of BC1-TagGFP2 carrying these framework mutations were generated (BC1^{S70R}-TagGFP2, BC1^{C92Y}-TagGFP2, BC1^{S113F}-TagGFP2) and compared to the original BC1-TagGFP2 CB upon co-expression with either mCherry-CTNNB1 or mCherry as control (**Figure 17A**). Comparative analysis of CB fluorescence revealed a slightly reduced mean fluorescence of the BC1^{S70R}-TagGFP2 and BC1^{S113F}-TagGFP2 mutants and a strong reduction for the BC1^{C92Y}-TagGFP2 mutant close to background fluorescence level. Comparison of each CB signal in mCherry- and mCherry-CTNNB1-co-transfected cells revealed that antigen-mediated stabilization determined for the mutant versions moderately increased from 1.75-fold for BC1-TagGFP2, to 2.06-fold for BC1^{S70R}-TagGFP2, and 2.2-fold for the BC1^{S113F}-TagGFP2 mutant (**Figure 17B**).

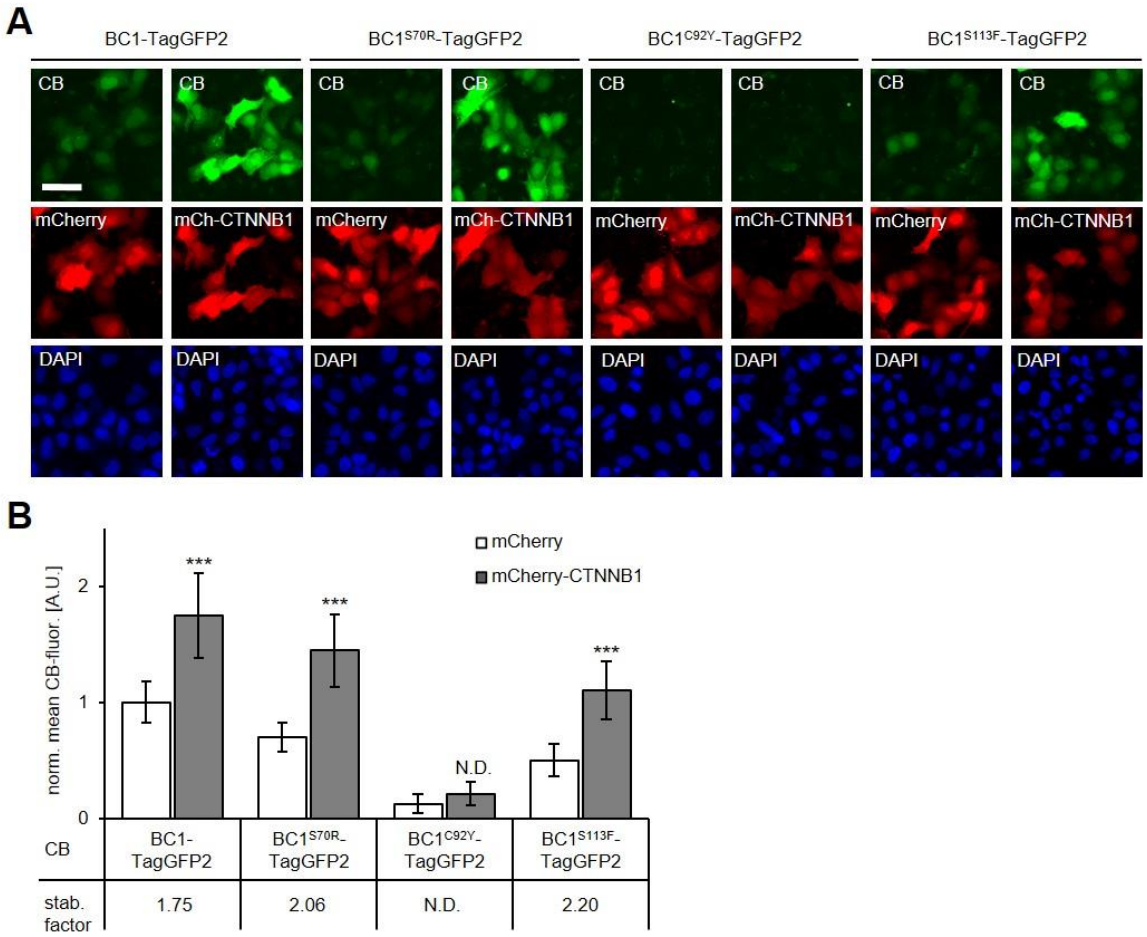

Figure 17 Microscopic analysis of destabilizing framework mutations of BC1-TagGFP2.
(A) *Representative fluorescence images of HeLa cells transiently co-transfected with the indicated BC1-CB variants and mCherry-CTNNB1 or mCherry as control. Nuclei were stained with DAPI, scale bar: 50 µm.* ***(B)*** *Quantification of mean CB fluorescence intensity in mCherry- and mCherry-CTNNB1 expressing cells. The intensity of each BC1-CB variant was normalized to the signal of the unmodified BC1-TagGFP2 in mCherry co-transfected cells (N=3, >200 cells each). The fold changes in CB fluorescence intensity after ectopic mCherry-CTNNB1 expression compared to the mCherry control are presented below the bar chart. Error bars: S.D., for statistical analysis student's t-test was applied, *** p < 0.001.*

However, when the antigen binding of the CBs was analyzed by intracellular co-immunoprecipitation of CTNNB1, CTNNB1 could not be detected in the bound fraction of the low expressing BC1^{C92Y}-TagGFP2 variant, indicating that this framework mutation might abolish binding to CTNNB1 (**Figure 18**).

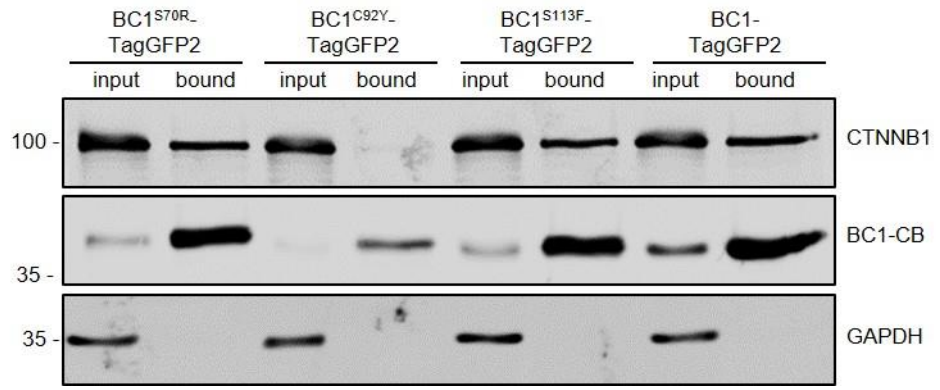

Figure 18 Intracellular co-immunoprecipitation of endogenous CTNNB1 with destabilized BC1-CBs.
HEK293T were transiently transfected with the indicated BC1-CB variants. 8 h post transfection cells were stimulated with 10 µM CHIR99021 for 16 h. Subsequently, cells were lysed using a 0.5 % NP40 lysis buffer and the soluble protein fraction was subjected to immunoprecipitation of the CBs with the GFP-Trap. 1 % of input and 20 % of bound fraction was loaded onto SDS-PAGE gels and protein level of CTNNB1, BC1-CB and GAPDH were analyzed via western blot.

With respect to the obtained findings, the strategy of using framework mutations to reduce the amount of unbound CBs in a cellular system could improve antigen-dependent responsiveness but also bears the risk in the generation of non-functional binding molecules. Hence, other strategies to reduce ground level of CBs were pursued, which should not interfere with antigen binding.

5.3.2 Elucidating the degradation pathway of the αCA-CB

In order to develop a different strategy resulting in reduced CB ground levels, it was first tested whether CBs are degraded via the ubiquitin proteasome system (UPS) or by lysosomal protein degradation. The described experiments in this chapter were conceived and conducted in collaboration with Dr. Björn Tränkle and Kathy-Ann Secker (Secker, 2016). To address this question, the HeLa_αCA-mCherry cell line was chosen for the analysis, since this cell line lacks an endogenous binding partner of the αCA-CB, because this model allows the analysis of the degradation pathway irrespective of antigen binding. Cells were either treated with the proteasome inhibitor MG132 or with NH_4Cl, which inhibits lysosomal degradation (Seglen & Reith, 1976) followed by continuous imaging of the cells in an hourly interval for up to 10 h. The images revealed a clear increase of CB fluorescence after treatment with the proteasome inhibitor MG132, while treatment with NH_4Cl did not alter

fluorescence intensity of the CB during the monitored period (**Figure 19A, B**). Considering the high similarity of CB sequence and structure, it can be assumed that most CBs are likely degraded via the UPS.

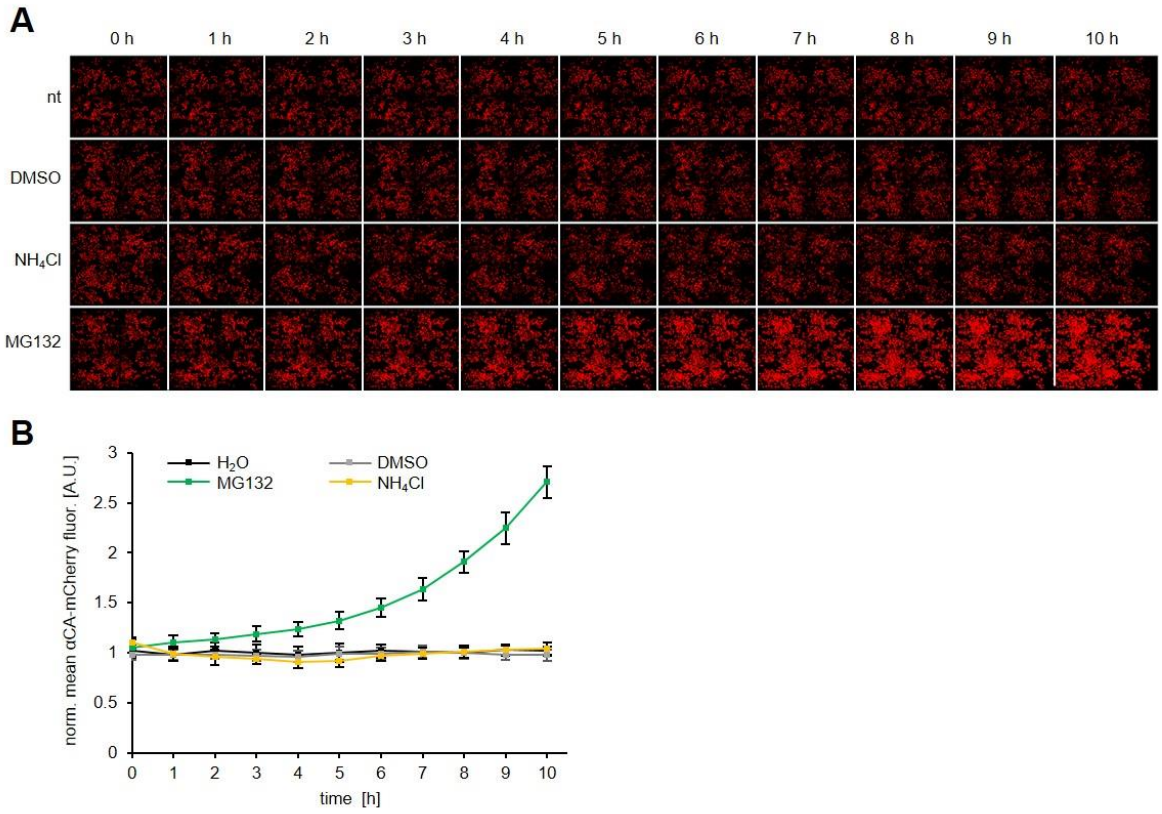

Figure 19 Chromobodies are degraded via the proteasomal pathway.
*(**A**) HeLa cells stably expressing αCA-mCherry CB (HeLa_αCA-mCherry) were treated with either MG132 to inhibit the proteasomal degradation or with NH_4Cl for inhibition of the lysosomal degradation pathway. Control cells were either left untreated (nt) or treated with DMSO. Cells were subjected to time-lapse imaging and fluorescence images were acquired every hour. (**B**) Quantification of αCA-mCherry mean fluorescence intensity. Graph illustrates mean CB fluorescence intensities normalized to their respective control (DMSO for MG132 and nt for NH_4Cl) and plotted against time (n=3, >200 cells), error bars: S.D. These results were conceived and conducted in collaboration with Dr. Björn Tränkle and Kathy-Ann Secker (Secker, 2016).*

5.3.3 Addition of a destabilizing PEST sequence to reduce CB half-life

To reduce ground level of the CBs without interfering with their binding capacity, CBs were C-terminally modified with a PEST sequence, derived from the ornithine decarboxylase (Rogers et al, 1986). PEST sequences directly affect the half-life of a protein by leading to rapid protein degradation of the modified protein (Rechsteiner & Rogers, 1996). Moreover, PEST sequence addition was already successfully applied to reduce the ground level of different gene reporters fused to different proteins like GFP or firefly luciferase (Li et al, 1998; Leclerc et al, 2000). The generation of PEST-tagged CB expression constructs and the

following analysis after transient expression in HeLa cells were independently performed and analyzed by the former Master student Kathy-Ann Secker (Secker, 2016).

At first, the ornithine decarboxylase-derived PEST sequence was C-terminally added to the BC1-TagGFP2 (BC1-TagGFP2-PEST) and the αCA-mCherry (αCA-mCherry-PEST). Next, BC1-TagGFP2-PEST was transiently co-expressed in HeLa cells, together with either mCherry-CTNNB1 or mCherry as control. The CB fluorescence was microscopically analyzed 17 h post transfection because after 24 h an onset of cell death was noticed. Analysis of transient BC1-TagGFP2 expressing cells revealed that after addition of the PEST sequence CB fluorescence was close to background and antigen co-expression led to an elevation of BC1-TagGFP2-PEST fluorescence (**Figure 20A**). Direct comparison with the original BC1-TagGFP2 CB illustrates a ~60 % reduced basal fluorescence in absence of the cognate antigen and the stabilization factor was slightly enhanced after addition of the PEST sequence (**Figure 20B**).

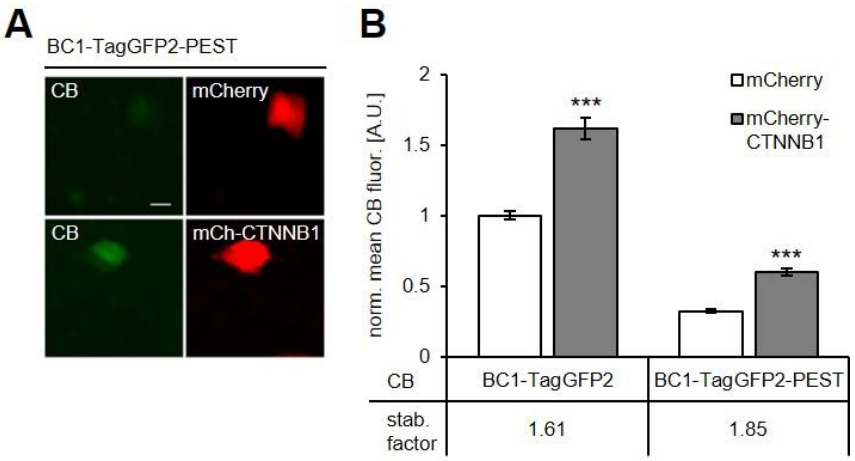

Figure 20 Addition of C-terminal PEST sequence to BC1-TagGFP2 reduces CB ground level.
*(Secker, 2016), (**A**) Parental HeLa cells were transiently co-transfected with BC1-TagGFP2-PEST and either with the corresponding antigen mCherry-CTNNB1 or mCherry as control. Shown are representative images 17 h post transfection, scale bar: 20 µm. (**B**) Bar chart of mean BC1-TagGFP2 and BC1-TagGFP2-PEST fluorescence in mCherry- or mCherry-CTNNB1-expressing cells analyzed 17 h post transient transfection. Mean CB fluorescences were normalized to cells expressing the non-modified BC1-TagGFP2 CB in mCherry transfected cells (n=3, >600 cells). Stabilization factors of fluorescence derived from antigen-negative and -positive cells are presented below the graphs. Error bars: S.E.M., for statistical analysis student's t-test was used.*

Secondly, CB fluorescence of αCA-mCherry-PEST 24 h post transient expression in HeLa cells was analyzed in presence and absence of the antigen GFP-CA. In the absence of the antigen αCA-mCherry-PEST fluorescence was reduced to ~60 % compared to the unmodified αCA-mCherry CB and the co-expression of the cognate antigen led to an enhanced stabilization factor for the PEST-modified CB (**Figure 21A, B**).

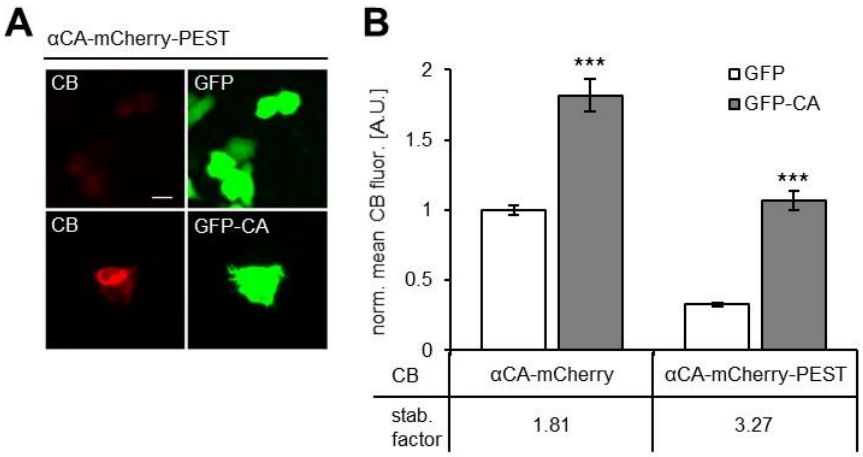

Figure 21 PEST sequence addition reduces αCA-CB ground level while enhancing the antigen-mediated stabilization factor.
*(**A**) Parental HeLa cells were transiently co-transfected with αCA-mCherry-PEST and either with the corresponding antigen GFP-CA or GFP as control. Illustrated are representative images 24 h post transient transfection. (**B**) Bar chart of mean αCA-mCherry and αCA-mCherry-PEST fluorescence in GFP- or GFP-CA-expressing cells analyzed 24 h post transient transfection. Mean fluorescence of the CB variants was normalized to cells expressing the non-modified αCA-mCherry CB in GFP transfected cells (n=3, >600 cells). Stabilization factors of fluorescence derived from antigen-negative and -positive cells are presented below the graphs. Error bars: S.E.M., for statistical analysis student's t-test was used.*

In conclusion, the addition of the PEST sequence to increase the CB turnover showed inconsistent results. Although this modification reduced the basal CB level and improved the associated stabilization factor for the αCA-CB, this approach was only partially applicable for the BC1-CB, since an accelerated cell death was observed after addition of the PEST sequence and in this example the stabilization factor did only slightly improve. Considering these findings, it was decided that this strategy is not generally suited to enhance the turnover of CBs.

5.3.4 Turnover-accelerating N-terminal amino acids

In another attempt to employ the proteasomal degradation pathway to reduce the CB ground level within a cellular expression system, the N-end rule, a key determinant of a protein's half-life, was utilized (Bachmair et al, 1986; Varshavsky, 2011). This method was already successfully applied to generate sensitive gene expression reporter by reducing the ground level of a reporter construct (Worley et al, 1998; Dantuma et al, 2000). Based on the N-end rule, the N-terminal amino acid of a protein is recognized by E3 ubiquitin ligases, which initiate ubiquitinylation of accessible nearby lysine residues, thereby priming the protein for proteasomal degradation. To screen for N-terminal amino acids leading to accelerated CB degradation, the ubiquitin fusion technique was implemented. This approach is based on the ratio that when ubiquitin (Ub) is expressed at the N-terminus of any POI, it is co-

translationally cleaved off from the fusion protein, resulting in exposure of a new N-terminal amino acid of the POI (Varshavsky, 2005; Bachmair et al, 1986).

To implement this method, an expression construct as outlined in **Figure 22A** was designed to generate Ub-CB fusions displaying different N-terminally exposed amino acid residues. Firstly, transient expression of the construct containing a N-terminal Ub fused to the BC1-TagGFP2 CB (Ub-M-BC1-TagGFP2) was tested in parental HeLa cells, which showed a dispersed distribution of the CB constructs in the nucleus and the cytosol of the cells without displaying aggregates (**Figure 22B**). Secondly, to test whether the Ub-CB fusion was processed according to the literature (Varshavsky, 2005), the original BC1-TagGFP2, Ub-M-BC1-TagGFP2 and the non-cleavable mutant Ub^{G76V}-M-BC1-TagGFP2 (Dantuma et al, 2000) were transiently expressed in HEK293T cells followed by comparative western blot analysis of the molecular weight of the matured CB variants (**Figure 22C**). No size difference was observed between the BC1-TagGFP2 CB and the Ub-CB fusion (Ub-M-BC1-TagGFP2), whereas Ub^{G76V}-M-BC1-TagGFP2 showed a size shift towards a higher molecular weight. These results indicate that the Ub-CB fusion is processed as intended and can be successfully expressed in HeLa and HEK293T cells.

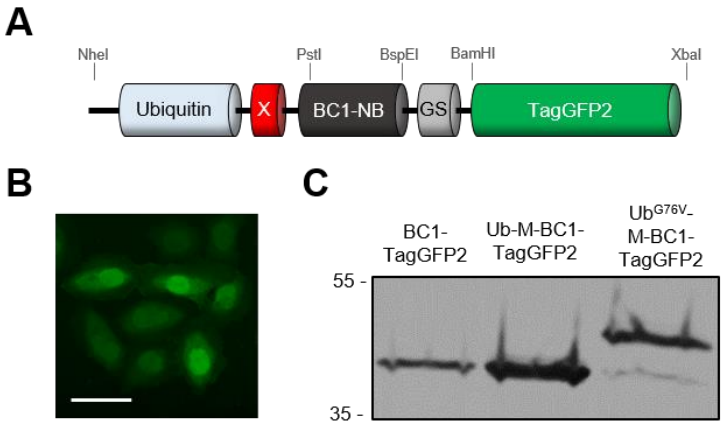

Figure 22 Implementation of the ubiquitin fusion technique for BC1-CB expression.
*(**A**) Schematic illustration of the chromobody expression construct generated to express CBs exposing different N-terminal residues. The indicated restriction sites allow an easy exchange of every CB component. (**B**) Representative image of parental HeLa cells transiently transfected with the generated Ub-M-BC1-TagGFP2 plasmid acquired 24 h post transfection, scale bar: 50 µm. (**C**) HEK293T cells were transiently transfected with expression constructs encoding the original BC1-TagGFP, Ub-M-BC1-TagGFP2 and the cleavage-deficient mutant Ub^{G76V}-M-BC1-TagGFP2. 24 h post transfection cells were lysed and soluble protein fraction was subjected to SDS-PAGE followed by immunoblot analysis.*

5.3.4.1 Screening for BC1-TagGFP2 turnover-accelerating N-terminal amino acid residues

After demonstrating that Ub-CB fusions are expressible in mammalian cells, where they are processed as intended, a set of 20 CB expression constructs, differing only in the N-terminal amino acid after Ub cleavage, were generated by site-directed mutagenesis. To screen for CB turnover-accelerating N-terminal amino acids, parental HeLa cells were transfected with the 20 generated constructs followed by quantitative image analysis of mean CB fluorescence. The analysis revealed that phenylalanine (F), alanine (A), lysine (K), tryptophan (T), arginine (R) and tyrosine (Y) (highlighted in grey) resulted in a reduced CB fluorescence of 40 - 60 % compared to the methionine (M) variant. In contrast to this, serine (S, hatched) showed the highest CB fluorescence when exposed at the N-terminus (**Figure 23**).

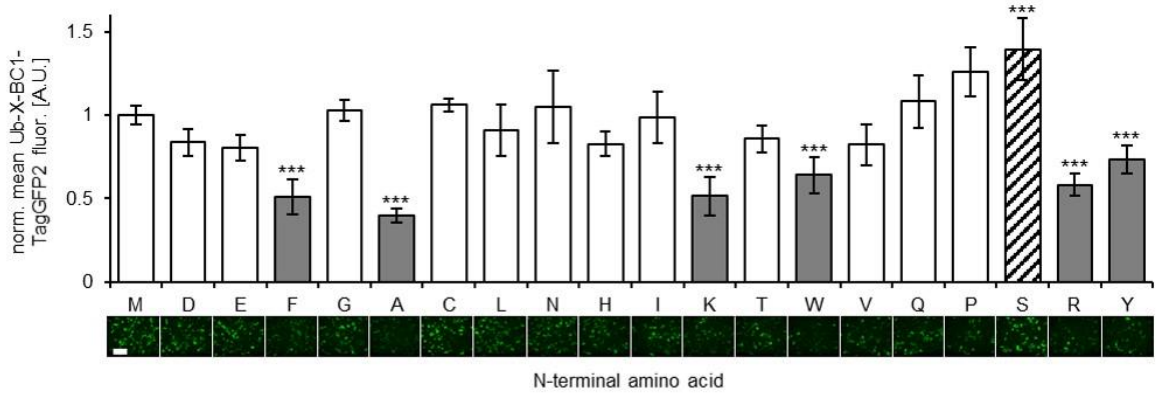

Figure 23 Screening for turnover-accelerating N-terminal residues of the Ub-X-BC1-TagGFP CB.
*Parental HeLa cells were transiently transfected with the indicated N-terminal Ub-X-BC1-TagGFP2 variants containing all possible amino acids at their N-terminus. To allow automated image segmentation, cells were co-transfected with mCherry and mean CB fluorescence was determined based on segmentation of the mCherry signal. Mean CB fluorescences were normalized to Ub-M-BC1-TagGFP2 (N=2, >200 cells each), error bars: S.D., for statistical analysis student's t-test was used, *** p < 0.001. Below the bar chart representative images of CB fluorescence are shown, scale bar: 200 µm.*

5.3.4.2 Verification of the identified turnover-accelerating amino acids by blocking the novel CB translation with cycloheximide

According to the experimental design, differences in CB fluorescence intensity detected in the initial screen should arise from the differences in CB degradation. To test this assumption in more detail, CB fluorescence of Ub-M-BC1-TagGFP2, Ub-F-BC1-TagGFP2, Ub-A-BC1-TagGFP2, Ub-R-BC1-TagGFP2 (Phe, Ala, Arg as variants with lowest CB fluorescence), and Ub-S-BC1-TagGFP (highest CB fluorescence) was monitored after

transient expression in HeLa cells following inhibition of protein translation by addition of cycloheximide (CHX) (**Figure 24A**). Compared to Ub-M-BC1-TagGFP2 and Ub-S-BC1-TagGFP2, which displayed 69 % and 80 % of the initial fluorescence after six hours, CB fluorescence with N-terminally exposed Phe, Ala or Arg decreased more rapidly to ~30 % of their respective initial fluorescence upon CHX treatment after six hours (**Figure 24B**). From this experiment it can be can be concluded that Phe, Ala and Arg were turnover-accelerating amino acids, which conferred rapid CB degradation.

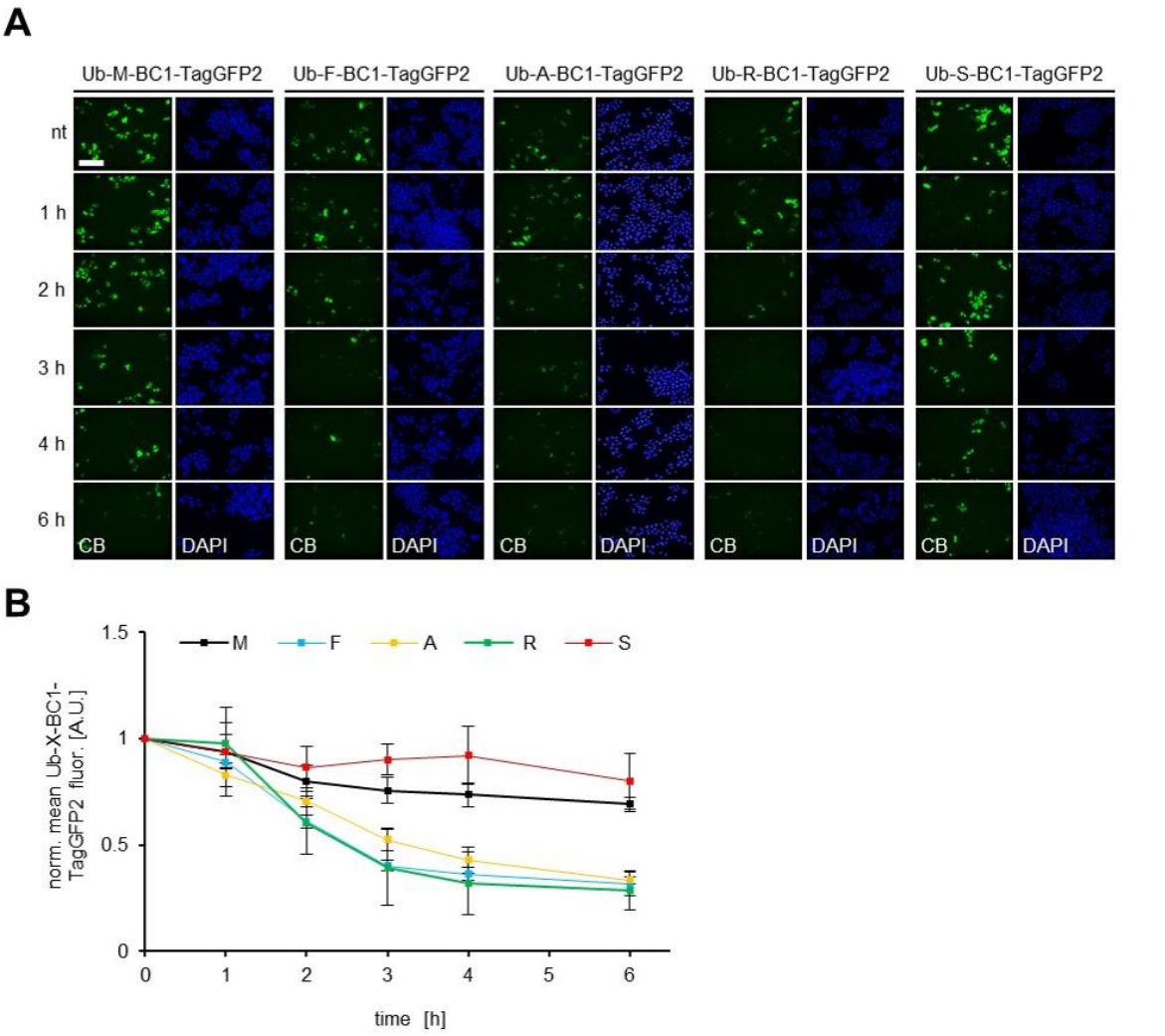

Figure 24 N-terminal residues Arg, Ala and Phe enhance turnover of Ub-X-BC1-TagGFP2.
*(**A**) Parental HeLa cells were transiently transfected with the indicated N-terminal variants of the Ub-X-BC1-TagGFP2 CB and mCherry as transfection control (not shown). 24 h post transfection cells were either left untreated or were treated with 0.1 mg/ml cycloheximide (CHX). At indicated time points cells were fixed and nuclei were stained with DAPI. Illustrated are representative fluorescence images of three biological replicates, scale bar: 200 µm. (**B**) Quantification of Ub-X-BC1-TagGFP2 mean fluorescence after blocking of protein translation using CHX. Mean fluorescence intensity of each CB variant was normalized to the respective non-treated control and normalized values were plotted against time (N=3, >200 cells each). Error bars: S.D.*

5.3.4.3 CB turnover-accelerating amino acids in other mammalian cell lines

As the expression of ubiquitin ligases might vary between different cell lines, fluorescence of the modified CBs (Ub-M-BC1-TagGFP2, Ub-F-BC1-TagGFP2, Ub-A-BC1-TagGFP2, Ub-R-BC1-TagGFP2and Ub-S-BC1-TagGFP2) was additionally analyzed in U2OS and A549 cell lines (**Figure 25A, B**). Therefore, the corresponding constructs were transiently expressed in these two cell lines followed by a quantitative analysis of CB fluorescence intensity segmented in mCherry-co-transfected cells. The analysis revealed highly similar CB signal intensities as detected in HeLa cells, except a weaker turnover-accelerating effect for the Ub-F-BC1-TagGFP2 variant. These results indicated that Ala and Arg, confer a high CB turnover in various cell lines.

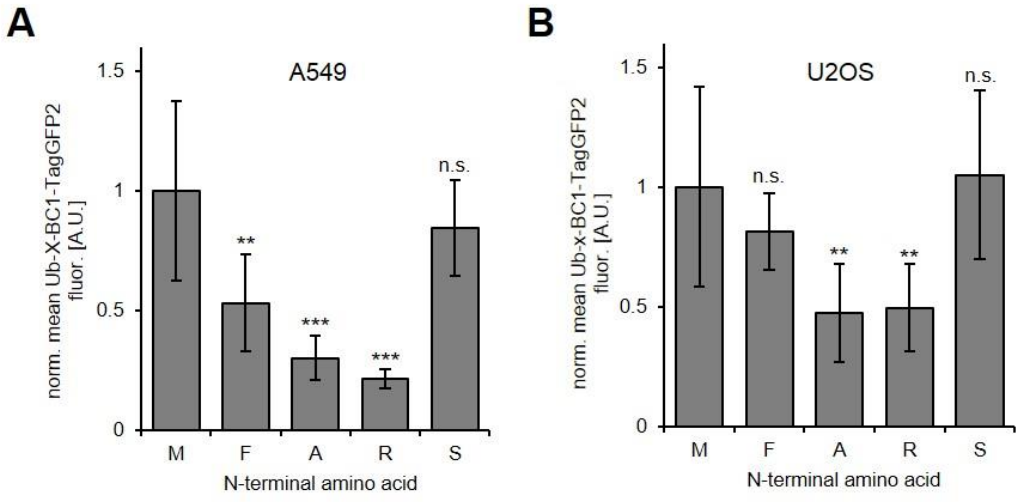

Figure 25 Differences in Ub-X-BC1-TagGFP2 turnover are transferable to A549 and U2OS cell lines. *Parental A549 (**A**) and U2OS (**B**) cells were transiently co-transfected with the indicated Ub-X-BC1-TagGFP2 variants and mCherry as transfection control. Mean CB fluorescence was analyzed by quantitative imaging, determining the CB fluorescence in mCherry-transfected cells. Bar charts illustrate mean fluorescence of CB variants normalized to the respective Ub-M-BC1-TagGFP2 variant (n=3, >200 cells). Error bars: S.D., for statistical analysis student's t-test was used, *** $p < 0.001$; ** $p < 0.01$; n.s. $p > 0.05$.*

5.3.4.4 Transfer of turnover-accelerating amino acids to other CBs

To test whether the effect of the identified turnover-accelerating amino acids is transferable to CBs targeting different antigens, the BC1-NB was replaced by the αCA- or VB6-NB within the generated CB expression constructs containing Met, Phe, Ala, Arg and Ser at their N-terminus using PstI and BspEI restriction sites (**Figure 22A**). For a comparative analysis all modified CBs were expressed in HeLa cells together with mCherry as transfection control followed by quantitative fluorescence imaging (**Figure 26A, B**). This experiment revealed a

significantly reduced fluorescence for all CBs displaying a N-terminal Phe and Arg residue as well as an enhanced fluorescence intensity for the Ser variants. Notably, the strong effect of Ala initially detected for the BC1-CB was neither observable for Ub-A-VB6-TagGFP2 nor for Ub-A-αCA-TagGFP2. Consequently Ala containing CB expression plasmids were excluded from further analyses.

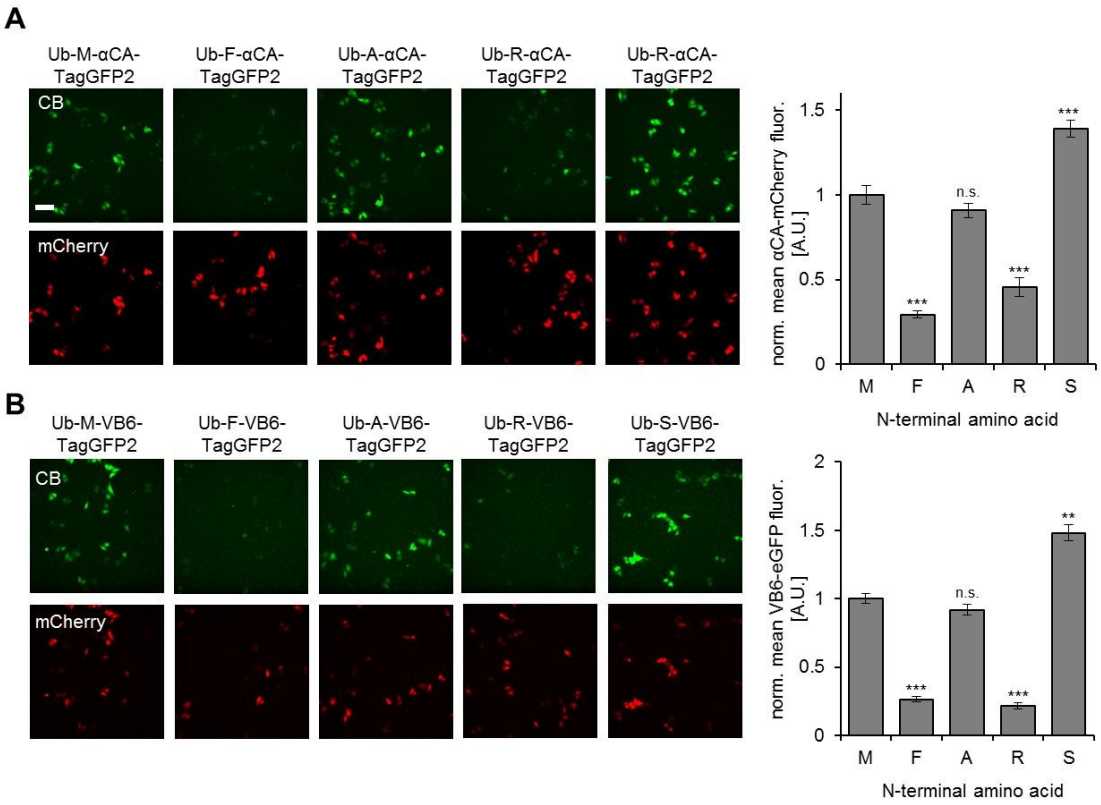

Figure 26 Turnover-accelerating N-terminal residues are transferable to other CBs.
*Parental HeLa cells were transiently co-transfected with the indicated Ub-X-αCA-TagGFP2 (**A**) or Ub-X-VB6-TagGFP2 (**B**) variants and mCherry as control. Shown are representative images, scale bar: 100 µm. Bar chart of mean CB fluorescence in mCherry expressing cells, normalized to the Met containing CB variant (n=3, >200 cells). Error bars: S.D., for statistical analysis student's t-test was used, *** $p < 0.001$; ** $p < 0.01$; n.s. $p > 0.05$.*

5.3.4.5 Influence of linker length

For the initiation of proteasomal degradation, unstructured amino acid regions are required (Yu et al, 2016). Within the CB, the nanobody moiety and the fluorescent protein are connected via a Gly-Ser-$(G_4S)_3$ linker, which represents an unstructured region and probably might serve as initiation site for proteasomal degradation. Thus, the impact of the linker length in context of AMCBS was evaluated. Consequently, the original $(G_4S)_3$ linker was substituted within the Ub-M-BC1-TagGFP2 construct towards a shorter $(G_4S)_2$ or a longer $(G_4S)_4$ version. These three linker variants of the CB were co-expressed in HeLa cells with

either mCherry-CTNNB1 or mCherry as control. Analysis of CB fluorescence revealed neither significant differences for the CB fluorescence in antigen absence nor in presence of the antigen (**Figure 27**), which indicates a negligible role of the linker length for AMCBS.

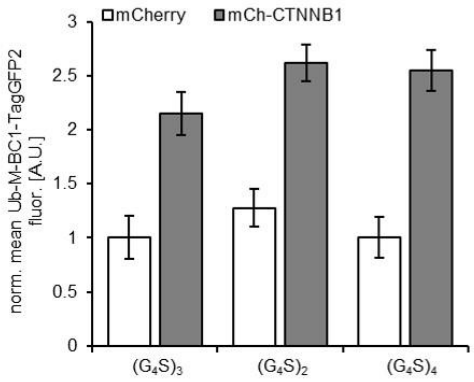

Figure 27 Influence of the length of the Gly-Ser linker connecting the chromobody binding moiety with the FP.
Parental HeLa cells were transiently co-transfected with Ub-M-BC1-TagGFP2 constructs comprising different variants of the Gly-Ser linker ($(G_4S)_3$, $(G_4S)_2$ and $(G_4S)_4$) and mCherry or mCherry-CTNNB1. Bar chart represents the mean CB fluorescence normalized to fluorescence signal detected in cells expressing the Ub-M-BC1-TagGFP2 comprising the $(G_4S)_3$ linker in combination with mCherry (n=3, >200 cells). Error bars: S.D.

5.3.4.6 Influence of fluorescent protein on CB degradation velocity

To evaluate a potential impact of the FP on CB turnover, TagGFP2 was either substituted by eGFP, mCherry or TagRFP in the N-terminally modified BC1-CB constructs displaying Met, Phe, Ala, Arg and Ser as N-terminally amino acid residues. After transient expression in HeLa cells, CB degradation velocities in the presence of CHX were monitored by fluorescence imaging for up to six hours followed by quantitative analysis (**Figure 28A, B, C**). The most rapid degradation to 26 % could be detected for Ub-R-BC1-eGFP, whereas corresponding CB constructs comprising either mCherry or TagRFP were less degraded to 43 % or 57 %, respectively. Although some differences among the FPs were observed, the turnover-accelerating effect of Arg and Phe was evident for all three additionally investigated FPs.

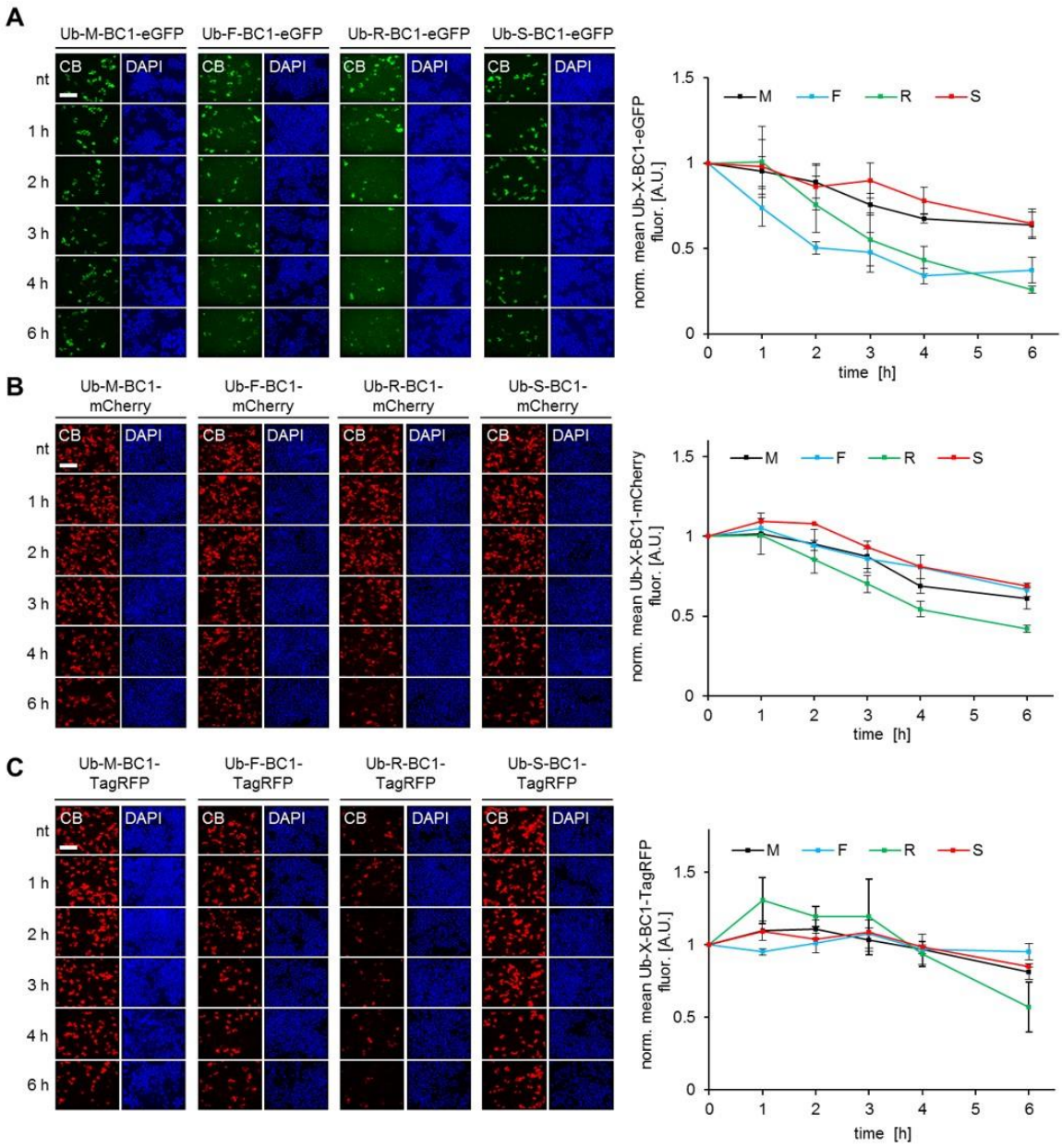

Figure 28 Impact of the fluorescent moiety on turnover velocity of N-terminally modified BC1-CB variants. *(**A**-**C**) New expression constructs of Ub-X-BC1-TagGFP2 containing Met, Phe, Arg and Ser were generated by replacing TagGFP2 by either eGFP (**A**), mCherry (**B**) or TagRFP (**C**). Left panel (A-C) shows fluorescent images of parental HeLa cells transiently expressing the indicated Ub-X-BC1-FPs. 24 h after transfection cells were either left non-treated (nt) or were treated with 0.1 mg/ml CHX. At the indicated time points cells were fixed and nuclei stained with DAPI. Shown are representative images of three biological replicates (N=3), scale bar: 200 µm. Right panel illustrates the mean fluorescence of the Ub-X-BC1-FP variants, each normalized to the respective non-treated control and plotted against time (N=3, >200 cells each). For segmentation a co-transfected control protein (mCherry in case of Ub-X-BC1-eGFP or GFP in case of Ub-X-BC1-mCherry and Ub-X-BC1-TagRFP) was used (for simplification data of co-transfection are not shown). Error bars: S.D.*

5.3.4.7 Antigen-mediated CB stabilization of turnover-accelerated BC1-CB variants

After demonstrating that the N-end rule is suitable to reduce CB ground level within cells, the next question was whether these modified CBs can be stabilized via their antigen and exhibit improved stabilization factors. To analyze the stabilization effect of CTNNB1, the BC1-CB variants Ub-M-BC1-TagGFP2, Ub-F-BC1-TagGFP2, Ub-R-BC1-TagGFP2 and Ub-S-BC1-TagGFP2 were compared. Thus, the CB constructs were transiently co-expressed in parental HeLa cells with either mCherry-CTNNB1 or mCherry as control and the CB fluorescence intensity was determined within co-transfected cells. Based on the degree of CB stabilization N-terminal Met and Ser behaved similar, displaying stabilization factors of 1.8 and 1.9, respectively. For the turnover-accelerating amino acids Phe and Arg stabilization factors of 2.2 and 2.3 were determined (**Figure 29A, B**). This observation illustrates that the ground level reduction of the BC1-CB variants exposing Phe and Arg at the N-terminus led to elevated stabilization factors.

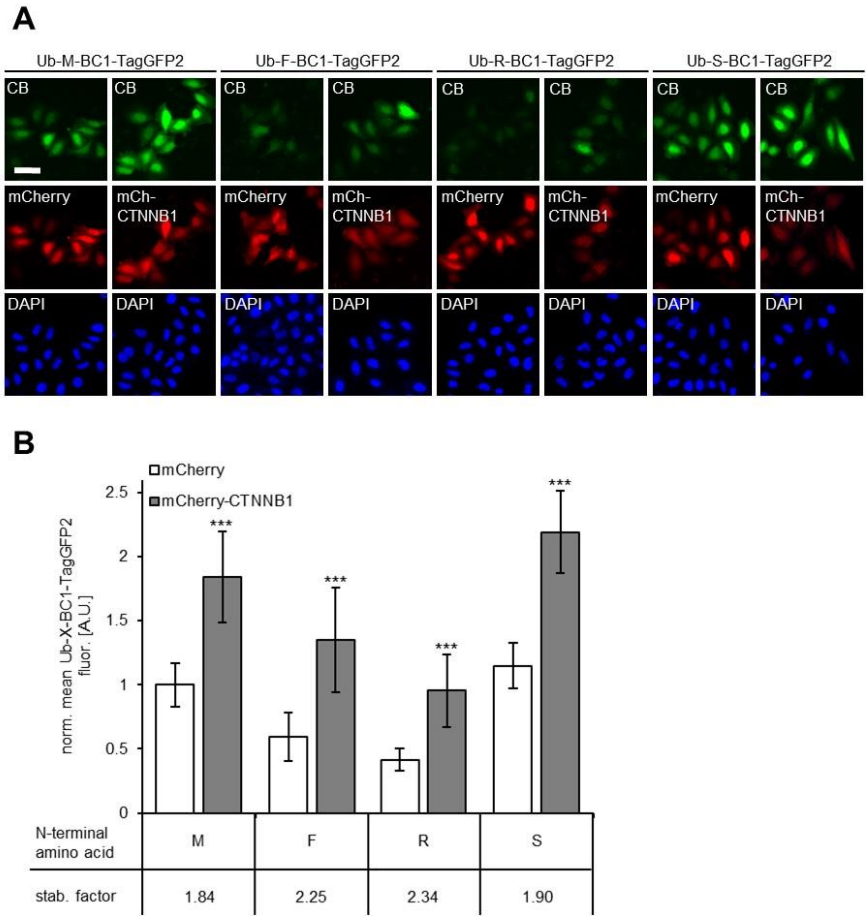

Figure 29 CTNNB1-dependent stabilization of N-terminally modified Ub-X-BC1-TagGFP2 variants
Parental HeLa cells were transiently co-transfected with respective Ub-X-BC1-TagGFP2 variant in combination with either mCherry or mCherry-CTNNB1. 24 h after transfection cells were fixed and nuclei

*were stained with DAPI. (**A**) Representative fluorescence images of parental HeLa cells transiently expressing BC1-CB and mCherry or mCherry-CTNNB1, scale bar: 50 µM. (**B**) Bar chart of mean CB fluorescence intensity detected in mCherry- or mCherry-CTNNB1-expressing cells. CB fluorescence intensity was normalized to the fluorescence detected in mCherry transfected cells. Mean fluorescence was calculated from three different samples (n=3), comprising >200 cells. Error bars: S.D., for statistical analysis student's t-test was performed, *** p < 0.001. Corresponding stabilization factors are indicated below the graph.*

5.3.4.8 CTNNB1-binding capacity of N-terminally modified BC1-CB variants

To exclude an interference of the N-terminal modification on antigen binding, intracellular co-immunoprecipitation (IC-IP) was performed. Hence, HEK293T were transiently transfected with plasmids encoding for the original BC1-TagGFP2 construct, the newly generated Ub-M-BC1-eGFP, the turnover-accelerated Ub-R-BC1-eGFP or GFP as control. Subsequently, cells were treated with 10 µM CHIR to elevate the level of endogenous CTNNB1. After lysis CBs were precipitated with GFP-Trap followed by analysis of respective input and bound fractions by western blot (**Figure 30**). Antibody staining revealed that all three CBs successfully bound similar levels of endogenous CTNNB1. Obviously, the N-terminal BC1-CB modification did not affect CTNNB1 binding capacity.

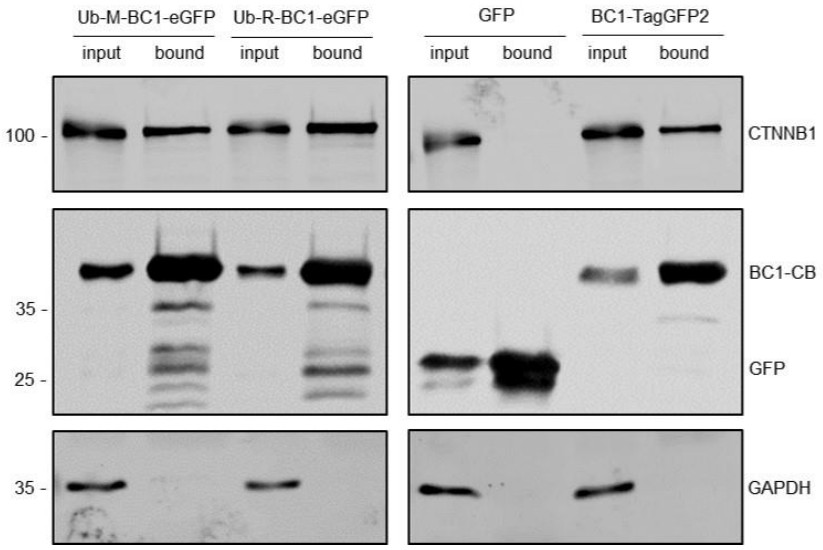

Figure 30 N-terminal modification of the BC1-CB does not affect intracellular binding to CTNNB1.
HEK293T cells were transiently transfected with the indicated CB variants or GFP as control. 8 h post transfection, cells were stimulated with 10 µM CHIR for additional 16 h. Cells were lysed using a 0.5 % NP40 lysis buffer and CBs were precipitated from the soluble fraction using the GFP-Trap. Input (1 %) and bound (20 %) fractions were subjected to SDS-PAGE followed by immunoblot analysis.

5.3.4.9 Influence of fluorescent moiety on CTNNB1-mediated stabilization of turnover-accelerated BC1-CBs

Here, the set of turnover-accelerated CBs applied in chapter 5.3.4.6 containing either eGFP, mCherry and TagRFP as fluorescent moiety were used to evaluate whether the type of the FP has an effect on CB stabilization mediated by CTNNB1. Therefore, the CB constructs were co-expressed in parental HeLa cells with either the corresponding antigen or the respective FP as control. Fluorescence images were acquired followed by quantification of CB signals in co-expressing cells (**Figure 31**). The stabilizing effect of CTNNB1 was observable for each CB construct and comparable stabilization effects were determined as previously observed for the TagGFP2-containing CB variants. Notably, the stabilization factors of all Arg containing FP variants were the highest among each CB set.

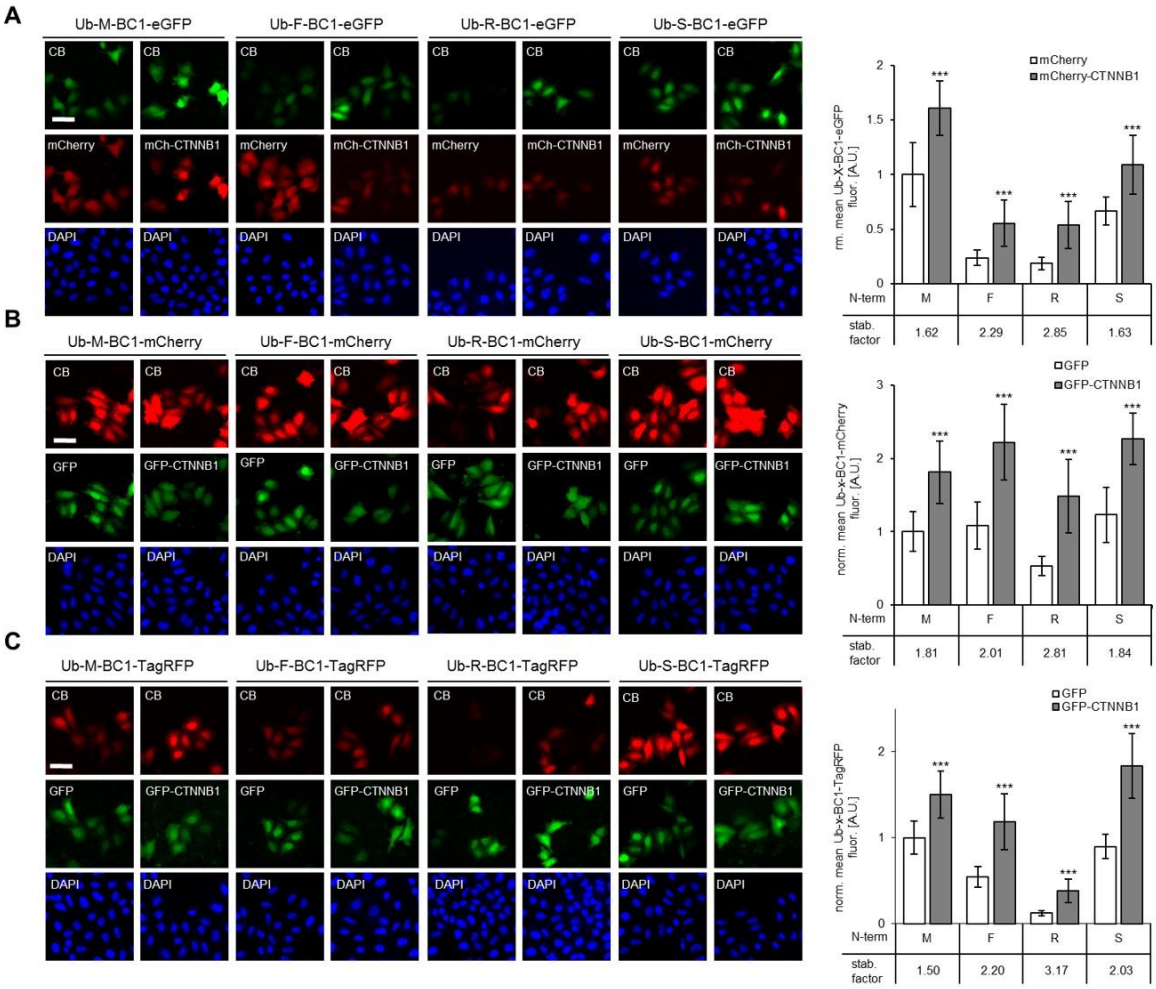

Figure 31 Effect of fluorescent moiety on antigen-mediated stabilization of N-terminally modified Ub-X-BC1-CB variants.
*(**A-C**) To analyze the effect of the fluorescent moiety on antigen-mediated stabilization of N-terminally modified Ub-X-BC1-CBs, expression constructs of the Met, Phe, Arg and Ser CB containing either eGFP (**A**), mCherry (**B**) or TagRFP (**C**) were used. Left panel (A-C) shows fluorescent images of parental HeLa cells transiently expressing the indicated Ub-X-BC1-CBs and the respective antigen or control-FP (mCherry and mCherry-*

*CTNNB1 in case of Ub-X-BC1-eGFP or GFP and GFP-CTNNB1 for Ub-X-BC1-mCherry and Ub-X-BC1-TagRFP). 24 h after co-transfection cells were fixed and nuclei stained with DAPI. Shown are representative images of three biological replicates (N=3), scale bar: 50 µm. Right panel illustrates the mean fluorescence of the Ub-X-BC1-FP variants, each normalized to the respective co-transfected control protein (N=3, >200 cells each). Error bars: S.D. For statistical analysis student's t-test was used, *** p < 0.001. Corresponding stabilization factors are shown below bar charts.*

5.3.4.10 Antigen-mediated stabilization of Ub-R-αCA-TagRFP

Next, the effect of antigen-mediated stabilization was tested for the Arg modification in context of the αCA-CB. Thus, the BC1-NB was replaced by the αCA-NB within the Met and Arg containing BC1-TagRFP expression constructs. Here, TagRFP as fluorescent moiety was chosen because the available expression construct for the antigen CA contained GFP as fluorescence moiety (GFP-CA). After cloning, the generated expression constructs (Ub-M-αCA-TagRFP and Ub-R-αCA-TagRFP) were transiently co-expressed in parental HeLa cells with either GFP-CA or GFP as control. In the absence of the antigen GFP-CA, the basal fluorescence of Ub-R-αCA-TagRFP was close to background level, whereas a moderate fluorescence was observed for the Met-containing variant (**Figure 32A**). Upon antigen exposure a stabilization factor of ~5 was calculated for Ub-M-αCA-TagRFP whereas the turnover-accelerated Arg variant showed a stabilization factor increased to ~14 (**Figure 32B**).

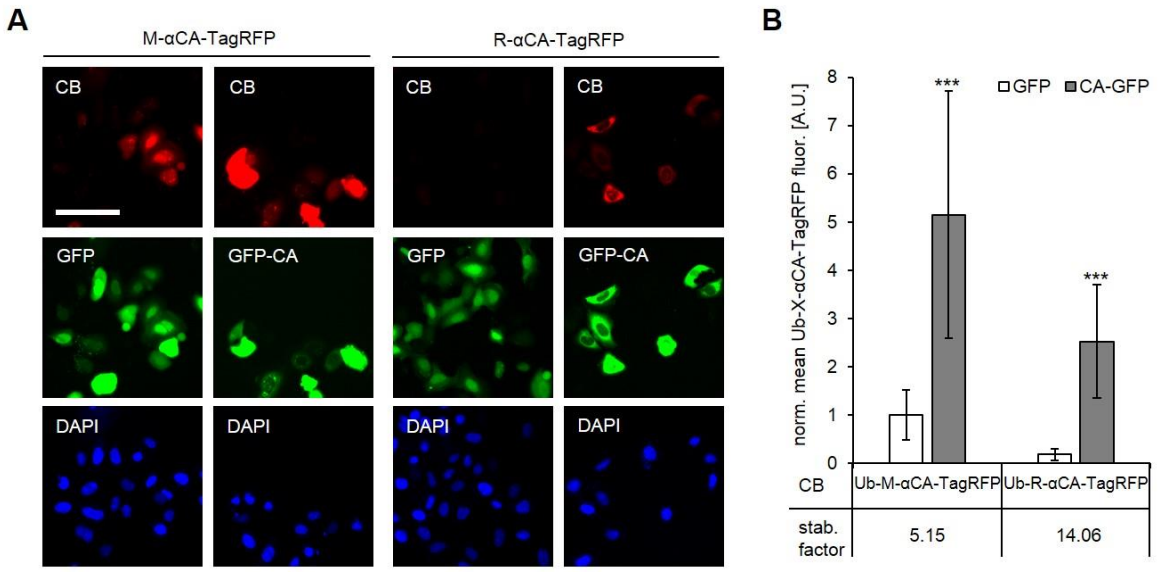

Figure 32 Antigen-mediated stabilization of N-terminally modified αCA-CB variants.
*(**A**) Representative fluorescence images of parental HeLa cells transiently expressing N-terminally modified Ub-X-αCA-TagRFP variants containing Met or Arg and GFP or GFP-CA. Nuclei were stained with DAPI, scale bar: 50 µM. (**B**) Bar chart of mean CB fluorescence intensity detected in GFP- or GFP-CA-expressing cells. CB fluorescence intensity was normalized to the fluorescence detected in GFP transfected cells. Mean fluorescence was calculated from three biological replicates (N=3), comprising >200 cells. Error bars: S.D., for statistical analysis student's t-test was used.*

5.3.4.11 Expression as ubiquitin fusion reduces aggregation of CBs after transient expression

The majority of current CB expression systems are utilizing the CMV promoter, which results in a high level of ectopically expressed CBs. However, strong CB expression can be accompanied by the formation of aggregates within the cell. As a consequence, aggregation might interfere with the respective analysis method, lead to artifacts in analysis or might even have toxic effects to the cells (Vavouri et al, 2009; Halff et al, 2014). In this context it was described that the ubiquitin fusion technique can be used to increase solubility and functionality of ectopically expressed proteins (Varshavsky, 2005).

The recently described Lamin-CB (LMN-TagGFP2) (Zolghadr et al, 2012) suffers from the formation of aggregates after transient expression in HeLa cells (**Figure 33A**). To test whether the ubiquitin fusion technique is effective to decrease aggregation of LMN-TagGFP2, expression constructs containing a N-terminal ubiquitin with either Met and Arg were produced by replacing the BC1-NB by the LMN-NB within the Ub-CB expression construct.

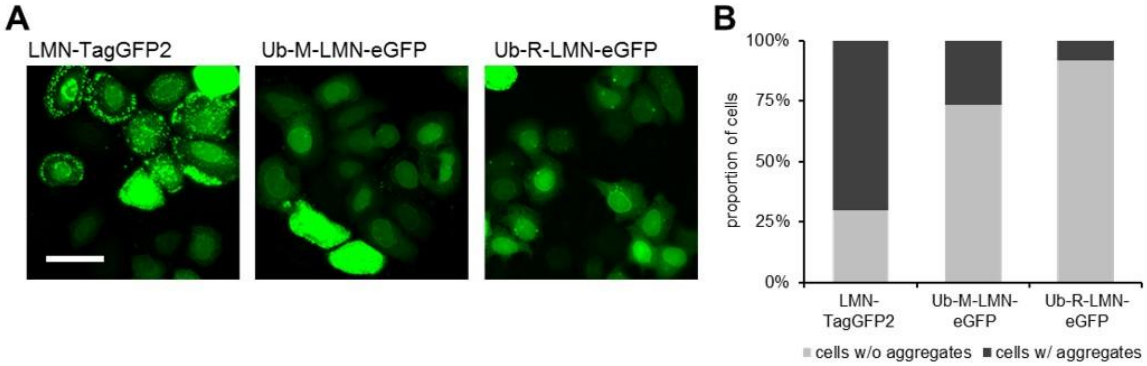

Figure 33 Comparative analysis of N-terminally modified Lamin-CB variants after transient expression in HeLa cells.
*Parental HeLa cells were transiently transfected with expression constructs encoding LMN-CB, Ub-M-LMN-CB and Ub-R-LMN-CB. (**A**) Shown are representative images of three biological replicates of Lamin-CB-expressing HeLa cells, scale bar 50 µM. (**B**) Quantification of aggregates proportion in HeLa cells transiently expressing the indicated Lamin-CB variants. Number of analyzed cells: LMN-CB: 157; Ub-M-LMN-CB: 142, and Ub-R-LMN-CB: 155.*

Next, parental HeLa cells were transiently transfected with expression constructs coding for LMN-TagGFP2, Ub-M-LMN-eGFP and the turnover-accelerated Ub-R-LMN-eGFP variant followed by fluorescence imaging of the CB-expressing cells (**Figure 33A**). Subsequently, the proportion of cells containing aggregates was determined for a statistically relevant number of cells (**Figure 33B)**. For the original LMN-TagGFP2 CB the majority of

transfected cells (~70 %) displayed fluorescent aggregates. The transient expression as ubiquitin fusion containing N-terminal Met reduced aggregation to ~27 % and the expression as turnover-accelerated Ub-R-LMN-eGFP further reduced the aggregation to ~8 %.

In summary, these results illustrate that besides reducing CB ground level another major benefit in the application of the ubiquitin fusion technique is a reduction of CB aggregate formation after transient expression. Notably, after transient expression of the unmodified LMN-CB the nuclear lamina was hardly detectable in the majority of the cells, whereas both ubiquitin fusions led to more prominent fluorescent targeting of the lamina.

5.3.4.12 Summary of CB turnover optimization

To reduce the amount of antigen-independent CB within a cellular system, the application of the N-end rule turned out to be well suited for the generation of turnover-accelerated CBs by reducing CB ground level. The Arg-modified BC1 construct exhibited the most rapid turnover (**Figure 24B**), lowest fluorescence in absence of the antigen and the greatest stabilization after ectopic antigen expression (**Figure 29**). Importantly, these observations were evident irrespective of the fluorescent moiety (**Figure 28**, **Figure 31**) or the binding moiety (**Figure 26**) of the CB and the used cell line (**Figure 25**). Further, the Arg-modification was successfully transferred to the αCA-CB resulting in a nearly tripled stabilization effect as compared with a version containing an N-terminal Met (**Figure 32**). Notably, the expression of a CB as Arg comprising ubiquitin fusion substantially increased the amount of functional CB upon transient expression by reducing the amount of aggregated CB (**Figure 33**).

Based on these findings, the N-terminal Arg modification was utilized as feature for the generation of new stable CB expressing cell lines.

5.4 Generation of stable cell lines expressing the turnover-accelerated Ub-R-BC1-eGFP CB

A major benefit of the AMCBS approach compared to endpoint assays is its applicability to continuously monitor time-dependent changes in POI concentration in living cells. Previously, it could be demonstrated that an increase of endogenous CTNNB1 upon compound treatment can be visualized by real-time imaging of the CB signal in HeLa_BC1-TagGFP2 cells (Traenkle et al, 2015). However, upon a more detailed characterization within this thesis it turned out that this cell line has only a limited use to monitor decreasing CTNNB1 levels. This was mainly caused by high CB ground levels and a discrepancy in half-life of CB and antigen. This issue was now addressed by the generation of a turnover-accelerated CBs as described in the previous chapter. As a result of enhanced CB degradation, turnover-accelerated CBs were assumed to detect decreasing and small changes more precisely.

Since transient CB expression results in substantial heterogeneity of intracellular CB level, two novel cell lines stably expressing the turnover-accelerated Ub-R-BC1-eGFP CB (HeLa_Ub-R-BC1-eGFP and U2OS_Ub-R-BC1-eGFP) were generated as illustrated in **Figure 34**.

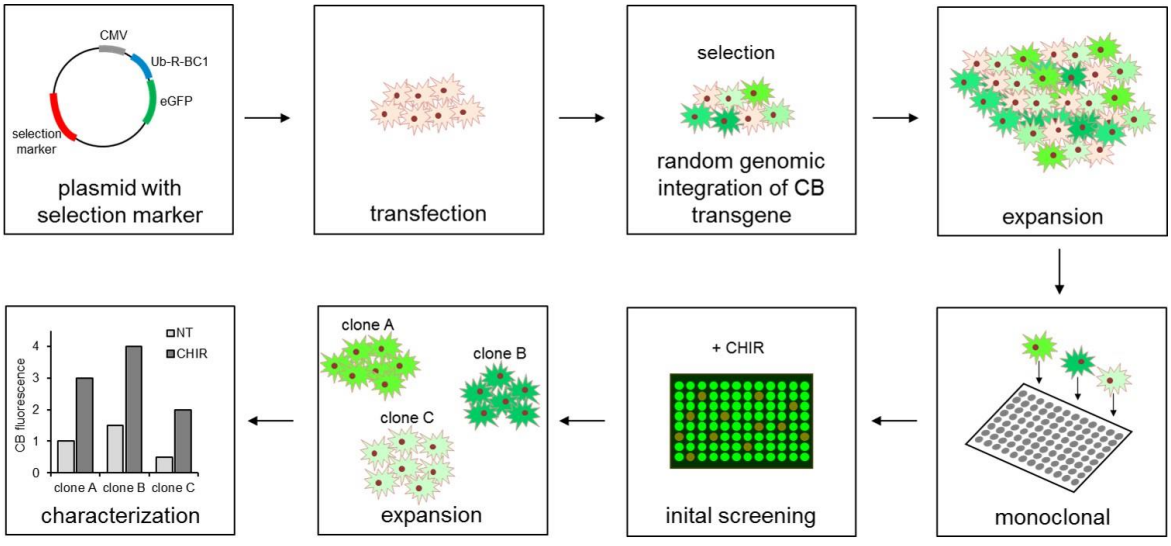

Figure 34 Schematic overview of stable Ub-R-BC1-CB cell line generation.
Shown is the typical workflow of stable cell line generation following random genomic transgene integration. Parental cells were transfected with a plasmid coding for the turnover-accelerated CB, driven by a CMV promoter and a selection marker. Subsequent selection with the appropriated antibiotics resulted in random genomic integration of CB transgene. After expansion monoclonal cells were isolated. By an initial screen, cells were treated with CHIR to elevate the endogenous amount CTNNB1, which led to an increase in CB fluorescence. Single clones displaying rising CB levels in response to the CHIR-induced CTNNB1 increase were further expanded and characterized.

At first, parental HeLa and U2OS cells were transiently transfected with an expression plasmid containing the turnover-accelerated Ub-R-BC1-eGFP CB under a constitutive CMV promoter and the *neoR* resistance gene. One day after plasmid transfection, cells were continuously cultivated with 0.5 mg/ml G418 for a two week period (concentration determined by kill curve, data not shown) and after selection monoclonal cells were isolated. Initial characterization of the isolated Ub-R-BC1-eGFP expressing HeLa and U2OS clones was performed by monitoring the CB level after treatment with 10 µM CHIR for 16 h using fluorescence microscopy (**Figure 35**). The acquired images illustrate the CB steady-state level (nt) as well as elevated fluorescence signals upon CHIR treatment. Notably, the ground level differed substantially between the different clones, ranging from clones with basal CB intensities near background level (HeLa_Ub-R-BC1-eGFP clone D4 and U2OS_Ub-R-BC1-eGFP clone F11) to clones displaying higher basal fluorescence signals. Although the calculated stabilization factors differed among the cell lines and the clones, the stabilizing effect of CTNNB1 was evident for all tested CB-expressing clones.

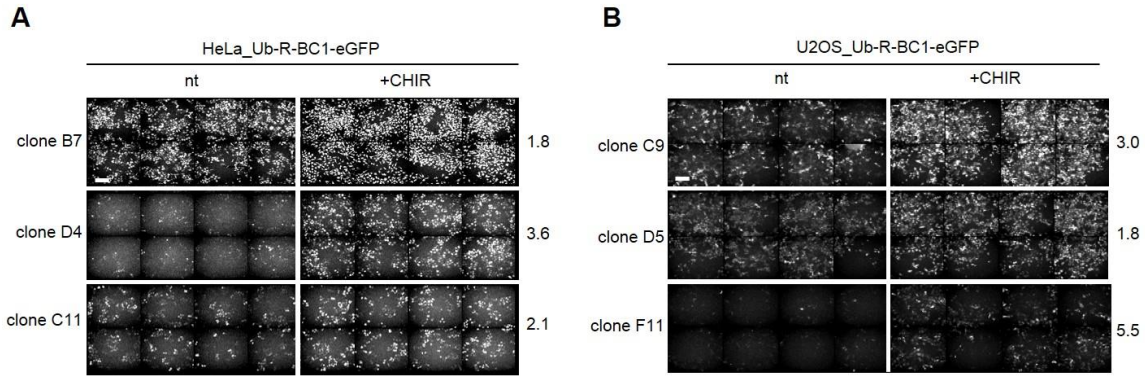

Figure 35 Initial characterization of three representative HeLa and U2OS cell clones stably expressing the turnover-accelerated Ub-R-BC1-eGFP.
*Parental HeLa and U2OS cells were transfected with expression construct coding for the turnover-accelerated Ub-R-BC1-eGFP CB. 24 h post transfection cells were subjected to selection with 0.5 mg/ml G418 for two weeks followed by single cell separation and cell expansion. Stable HeLa_Ub-R-BC1-eGFP cells (clone B7, D4 and C11 (**A**)) and stable U2OS_ Ub-R-BC1-eGFP (clones C9, D5 and F11 (**B**)) were treated with 10 µM CHIR for 16 h followed by quantitative imaging. Shown are representative images, scale bar 200 µm. Stabilization factor between non-treated and CHIR-treated cells are indicated on the right side of the respective image of each monoclonal cell line.*

As HeLa_Ub-R-BC1-eGFP (clone D4) and U2OS_Ub-R-BC1-eGFP (clone F11) exhibited the lowest CB ground level in combination with the strongest CTNNB1-mediated stabilization, these monoclonal cell lines were characterized in more detail. Thus, both cell lines were treated with a set of CTNNB1 level-elevating compounds (10 µM CHIR, 5 µM 6-bromoindirubin-3-oxime (BIO), 20 mM LiCl or the respective controls) and subjected to fluorescence live-cell microscopy followed by automated image quantification of CB

fluorescence (**Figure 36A, B**). All three tested compounds increased the CB fluorescence continuously for up to 24 h, whereas CHIR treatment in both cell lines had the most potent effect leading to ~19-fold elevated CB fluorescence for HeLa_Ub-R-BC1-eGFP and a 33-fold CB fluorescence increase for U2OS_Ub-R-BC1-eGFP normalized to the respective CB intensity at 0 h. After 24 h, treatment with LiCl resulted in ~7-fold and with BIO in ~4-fold enrichment of the turnover-accelerated CB in HeLa cells, whereas for the U2OS cell line the response to BIO led to ~10-fold and LiCl to ~6-fold enrichment, respectively.

Taken together, HeLa_Ub-R-BC1-eGFP (clone D4) and U2OS_Ub-R-BC1-eGFP (clone F11) were characterized to show weak CB ground level and display a strong stabilizing effect mediated by different compounds, which are described to elevate endogenous level of CTNNB1. For simplification both cell lines are referred to without indication of the respective clone ID in the following chapters.

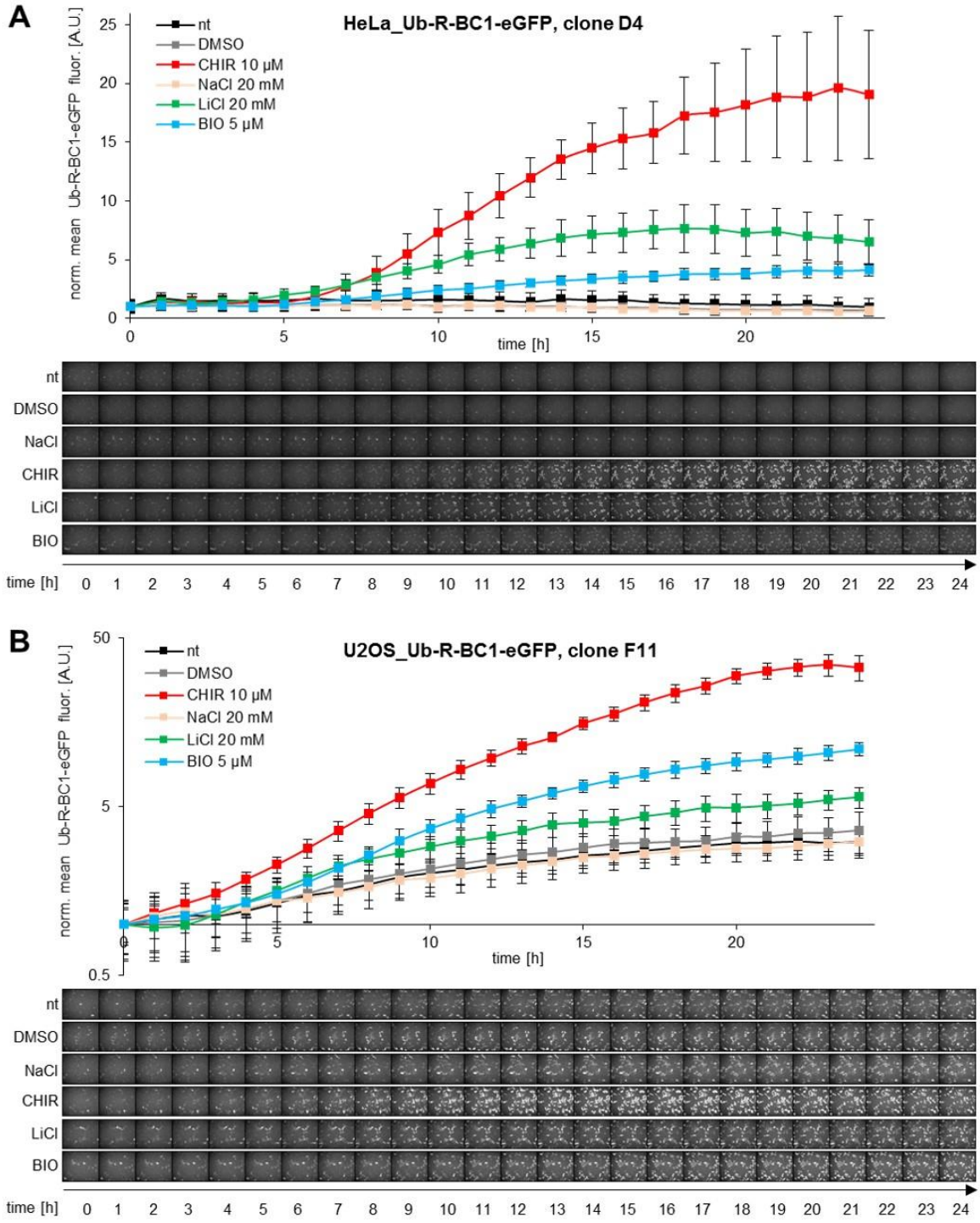

Figure 36 Characterization of HeLa and U2OS cell clones stably expressing the turnover-accelerated Ub-R-BC1-eGFP CB.

*(**A**) HeLa_Ub-R-BC1-eGFP (clone D4) and (**B**) stable U2OS_ Ub-R-BC1-eGFP (clone F11) were either treated with 10 µM CHIR, 5 µM 6-bromoindirubin-3-oxime (BIO) or 20 mM LiCl, or with respective controls (H_2O (nt) for CHIR, 0.01 % DMSO for BIO or 20 mM NaCl for LiCl treatment). Subsequently, cells were subjected to fluorescence live-cell imaging for 24 h followed by image quantification of CB fluorescence determined in nuclei, stained with Hoechst33258. Respective CB fluorescence was normalized to its value at 0 h and normalized values were plotted against time (n=2, >500 cells). Error bars: S.D. Below each graph representative images displaying CB fluorescence of each treatment over time are shown.*

5.4.1 Comparison of HeLa_BC1-TagGFP2 and HeLa_Ub-R-BC1-eGFP CB performance

To analyze whether the newly generated HeLa-Ub-R-BC1-eGFP cell line can be utilized to monitor changes in endogenous CTNNB1 more precisely compared to the original HeLa_BC1-TagGFP2 cell line, a detailed characterization was performed. To this end, changes of endogenous CTNNB1 upon treatment with CHIR for 20 h were analyzed in a population-wide manner by immunofluorescence staining in combination with the detection of Ub-R-BC1-eGFP CB fluorescence. Quantitative fluorescence imaging of HeLa-Ub-R-BC1-eGFP cells revealed that in absence of CHIR, CB fluorescence is nearly indistinguishable from autofluorescence of parental HeLa cells, whereas elevating endogenous CTNNB1 levels following CHIR treatment can be monitored by strongly increased CB fluorescence (**Figure 37A, B**). Notably, *in situ* detection of CTNNB1 showed that the mean CTNNB1 concentration was highly similar in parental HeLa and HeLa-Ub-R-BC1-eGFP cells, indicating that expression of the turnover-accelerated BC1-CB did not interfere with the amount of endogenous CTNNB1.

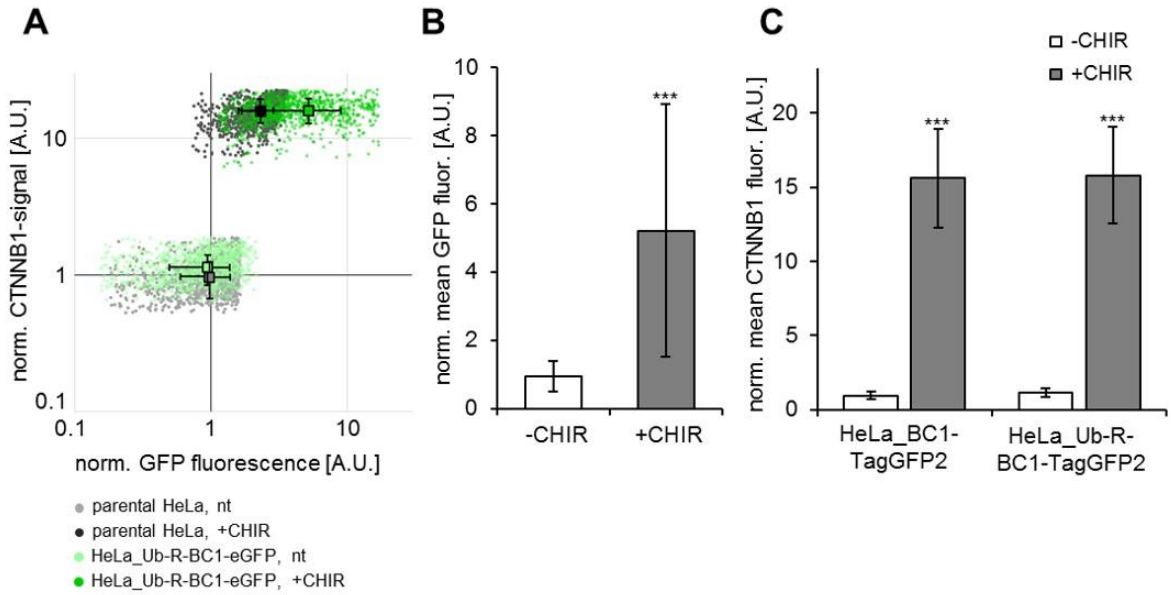

Figure 37 Further characterization of HeLa_Ub-R-BC1-eGFP.
*(**A-C**) Parental HeLa and HeLa_Ub-R-BC1-eGFP cells were treated with CHIR for 16 h and after fixation cells were stained with an antibody specific for CTNNB1. Cells were subjected to quantitative fluorescence imaging. (**A**) Population wide analysis of CTNNB1 immunofluorescence and Ub-R-BC1-eGFP signal intensity in HeLa_Ub-R-BC1-eGFP cells or autofluorescence in parental HeLa cells. Depicted are normalized fluorescence values within the 5th to 95th percentile of all analyzed cells. Number of analyzed cells: HeLa_Ub-R-BC1-eGFP – nt: n=1135, +CHIR: n=895; parental HeLa – nt: n=1053, +CHIR: n=1285. Squares illustrate mean fluorescence intensity of the analyzed population. Error bars: standard deviation (S.D.). (**B**) Bar chart of mean CB fluorescence of HeLa_Ub-R-BC1-eGFP cells analyzed in (A), error bars: S.D. (**C**) Bar chart of mean CTNNB1 antibody staining of non-treated and CHIR-treated parental HeLa and HeLa_Ub-R-BC1-eGFP*

*cells from (A). (B and C) Average fluorescence intensity was normalized to the non-treated control cells. Error bars: S.D., for statistical analysis student's t-test was performed, *** p < 0.001.*

To further compare the functionality of both BC1-CB variants, intracellular co-immunoprecipitation of Ub-R-BC1-eGFP was performed and compared with CB precipitation from HeLa_BC1-TagGFP2 cells. Therefore, cells were either left untreated or cultured in the presence of CHIR. After cell lysis, CBs were precipitated using the GFP-Trap. Western blot analysis of the input and bound fractions revealed that endogenous CTNNB1 is bound to a similar extent by both variants of the BC1-CB. (**Figure 38**).

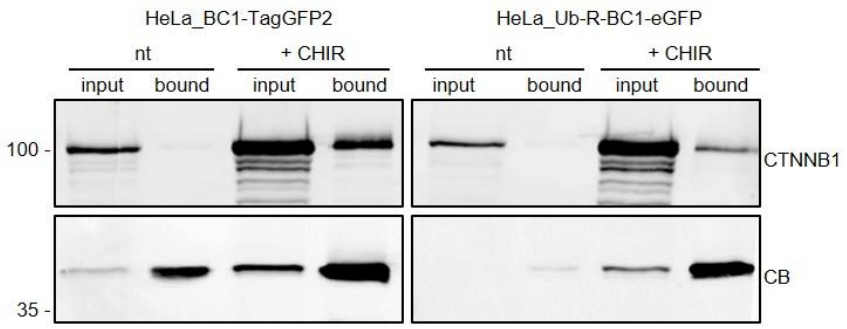

Figure 38 Turnover-accelerated Ub-R-BC1-eGFP intracellularly binding to endogenous CTNNB1 in HeLa_Ub-R-BC1-eGFP cells.
Stably expressing HeLa_BC1-TagGFP2 and HeLa_Ub-R-BC1-eGFP were stimulated with 10 µM CHIR for 20 h. After cell lysis CBs were precipitated with the GFP-Trap and input and bound fractions were subjected to SDS-PAGE followed by western blot analysis using CTNNB1-, TagGFP2- and eGFP-specific antibodies.

After successful demonstration that CHIR-induced CTNNB1 elevation was accompanied by rising CB level in HeLa_Ub-R-BC1-eGFP and verification of the binding capacity, the ability of utilizing the CB fluorescence to monitor reversible changes of endogenous CTNNB1 levels was directly compared between the original HeLa_BC1-TagGFP2 and the HeLa_Ub-R-BC1-eGFP cell line. Thus, both cell lines were cultivated in the presence of CHIR for 16 h. Subsequently, cells were washed and continuously cultivated. At the indicated time points after CHIR removal, cells were fixed and endogenous CTNNB1 levels were detected *in situ* by immunostaining. CTNNB1 antibody staining and BC1-CB fluorescence was detected by fluorescence imaging (**Figure 39A**). In both cell lines as well as in parental HeLa cells a ~12-fold increase of endogenous CTNNB1 upon CHIR treatment was calculated from the fluorescence images. Four hours after CHIR removal the levels of endogenous CTNNB1 returned to base level in both cell lines (**Figure 39B**). Accordingly, BC1-CB levels were also elevated upon treatment with CHIR after 16 h in both CB expressing cell lines. Notably, in cells expressing Ub-R-BC1-eGFP, the CB fluorescence

increased more strongly compared to the non-modified BC1-TagGFP2. Moreover, the CB fluorescence decreased more rapidly after CHIR removal, while in cells expressing BC1-TagGFP2 the CB signal remained at higher levels after removal of CHIR (**Figure 39C**).

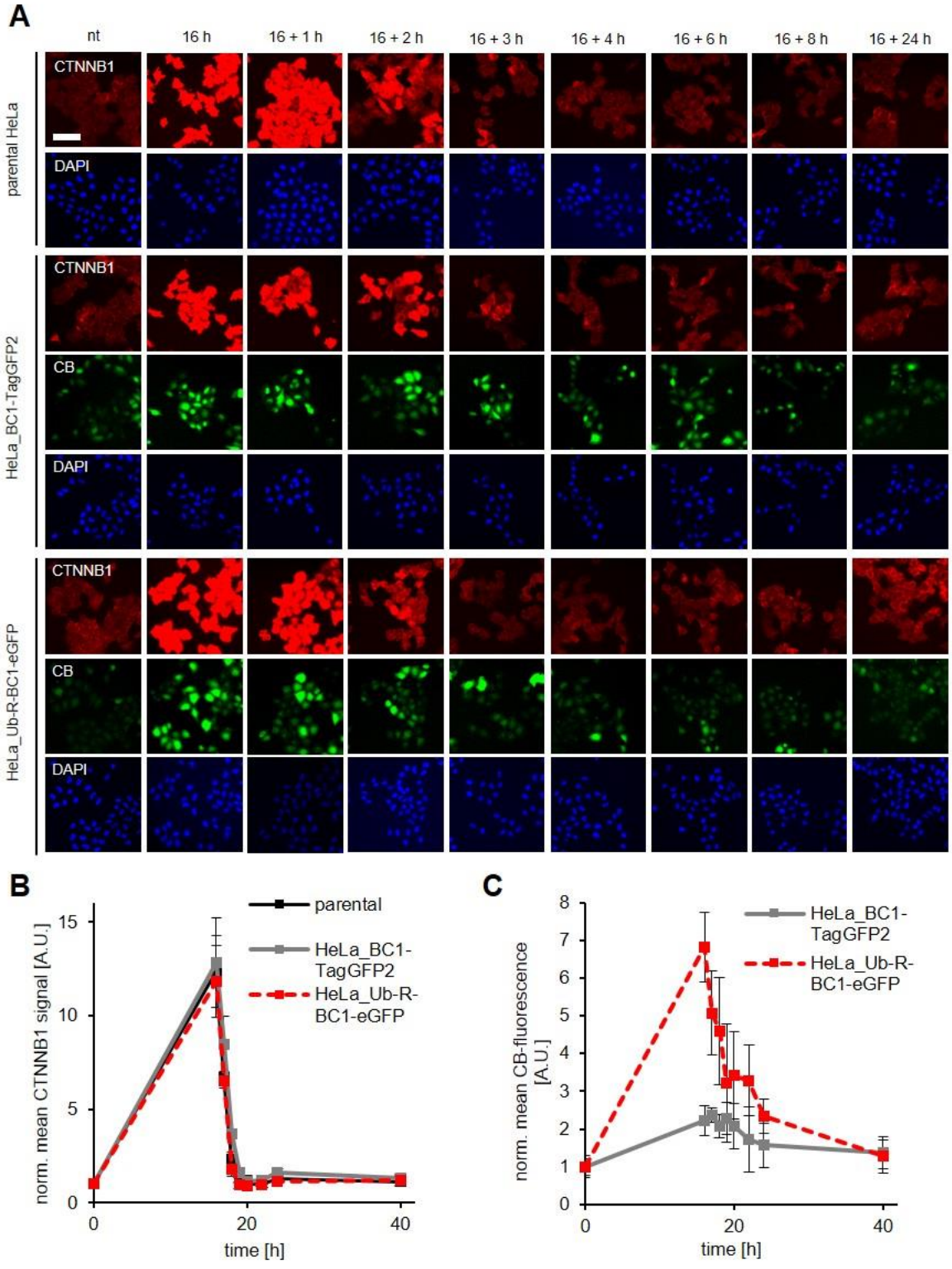

Figure 39 Microscopic analysis of CB dynamics in HeLa_Ub-R-BC1-eGFP and HeLa_BC1-TagGFP2 cells.

*(**A**) Parental HeLa, HeLa_BC1-TagGFP2 and HeLa_Ub-R-BC1-eGFP cells were either left non-treated (nt) or were treated with 10 µM CHIR for 16 h. CHIR was removed and after three times of washing cells were cultivated for up to additional 24 h. At the indicated time points, cells were fixed and immunostained with a CTNNB1-specific antibody. Shown are representative fluorescence images of the CTNNB1-staining and the CB signal. Nuclei were stained with DAPI, scale bar: 50 µm. (**B** and **C**) Quantification of CTNNB1 antibody-staining (B) and CB-fluorescence (C) in cell lines at the indicated time points as described in (A). Mean CTNNB1 signal intensity and mean CB fluorescence was normalized to the respective non-treated control in each cell line and the normalized values were plotted against time (n=3, >500 cells). Error bars: S.D.*

To assess the accuracy of CTNNB1 estimation by BC1-CB fluorescence, the ratio of normalized mean fluorescence (CTNNB1 / BC1-CB) was plotted against time in a graph (**Figure 40**). In an ideal model, CB fluorescence would be proportional to the amount of CTNNB1 at any given time. Consequently, the ratio of the normalized fluorescence values would always be 1. Comparing the overall divergence from the ideal model, the newly generated HeLa_Ub-R-BC1-eGFP clearly outperformed the original cell line. Numerical integration of overall divergence from the ideal model results in a value of 6.7 for HeLa_Ub-R-BC1-eGFP, whereas an integrated overall divergence of 16.05 was estimated the original HeLa_BC1-TagGFP2 cell line.

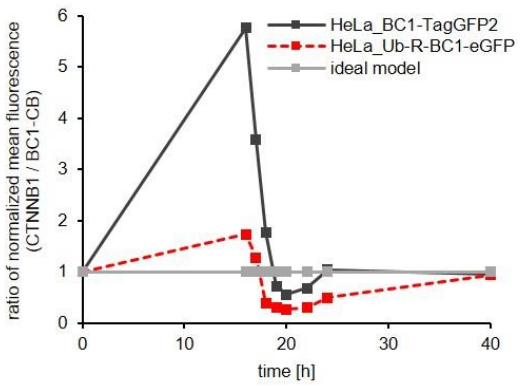

Figure 40 Comparison of CB performance in HeLa_BC1-TagGFP2 and HeLa_Ub-R-BC1-eGFP cells.
*The ratios of normalized CB fluorescence (CB / CTNNB1) derived from **Figure 39** were compared to an ideal model, where the ratio of the fluorescence values between the CTNNB1 signal and the CB fluorescence would be 1. This ideal situation is represented by the reference line parallel to x-axis. The graph shows that the overall divergence from an ideal model is smaller in the newly generated HeLa_Ub-R-BC1-eGFP cell line than compared to the old HeLa_BC1-TagGFP2 cell line.*

For additional validation, the CB's ability to monitor reversible changes of CTNNB1 was studied using a biochemical approach. Thus, cells were treated as described for **Figure 39**. At indicated time points, cells were harvested and soluble protein fractions were subjected to SDS-PAGE and immunoblotting. Subsequently, CTNNB1 and the CB levels were monitored by antibody staining (**Figure 41**). The results obtained from these biochemical studies are in line with the data obtained from fluorescence microscopy, which confirmed a

more rapid turnover of the Ub-R-BC1-eGFP upon removal of CHIR as compared with the original BC1-TagGFP2.

In summary, direct comparison of the original BC1-TagGFP2 and the turnover-accelerated Ub-R-BC1-eGFP clearly showed, that the turnover-accelerating modification substantially improved the ability of the CB to monitor reversible changes in the amount of endogenous CTNNB1 by AMCBS.

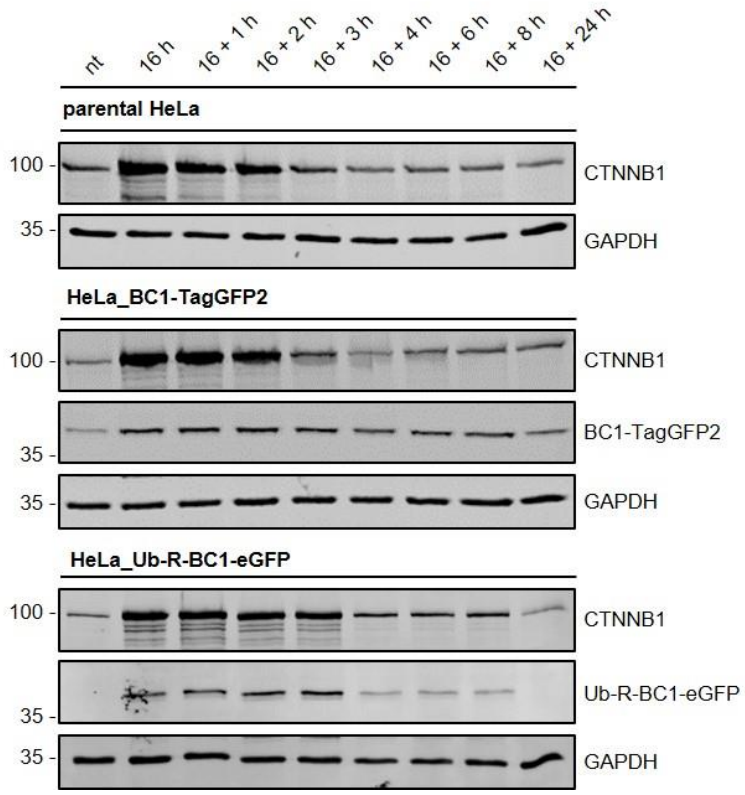

Figure 41 Comparison of CB performance by western blot analysis.
Parental HeLa, HeLa_BC1-TagGFP2 and HeLa_Ub-R-BC1-eGFP cells were treated as described in Figure 39. At the indicated time points soluble protein fractions were subjected to SDS-PAGE followed by immunoblot analysis. Shown are signals for endogenous CTNNB1, CBs (BC1-TagGFP2 and Ub-R-BC1-eGFP, detected with either TagCGY-specific or eGFP specific antibody) and GAPDH as loading control.

5.4.2 Monitoring the dynamics of turnover-accelerated BC1-CB in U2OS_Ub-R-BC1-eGFP cell line

To further validate the improved performance of the turnover-accelerated BC1-CB to monitor changes of endogenous CTNNB1, similar studies were performed in an additionally generated stable U2OS_Ub-R-BC1-eGFP cell line. Also in this cell line the basal CB expression was nearly indistinguishable from background fluorescence in non-treated cells (**Figure 42A**). Detection of endogenous CTNNB1 by antibody staining revealed that

treatment with CHIR resulted in ~5-fold elevated CTNNB1 level in parental U2OS and U2OS_Ub-R-BC1-eGFP cells, which recovered to basal level within 4 h after CHIR removal (**Figure 42B**). Moreover, the immunostaining shows that CTNNB1 dynamics was identical in the CB cell line and parental U2OS. This strengthens the assumption that the integration of the turnover-accelerated CB did neither impair endogenous CTNNB1 level nor CTNNB1 dynamics. The analysis of the CB dynamics demonstrated a corresponding ~5 fold increase induced by CHIR treatment, which recovered upon CHIR removal (**Figure 42B**). Based on these experimental data, U2OS_Ub-R-BC1 was implemented as a second model to monitor dynamic and reversible changes of endogenous CTNNB1.

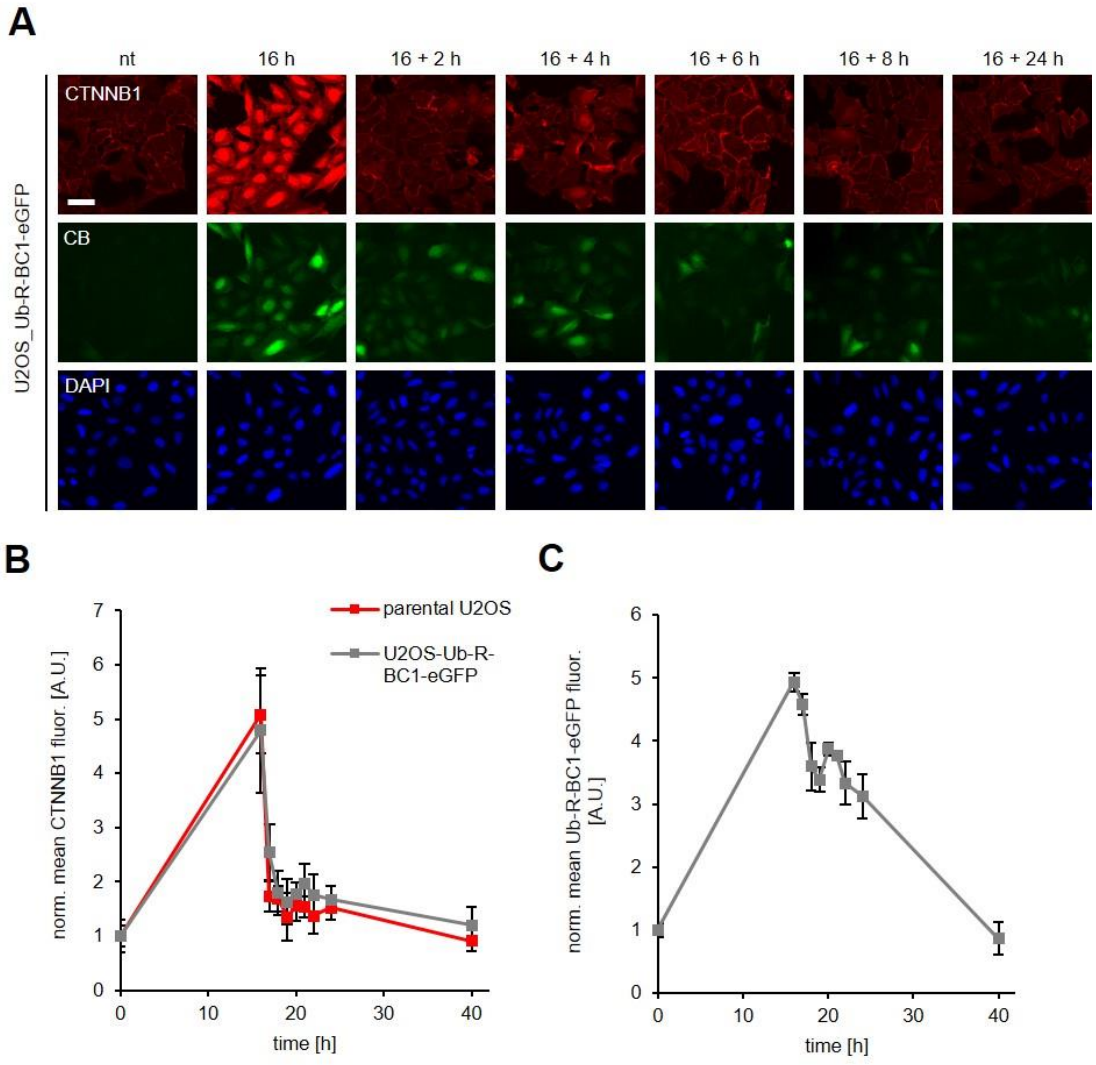

Figure 42 Dynamics of turnover-accelerated CB in U2OS_Ub-R-BC1-eGFP.
*U2OS_Ub-R-BC1-eGFP cells were either left non-treated (nt) or were treated with 10 µM CHIR for 16 h. Subsequently, CHIR was removed and after three times of washing cells were cultivated for up to additional 24 h. At indicated time points cells were fixed and immunostained with a CTNNB1-specific antibody.(**A**) Illustrated are representative fluorescence images of CTNNB1 staining and CB signal. Nuclei were stained with DAPI, scale bar: 50 µm. (**B** and **C**) Quantification of CTNNB1 antibody-staining (compared to parental U2OS cells, images not shown) (B) and CB-fluorescence (C). Mean CTNNB1 signal intensity and mean CB*

fluorescence was normalized to the respective non-treated control and the normalized values were plotted against time (n=3, >500 cells). Error bars: S.D.

Finally, to analyze a possible interference of the turnover-accelerated BC1-CB with CTNNB1 functionality, the expression levels of CTNNB1 and CTNNB1-responsive genes c-myc (MYC), axin-2 (AXIN2) and cyclin D1 (CCND1) were determined in parental and CB-expressing U2OS cells. MYC, AXIN2 and CCND1 are major WNT target genes that are upregulated upon WNT-pathway activation mediated by CTNNB1 activated transcription (He et al, 1998; Shtutman et al, 1999; Jho et al, 2002). For expression studies on RNA level, parental U2OS and U2OS_Ub-R-BC1-eGFP cells were either left untreated or treated with 10 µM CHIR for 8 and 16 h. Subsequently, mRNA was isolated from the cell lysates and reversely transcribed into cDNA followed by qRT-PCR analysis. No major differences in CTNNB1 or target gene expression were observed between parental and CB-expressing U2OS cells indicating that the presence of the CB did not impair CTNNB1 functionality as transcriptional co-activator (**Figure 43**).

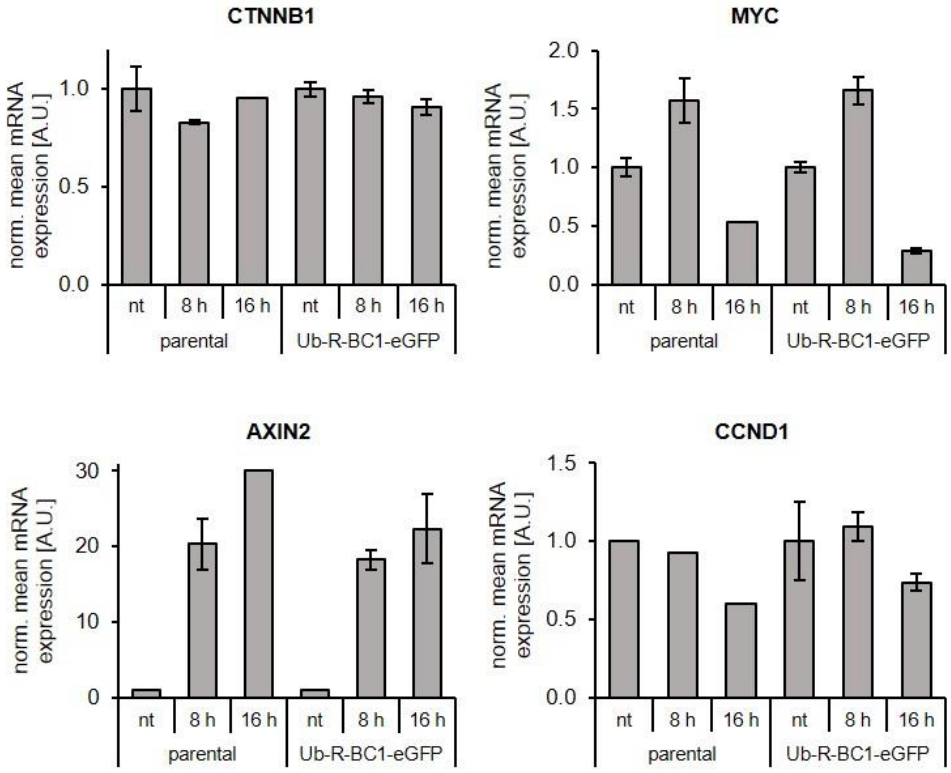

Figure 43 Analysis of CTNNB1 target gene expression in U2OS_Ub-R-BC1-eGFP cells.
Parental U2OS and U2OS_Ub-R-BC1-eGFP cells were either left non-treated (nt) or were treated with 10 µM CHIR for 8 and 16 h, respectively. Bar charts illustrate mRNA expression levels of CTNNB1, c-myc (MYC), axin-2 (AXIN2) and cyclin D1 (CCND1) quantified by qRT-PCR in relation to GAPDH (N=2). Error bars: S.D.

5.4.3 Application of U2OS_Ub-R-BC1-eGFP to monitor compound effects

In preclinical drug development the use of cellular *in vitro* models has strongly increased over the last years. These models serve as powerful tools to screen for novel drug candidates as well as to evaluate cellular compound efficacy. However, there are no methods available to continuously monitor dose-response and kinetics of drug action on the level of endogenous target proteins. Here, the turnover-accelerated BC1-CB expressing cell line U2OS_Ub-R-BC1-eGFP was applied to monitor the effect of two well established GSK3-β kinase inhibitors CHIR and BIO on endogenous CTNNB1 in a quantitative live-cell imaging setup by continuously imaging U2OS_Ub-R-BC1-eGFP cells upon incubation with different inhibitor concentration for up to 42 h. Images were taken every three hours (**Figure 44A**) and CB fluorescence was determined within cell nuclei (**Figure 44B**). For both inhibitors an overall dose dependency was detectable. Moreover, prolonged time-lapse image analysis revealed that higher inhibitor concentrations (>2.5 µM for CHIR and >5 µM for BIO) induced cell death after 30 – 36 h. Notably, differences in drug action kinetics were also detected. While concentration-independent for CHIR a maximum corresponding effect was observed after 22 h, which was then followed by a gradual decline of CB fluorescence, the effect of BIO reached a plateau at about 24 hours for non-toxic concentrations. Interestingly, the maximum tolerated concentration for both inhibitors (1 µM CHIR and 2.5 µM BIO) led to a similar increase in BC1-CB fluorescence of about 3.5-fold (**Figure 44B**). Although the molecular basis for the inhibitors' cytotoxicity might have multiple reasons including off-target effects, it could be possible that U2OS cells only tolerate a certain elevation of CTNNB1 for a defined period. Taken together, these data demonstrate that turnover-accelerated CBs in combination with quantitative imaging allow a precise determination of dose- and time-dependent compound effects on the level of individual endogenous proteins in living cells.

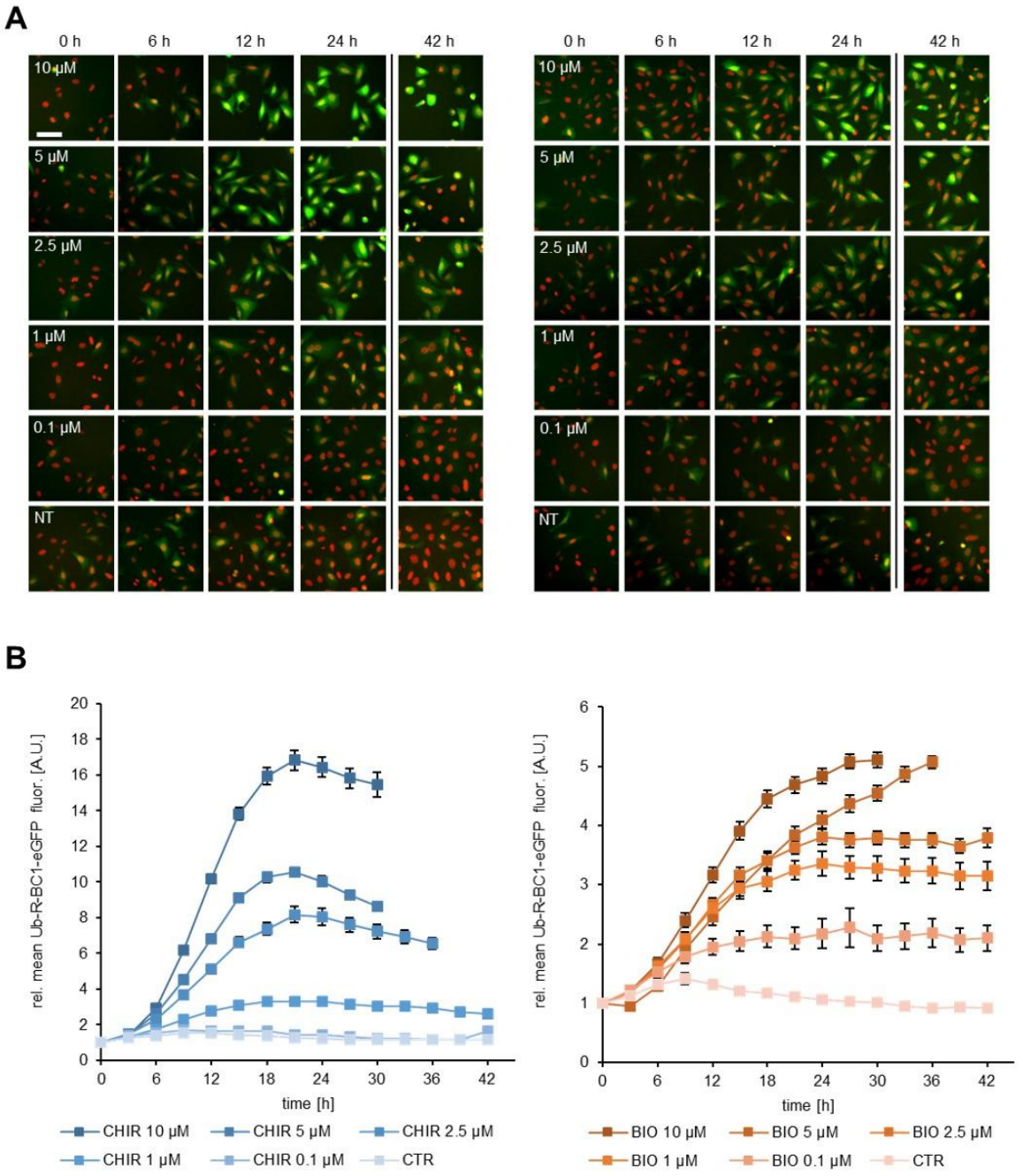

Figure 44 Monitoring kinetics of drug action in U2OS_Ub-R-BC1-eGFP cells
*(**A**) Respective fluorescence images of U2OS_Ub-R-BC1-eGFP cells either treated with indicated concentrations of CHIR (left panel) or 6-bromoindirumbin-3-oxime (BIO) (right panel) or with the respective NT controls (H_2O for CHIR and 0.01 % DMSO for BIO). For time-lapse imaging cells were stained with Hoechst33258 (depicted in red) and cells were continuously imaged every 3 h for up to 42 h. (B) Fluorescence intensity of nuclear CB-signal was quantified as described in **Figure 5**. Fluorescence values were normalized to the respective value at 0 h and plotted against time for a maximum of 42 h or until onset of cell death (N=2, >800 cells each). Error bars: S.E.M.*

5.5 Generation of cell lines expressing turnover-accelerated CBs stably integrated into the safe harbor AAVS1 locus

5.5.1 Long term expression stability of stable CB cell lines

To date, cell lines stably expressing a desired reporter system are widely used in biological and biotechnological research but generating a stable cell line, especially the isolation and characterization of a stable monoclonal cell line (as outlined in **Figure 34**) is still time consuming and labor intensive. Importantly, for larger screening campaigns using high-content imaging, the expression level of the reporter gene has to be consistently high over longer cultivation periods. As stable CB expressing cell lines are emerging tools in the field of high-content screening approaches (Schorpp et al, 2016), the expression level of the CB also needs a reliable consistency in cell culture. However, it was obsereved that quantitative imaging analysis often suffers from inconsistent CB expression levels and a strong cell-to-cell variance in CB fluorescence intensity (**Figure 45**).

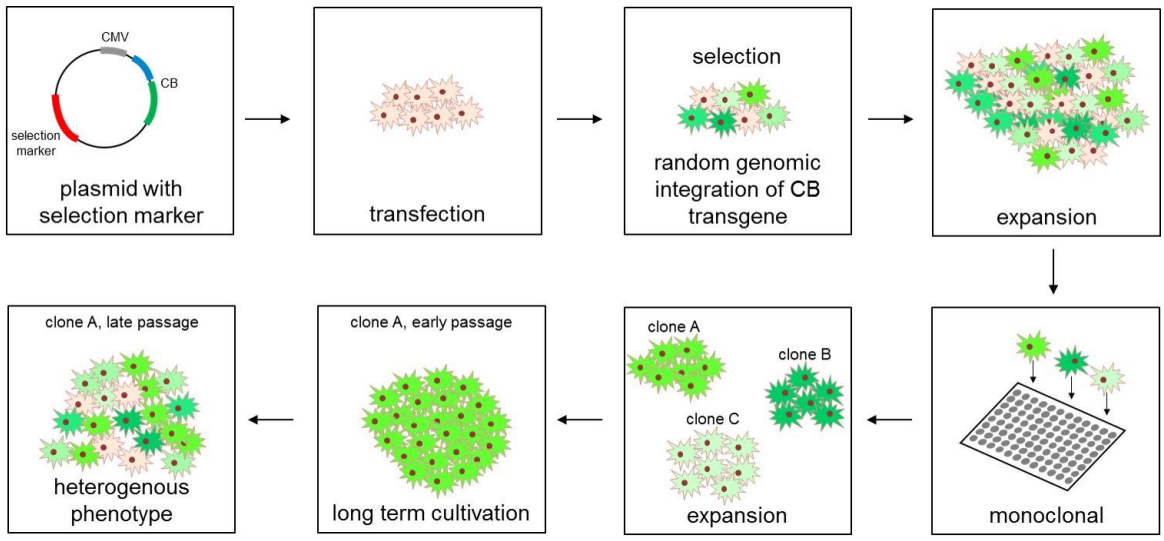

Figure 45 Schematic overview of stable CB cell line generation.
*Shown is the typical workflow of stable cell line generation following random genomic transgene integration (as described in **Figure 34**). The monoclonal cell line was characterized at an early passaged and displayed a homogenous phenotype regarding CB expression. However, at later passages (~20) the cell lines exhibit a heterogeneous CB expression, which limits their application in high-content image analysis.*

In general, the stability of the expression of a randomly integrated transgene (e.g. CB) over time can be affected by different effects. As the integration of the CB transgene occurs randomly, neither a prediction about the chromatin structure at the integration site can be made nor the number of transgene copies within the cellular can be foreseen. This genomic manipulation not only bears the risk to interfere with major cellular processes of the host cell

but can also lead to inconsistent CB signal intensities due to the integration of different copy numbers of the CB transgene and genomic position effects (Akhtar et al, 2013). Moreover, epigenetic silencing of the promoter upon continuous sub-culturing can occur (Xia et al, 2006). In addition, the generated stable cell line has to be cultured under constant selection pressure, which can alter cellular gene expression and metabolism (Rodolosse et al, 1998; Valera et al, 1994) or might directly affect genetic stability of the host cell (McDaniel & Schultz, 1993).

Notably, in the stable BC1-CB expressing HeLa cell line, which was generated by random integration of the CB expression cassette, an instability in CB expression over time was detected. Whereas low passages of the HeLa_BC1-TagGFP2 cells displayed a homogenous intercellular expression within this cell line, at high cellular passages the CB expression turned out to be quite heterogeneous within the monoclonal cell line (**Figure 46**).

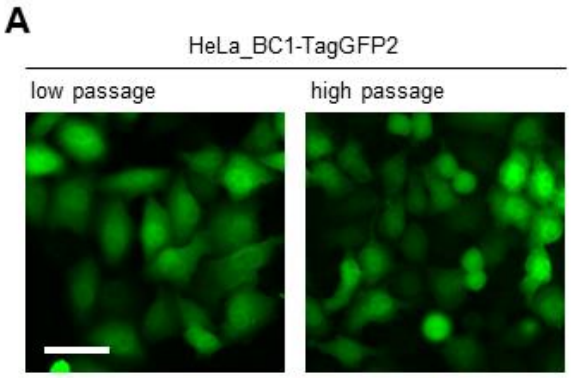

Figure 46 Stable HeLa_BC1-TagGFP2 cell line displays heterogeneity in CB expression at high cell passages.
Illustration of HeLa cells stably expressing the BC1-TagGFP2 CB in an early passage (passage number 4, left side) and at a high passage (passage number 20, right side). Scale bar: 50 µm.

To overcome these drawbacks in stable chromobody cell line generation, a new strategy was applied to generate stable cell lines with consistent CB expression over longer cultivation periods. Thus, it was aimed for a promoter less sensitive to epigenetic silencing in combination with targeted genomic integration of the CB transgene into the adeno-associated virus integration site 1 (AAVS1) safe harbor locus of human cells using CRISPR/Cas9 gene editing technology.

5.5.2 Comparison of transient CB expression from CMV-, EF1-α and β-actin promoter

To apply stable CB cell lines in high-content screening campaigns, a consistent high level transgene expression over an extended cultivation time is essential. One critical factor causing expression instability over time is epigenetic silencing of the transgene's promoter, which is mainly caused by DNA methylation (Krishnan et al, 2006; Yang et al, 2010) and histone modification (Paredes et al, 2013). The so far established stable CB expressing cell lines all contained a randomly integrated transgene driven by a constitutive CMV promoter, which is reported to be sensitive to silencing by DNA methylation (Hsu et al, 2010). To optimize the consistency of CB expression in long term culture, it was searched for a strong promoter, which is less prone to epigenetic silencing. In this context, the human elongation factor 1α (EF1-α) promoter and the human β-actin (h-βact) promoter were described to lead to medium-to-high expression levels within different cell lines (Damdindorj et al, 2014; Qin et al, 2010) and further both promoters maintain a stable expression level over several passages (Norrman et al, 2010; Damdindorj et al, 2012).

For comparative analysis the CMV promoter was replaced by the EF1-α or the β-actin promoter within the Ub-R-BC1-eGFP construct (**Figure 47A**). To analyze the expression level and the effect on AMCBS, the newly generated CB constructs were co-expressed in parental HeLa cells with either mCherry-CTNNB1 or mCherry as control and compared with the original CMV promoter containing CB construct. Fluorescence imaging revealed that the transient CB expression levels differed substantially between the different constructs (**Figure 47B, C**). CMV-driven CB expression led to the highest expression level within HeLa cells with a mean fluorescence intensity (MFI) of ~700 in mCherry transfected cells, which increased to a MFI of ~5,000 in the presence of the antigen. An intermediate strength in CB expression was determined for the EF1-α containing variant with mean fluorescence intensities of ~130 in absence and ~1000 in presence of mCherry-CTNNB1. The h-βact promoter driven expression resulted in very weak signals, which were close to background level. Interestingly, the antigen-mediated CB stabilization was not affected by the exchange of the promoter, as for all constructs similar factors of stabilization (8.5 – 9.7) were calculated, indicating that AMCBS was not affected by the promoter exchange (**Figure 47D**). Based on these results, the EF1-α appeared as promising candidate to generate stable CB cell lines combining expression strength with the maintenance of the stable expression level over prolonged cultivation time.

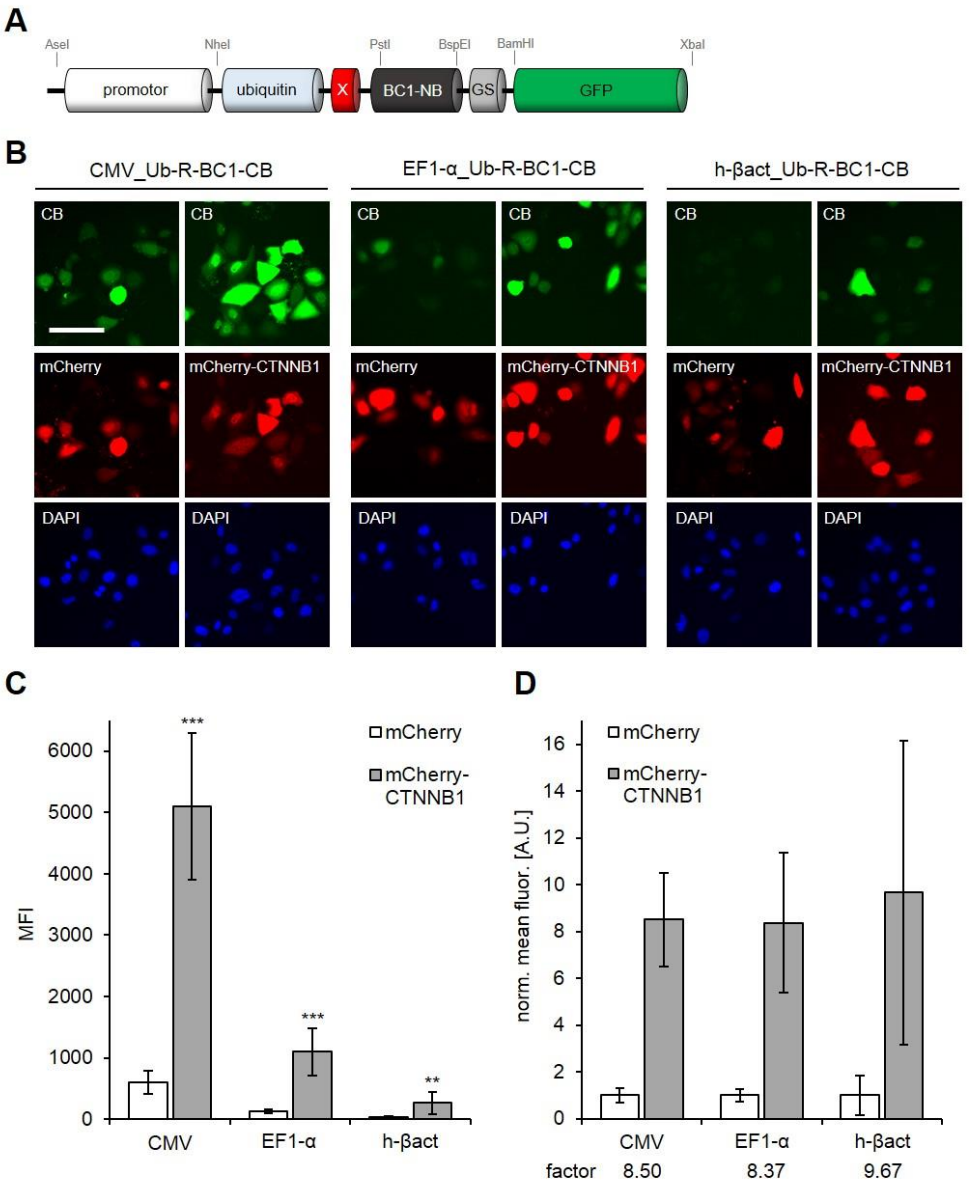

Figure 47 Quantitative image analysis of promoter-driven Ub-R-BC1-eGFP expression.
*(**A**) Schematic illustration of the chromobody expression construct containing AseI and NheI restriction sites to allow promoter exchange. (**B**) Representative images of HeLa cells transiently expressing the Ub-R-BC1-eGFP CB driven by different promoters (CMV, EF1-α and h-βact) in combination with either mCherry or mCherry-CTNNB1. Nuclei were stained with DAPI, scale bar: 50 µm. (**C**) Bar charts represent mean CB fluorescence detected in mCherry or mCherry-CTNNB1 co-expressing cells by quantitative fluorescence imaging (n=3, >100 cells each). (**D**) For every promoter construct mean fluorescence intensity (MFI) of the CB was normalized to the respective CB signal intensity determined in cells co-expressing mCherry, leading to the indicated stabilization factors. Error bars: S.D. Statistical analysis was performed using student's t-test, *** $p < 0.001$, ** $p < 0.01$.*

5.5.3 Design and construction of AAVS1 donor vector for site- directed stable integration of turnover-accelerated CBs

Besides using a constitutive promoter insensitive to silencing by DNA methylation, the selected genomic locus for the integration of the transgene plays a major role in the stability of the expression. Typically, the generation of stable CB cell lines is based on the

transfection of a cell line with a CB expression vector comprising a selection marker, which e.g. confers resistance to antibiotics.

Although this workflow was applied to generate numerous of stable CB cell lines some pitfalls have to be considered. As the integration of the CB transgene occurs randomly, the chromatin structure at the integration site can and the number of CB transgene copies within the cellular host cannot be predicted. Notably, the site of integration has a major effect on the cellular amount of the transgene summarized as positioning effect (Wurm, 2004). Additionally, such stable cell lines have to be continuously cultured under constant selection pressure, which has been reported to affect host cell physiology, genetic stability and metabolism (McDaniel & Schultz, 1993; Valera et al, 1994; Rodolosse et al, 1998). To address these shortcomings in the process of stable CB cell line generation and maintenance, a new protocol that allows site-directed integration of turnover-accelerated CBs into the host cell DNA by applying the CRISPR/Cas9 gene editing technique was established.

Recently, the adeno-associated virus site 1 (AAVS1, position 19q13.42), located in the first intron of the protein phosphatase 1 regulatory subunit 12C (PPP1R12C), was described as genomic safe-harbor (GSH) integration site (Kotin et al, 1992; Luo et al, 2014; Sekine et al, 2014; Oceguera-Yanez et al, 2016; Zhang et al, 2016; Sadelain et al, 2012). As transgene expression from this GSH integration site was previously reported to result in robust and persistent protein levels (Smith et al, 2008) and functional gRNAs for a CRISPR/Cas9-mediated integration have been described (Oceguera-Yanez et al, 2016), the AAVS1 locus was chosen as integration site for the turnover-accelerated CBs. For targeted engineering, a donor plasmid containing a turnover-accelerated CB expression cassette was designed, which is driven by an EF1-α promoter and flanked by AAVS1-specific homology arms (HA-L/R) (HA-L/R) (**Figure 48A**). Additionally, a puromycin resistance gene containing a splice acceptor site (SA) linked to a self-cleaving peptide sequence (T2A) was added. Upon correct genomic integration, the expression of the puromycin resistance will be driven by the endogenous PPP1R12C promoter, which allows specific selection of clones that underwent the desired CRISPR event. All fragments within the construct were sequence-optimized and the restriction sites as indicated (**Figure 48A**) allow an easy exchange of the different components including promoter, nanobody binding moiety and fluorescent marker. Additionally, a PCR-based genotyping strategy to verify clones comprising a correct transgene integration was adapted (illustrated in **Figure 48B**) (Oceguera-Yanez et al, 2016).

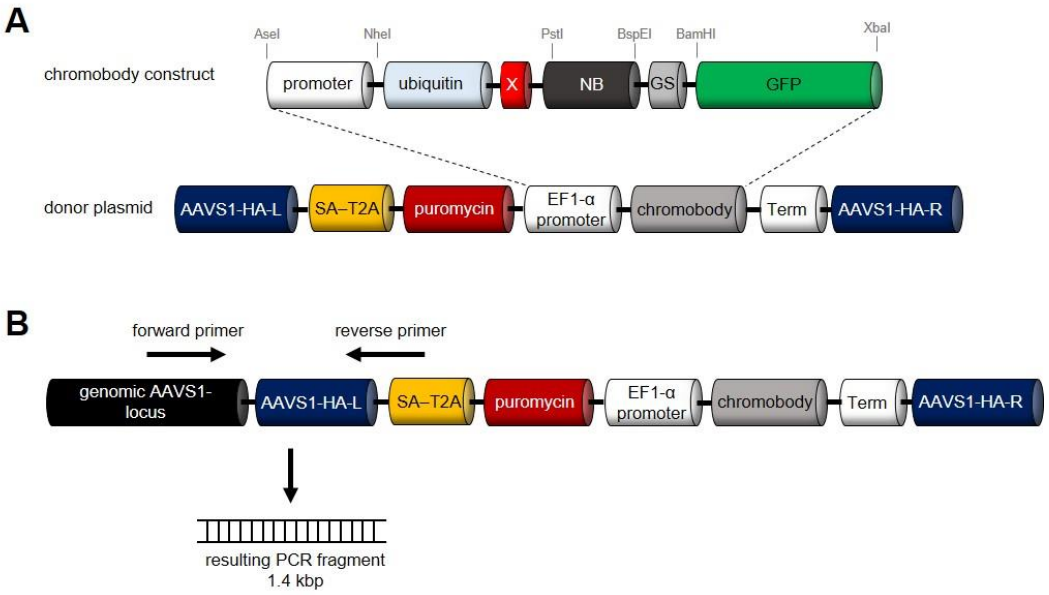

Figure 48 Strategy for stable integration of turnover-accelerated CBs into the human AAVS1 locus.
*(**A**) Schematic illustration of CB containing donor plasmid for stable integration into the human AAVS1 locus.*
*(**B**) Strategy for PCR-based genotyping of host cell DNA to verify site-directed integration.*

5.5.4 Site-directed integration of the turnover-accelerated Actin-CB into the AAVS1 locus

In order to test this strategy, a HeLa cell line with stable expression of an actin specific CB (ACT-CB) was generated (illustrated in **Figure 48**). The ACT-CB has been previously shown to bind to F-actin without affecting the dynamic reorganization of the cytoskeleton (Panza et al, 2015), thus the detection of the cytoskeleton provides a suitable read out to validate the functionality of the CB transgene upon CRISPR/Cas9 mediated integration. In a first step, HeLa cells were co-transfected with plasmids encoding for (i) Cas9 nuclease and the respective gRNA for the AAVS1 locus (Oceguera-Yanez et al, 2016) and (ii) donor plasmid containing the turnover-accelerated ACT-CB (Ub-R-ACT-CB). 24 h after transfection cells were subjected to selective pressure by addition of puromycin for two days to enrich cells that underwent stable AAVS1 integration of the CB transgene. Two cell clones clearly showing actin structures (referred as B5 and B6) were isolated (**Figure 49A**). Both cell clones were similar in cell morphology and size, and displayed a homogenous expression of the ACT-CB. However, it was noticed that the fluorescence intensity of clone B5 was slightly higher compared to clone B6 (**Figure 49B**). PCR-based genotyping (as outlined in Figure 48B) revealed for clone B6 an amplicon at the expected size of ~1400 bps (**Figure 49C**). This indicates that a correct CB transgene integration at the AAVS1 locus

was only obtained for clone B6, which was further verified by sequence analysis of the PCR fragment.

In addition, a qualitative comparison of the morphology of the novel CRISPR-engineered HeLa_AAVS1_Ub-R-ACT-CB cell line with a stable ACT-CB expressing HeLa cell line, previously generated by random integration of a CMV-driven non-turnover-accelerated ACT-CB, was performed (**Figure 49D**). In the CRISPR-modified HeLa_AAVS1-Ub-R-ACT-CB cells a more homogenous cell morphology and CB expression level was observed and additionally less CB aggregates were detected.

Taken together, these findings demonstrate that the outlined CRISPR strategy based on the stable integration of optimized CB transgenes in the AAVS1 locus of human cells is suitable and facilitates the generation of stable CB reporter cell lines.

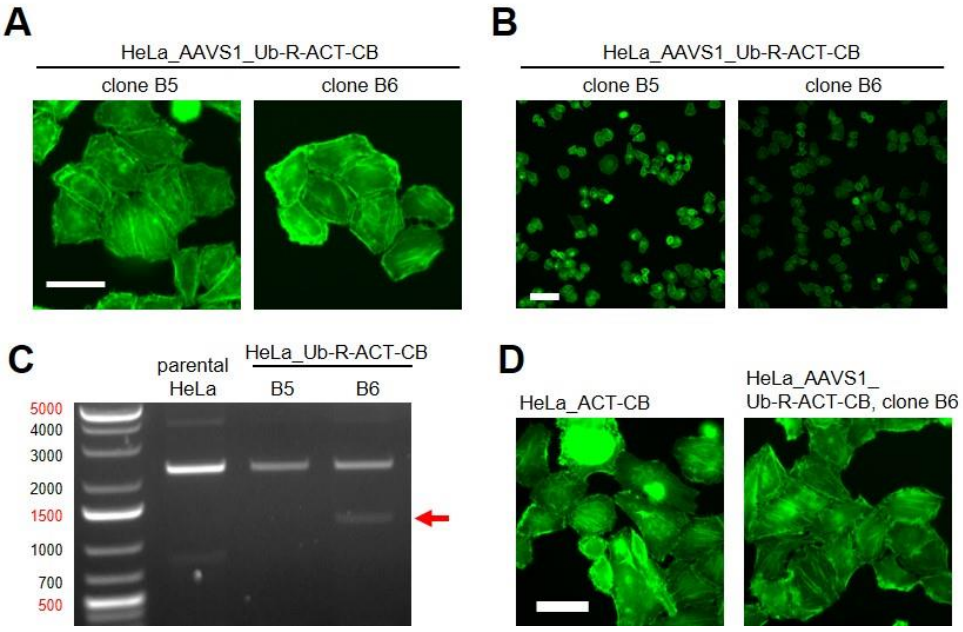

Figure 49 Generation of a HeLa cell line expressing Ub-R-ActinNB-eGFP stably integrated into the AAVS1 locus by using CRISPR/Cas9 technology.
*(**A**) Fluorescence images of two CRISPR-engineered HeLa cell clones expressing ACT-CB scale bar 50 µM. (**B**) Comparison of fluorescence intensity between HeLa_AAVS1_Ub-R-ACT-CB clone B5 and B6, scale bar 100 µm. (**C**) Genotyping of HeLa_AAVS1_Ub-R-BC1-CB clones B5 and B6 in comparison to parental HeLa cells. Genomic DNA of the monoclonal cells was extracted and subjected to PCR using the genotyping strategy illustrated in **Figure 48**. Shown are resulting PCR products (indicated by arrow) on a 1 % agarose gel stained with ethidiumbromide. (**D**) Representative fluorescence images of HeLa cells stably expressing the respective ACT-CB. Left image illustrates HeLa_ACT-CB cells generated by random integration of the non-modified ACT-CB. The right image shows HeLa_AAVS1_Ub-R-ACT-CB cells generated by site-directed integration of the ubiquitin-modified ACT-CB. Scale bar: 50 µm.*

5.5.5 Site-directed integration of the turnover-accelerated BC1-CB into the AAVS1 locus of human CRC cell lines

Finally, it was aimed to generate cell lines, which are suitable to monitor changes in endogenous protein concentration upon compound treatment by quantitative image analysis of the CB signal. In previous studies it was demonstrated that the CTNNB1-specific CB (BC1-CB) traces changes in the levels of transcriptionally active, hypophosphorylated CTNNB1 upon induction of the WNT pathway (Traenkle et al, 2015). Motivated by the studies of this thesis, the intention within this last chapter was to generate more sophisticated CB cell models to monitor the effects of compounds on the reduction of endogenous CTNNB1 levels by following the BC1-CB signal.

Colorectal cancer (CRC) is the third leading cause of cancer-related deaths in 2018 with over 1,000,000 new cases worldwide (Bray et al, 2018) and in ~90 % of CRC tumors WNT signaling pathway is mutated (The Cancer Genome Atlas Network, 2012) resulting in an accumulation of transcriptionally active CTNNB1 (White et al, 2012). As the WNT pathway is considered as major driver of colorectal carcinogenesis, it is not surprising that a lot of effort is put into the development of WNT modulating therapeutics. To date, several WNT modulating agents have been successfully identified within screening campaigns using TOP-flash reporter assays (Gonsalves et al, 2011; Emami et al, 2004; Huang et al, 2009). Although a broad range of inhibitors have been identified within this experimental setup, one major drawback is the endpoint assay nature by using a luciferase-based gene reporter. Analyzing drug response in living cells is preferable since information about drug kinetics can be obtained and no decision regarding the endpoint of the assay is required. As demonstrated with the U2OS_Ub-R-BC1-eGFP cell line, the turnover-accelerated BC1-CB is well suited to monitor drug action in response to WNT-inducing compounds (**Figure 44**). Consequently, the next question was whether the effect of inhibitory WNT-signaling compounds can be portrayed by the turnover-accelerated BC1-CB. Thus, two human colorectal carcinoma (CRC) cell lines DLD-1 and HCT116, which both are described to have elevated levels of active CTNNB1 (Ahmed et al, 2013), were used to generate stable cell lines expressing the turnover-accelerated BC1-CB.

For generation of the donor plasmid the actin binding moiety (ACT-NB) was replaced by the CTNNB1 binding nanobody BC1 using PstI and BspEI restriction site as outlined in **Figure 48** and the CRISPR strategy was followed as described above. Following puromycin

selection single clones of DLD-1 and HCT116 cells displaying green fluorescence were identified, which were isolated and further expanded (**Figure 50A**). To confirm correct CB integration at the AAVS1 locus PCR-based genotyping as illustrated in **Figure 48B** was performed (**Figure 50B**). In DLD-1_AAVS1_Ub-R-BC1-CB and HCT116_AAVS1_Ub-R-BC1-CB cells lines PCR products at ~1400 bps were detected (**Figure 50B**), which were absent in the parental cells. Sequence analysis of the amplicons further verified that the CB transgene was successfully integrated in both cell lines into the AAVS1 locus.

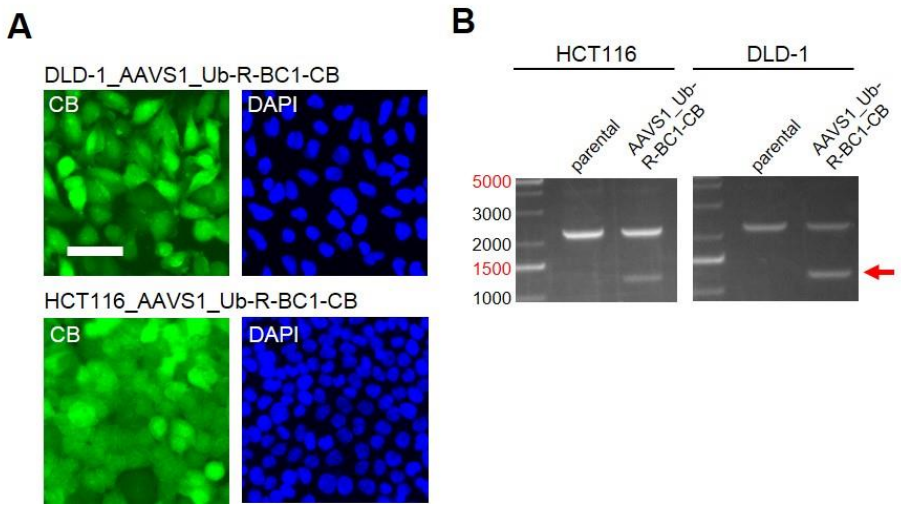

Figure 50 Generation of CRC cell lines with AAVS1 integration of turnover-accelerated BC1-CB.
*(**A**) Representative fluorescence images of isolated DLD-1 (upper panel) and HCT116 (lower panel) clones stably expressing Ub-R-BC1-CB. Nuclei were stained with DAPI, scale bar: 50 µm. (**B**) Genotyping of HCT116_AAVS1_Ub-R-BC1-CB and DLD-1_AAVS1_Ub-R-BC1-CB. Genomic DNA of host cells was extracted and subjected to PCR using genotyping strategy illustrated in **Figure 48** (PCR product indicated by arrow).*

In addition, the phenotype of a monoclonal DLD-1 cell line generated by random integration of the non-modified BC1-CB with the newly generated DLD-1_AAVS1_Ub-R-BC1-CB cell line was compared by fluorescence imaging. For the DLD-1_AAVS1_Ub-R-BC1-CB cells a more homogenous phenotype regarding cell size, shape and CB fluorescence, while the conventional DLD-1_BC1-CB cells displayed a more heterogeneous morphology accompanied by miscellaneous CB signal intensities.

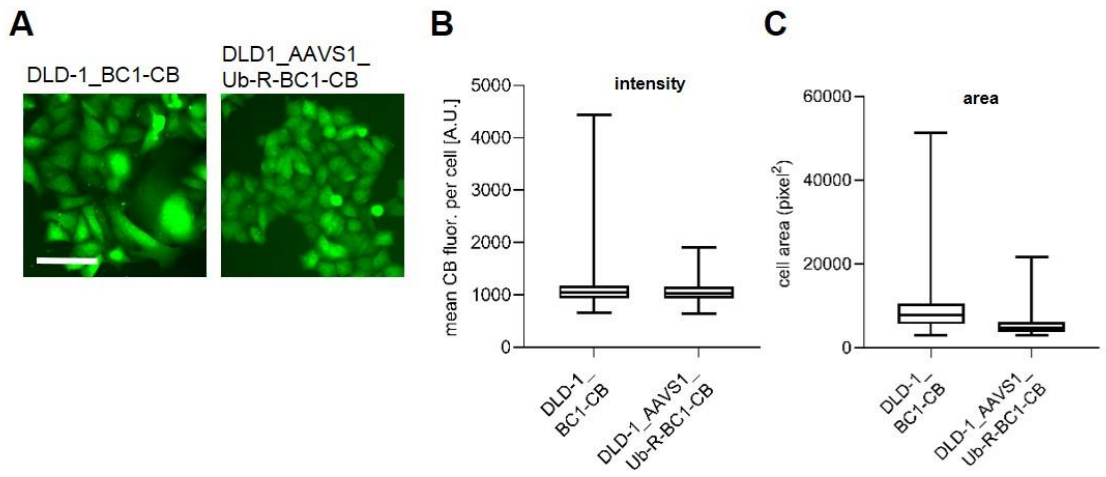

Figure 51 Comparative analysis of DLD-1_BC1-CB and DLD-1_AAVS1_Ub-R-BC1-CB cell line.
*(**A**) Representative fluorescence images of DLD-1 cell lines stably expressing the indicated BC1-CB. Left image shows DLD-1_BC1-CB cells generated by random integration of the non-modified BC1-CB. The right image shows DLD-1_AAVS1_Ub-R-BC1-CB cells generated by site-directed integration of the ubiquitin-fused BC1-CB. Scale bar: 50 µm. (**B** and **C**) Fluorescence images of DLD-1_BC1-CB cells and DLD-1_AAVS1_Ub-R-BC1-CB as shown in (A) were subjected to quantitative image analysis. Using a customized image segmentation algorithm the mean fluorescence of the CB (**B**) and the cell area (**C**) were determined for each individual cell. Number of analyzed cells: DLD-1_BC1: n=2478; DLD-1_AAVS1_Ub-R-BC1-CB: n=2090.*

Finally, the novel generated DLD-1_AAVS1_Ub-R-BC1-CB cell line was applied to monitor the effect of two compounds FH535 and XAV939, which were previously reported to affect the level of endogenous CTNNB1 (Handeli & Simon, 2008; Yao et al, 2011). Time-lapse imaging of DLD-1_AAVS1_Ub-R-BC1-CB was performed for 24 h followed by quantitative analysis of CB fluorescence in the nucleus upon incubation with different inhibitor concentrations (**Figure 52A, B**). By monitoring the BC1-CB fluorescence, a strong reduction of CTNNB1 to ~ 50% upon treatment with 10 and 50 µM of FH535 was observed after 6 h. For XAV939 milder effects indicated by a reduction to ~80 % at only the highest concentration of 10 µM after 12 h were detected. To verify whether the decreased CB fluorescence actually reflects a reduction of hypophosphorylated CTNNB1, immunoblot analysis of DLD-1_AAVS1-Ub-R-BC1-CB cells treated either with DMSO as control or 10 µM FH535 for 24 h was performed (experiments were performed by the Master student Melissa Weldle). While only a minor effect of compound treatment for total CTNNB1 was observed, hypophosphorylated CTNNB1 was clearly reduced upon treatment with FH535 in the soluble protein fraction.

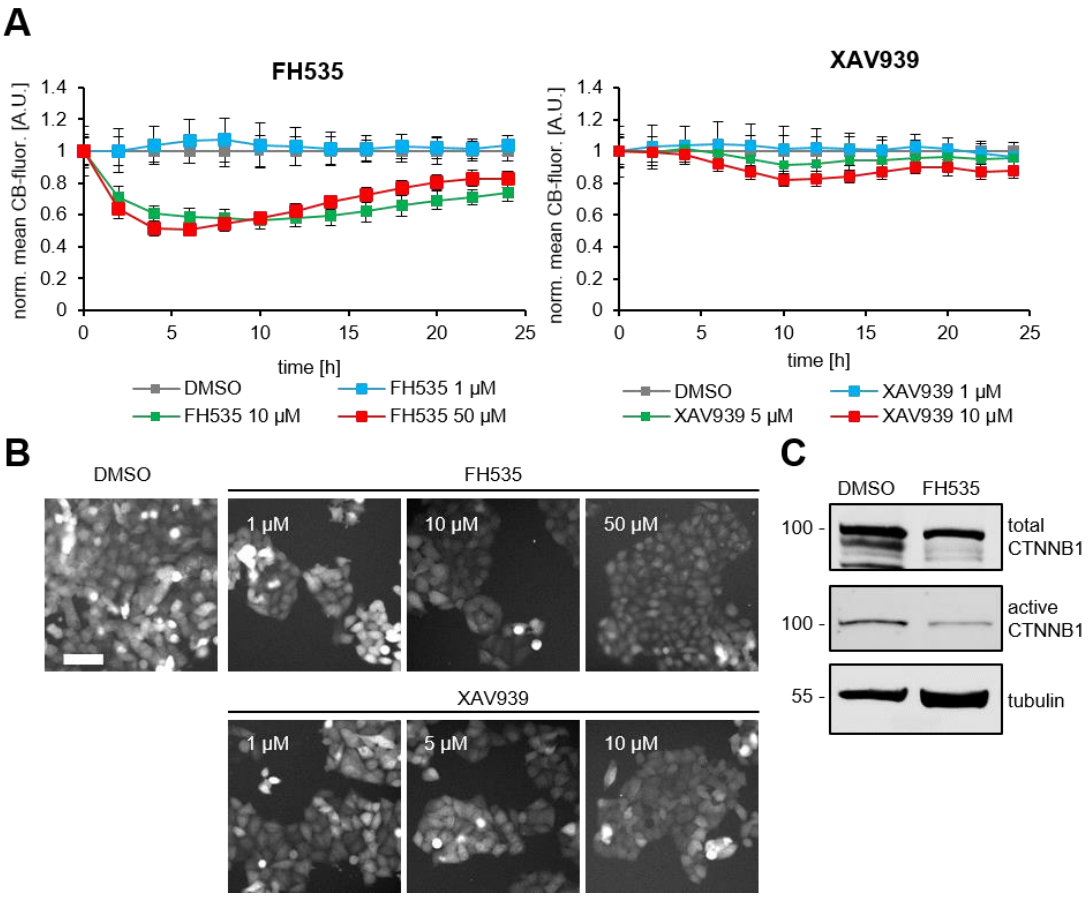

Figure 52 Quantification of nuclear CB fluorescence in DLD-1_AAVS1_Ub-R-BC1-CB cells upon compound treatment.
*(**A**) DLD-1_AAVS1_Ub-R-BC1-CB were either treated with the indicated concentrations of FH535 or XAV939 or with 0.01 % DMSO as control were continuously imaged every 2 h for up to 24 h. Fluorescence intensity of nuclear CB-signal was quantified and the fluorescence values were normalized to DMSO and plotted against time (n=2, >200 cells each). Error bars: S.D. (**B**) Fluorescence images of DLD-1_AAVS1_Ub-R-BC1-CB cells upon treatment with indicated compounds. Representative fluorescence images are shown 12 h after treatment, scale bar: 50 µM. (**C**) DLD-1_AAVS1_Ub-R-BC1-CB were either treated 10 µM FH535 or with 0.01 % DMSO as control for 24 h. Cells were lysed using 0.5 % NP40 lysis buffer and equal protein amounts of the soluble fraction were subjected to SDS-PAGE followed by immunoblot analysis using antibodies specific for total CTNNB1, active CTNNB1 and tubulin as loading control.*

Taken together, these data demonstrate that the CRISPR-based strategy to introduce turnover-accelerated CBs at a defined genomic locus results in CB cell models that enables a precise determination of dose- and time-dependent compound effects on the level of individual endogenous proteins in living cells using quantitative imaging.

6 DISCUSSION

The analysis of endogenous protein dynamics in living cells substantially contributes to a better understanding of physiological processes. During the last years, chromobodies have emerged as valuable scientific research tools to analyze spatiotemporal dynamics of corresponding endogenous antigens within living cells. Recently, it was noticed for the CTNNB1-specific BC1-CB that the CB technology not only allows to target and trace endogenous proteins but also the fluorescence intensity of the CB can be utilized for relative quantification of changes in endogenous protein concentration by an effect termed "**A**ntigen-**M**ediated **CB S**tabilization" (AMCBS) (Traenkle et al, 2015).

In this dissertation, further evidence of AMCBS was found for four different CBs targeting (i) the transcriptional co-activator CTNNB1, (ii) DNA-replication-associated PCNA, (iii) the intermediate filament vimentin and (iv) the HIV capsid protein (CA). The antigen levels in stably CB expressing cell lines have been either elevated by ectopic expression (CTNNB1, CA), or antigen expression was induced by chemical compounds (CHIR, BIO and LiCl for CTNNB1) or cytokines (TGF-β for vimentin). Additionally, siRNA-mediated antigen depletion was monitored by a corresponding decrease in CB fluorescence (vimentin and PCNA). Given the fact that similar observations of an antigen dependency of NBs and CBs have been described by other groups (Blanco-Toribio et al, 2010; Tang et al, 2016), here a depletion of the antigen was illustrated by following the CB fluorescence intensity for the first time. However, monitoring rapid changes in endogenous CTNNB1 concentration by the BC1-CB displayed an inaccuracy that could be explained by differences in turnover rates of CB and antigen. Furthermore, small changes in antigen concentration might not be detected as these minor changes might be lost in the noise of non-antigen bound CB. To precisely detect rapid as well as small changes in antigen concentration, a strong CB expression and a high CB turnover is required, which consequently lead to a low basal amount of antigen-independent CBs within a cellular expression system. To address these issues, turnover-accelerated CBs were generated by utilizing the N-end rule and the ubiquitin fusion technique, thereby identifying Arg as N-terminal residue contributing to an accelerated CB turnover. After generating a cell line stably expressing a turnover-accelerated version of the CTNNB1-specific CB (HeLa_Ub-R-BC1-TagGFP2), the CB was compared with the originally described BC1-CB (Traenkle et al, 2015). By analyzing the rapid decrease in CTNNB1 concentration upon induction and subsequent removal of CHIR, the turnover-accelerated Ub-R-BC1-eGFP CB clearly outperformed the original BC1-CB in regard to

accuracy. With a second generated stable cell line (U2OS_Ub-R-BC1-eGFP) dose response and kinetics of drug action were monitored for two CTNNB1-elevating compounds (CHIR and BIO), illustrating the potential application in preclinical drug development. Since in the development of stable reporter cell lines the maintenance of reporter expression over an extended cultivation time is essential, a protocol to stably integrate turnover-accelerated CBs into the AAVS1 safe harbor locus by applying CRISPR/Cas9 gene editing, was established. This approach was used to generate a HeLa cell line with site-directed safe harbor integration of a turnover-accelerated actin-specific CB (HeLa_AAVS1_Ub-R-ACT-CB). Additionally, by applying this strategy two colorectal cancer cell lines, comprising mutations within the WNT pathway, were genetically engineered to express the turnover-accelerated BC1-CB (DLD-1_AAVS1-Ub-R-BC1-eGFP and HCT116_AAVS1-Ub-R-BC1-eGFP) and applied in quantitative imaging using CTNNB1 targeting compounds.

In the following chapters the obtained results and observations are critically discussed with respect to the current state of the art in the analysis and quantification of endogenous proteins, established chromobody and intrabody systems and reporter cell line generation. Finally, an outlook addressing possible expansions and application opportunities of turnover-accelerated CBs will be provided.

6.1 Studying protein dynamics by chromobodies

Proteins are among the most important macromolecules of cells and living organisms and as they have to fulfill key regulatory functions for maintaining cellular functionality, these molecules need to be strictly regulated. Besides regulatory mechanisms as for instance PTMs, also the protein abundance itself can exhibit a regulatory function, which is orchestrated by the cellular amount of the specific protein. Thus, quantifying highly dynamic regulatory proteins like CTNNB1 not only contributes to the understanding of basic regulatory mechanisms but also helps to decipher the mechanisms of disease development and progression. However, the majority of the methods used to study endogenous proteins are endpoint assays, which require cell fixation and/or lysis. Considering the dynamic nature of proteins like CTNNB1, the analysis in living cells within the physiological environment is desirable. In addition, proteins such as CTNNB1 or VIM are strictly regulated in their intracellular levels and cannot be analyzed using an ectopic expression without altering the physiological state of the cells (Mendez et al, 2010; Spencer et al, 2006). Addressing this aspect, different CBs have been established to target and trace endogenous proteins in living

cells (Zolghadr et al, 2012; Traenkle et al, 2015; Panza et al, 2015; Maier et al, 2015; Burgess et al, 2012; Buchfellner et al, 2016; Irannejad et al, 2013). Moreover, some of these CBs have already been applied to monitor protein or DNA dynamics in whole organisms without functional interference (Panza et al, 2015; Jullien et al, 2016). Nevertheless, the ectopic expression of a CB and its possible interference within a cellular system has to be critically evaluated for each developed molecular probe. Given the fact that CBs can bind to concave-shaped epitopes (e.g. active sites of enzyme), this characteristic of affinity binders can lead to a functional interference (Genst et al, 2006). Notably, in their initial study in 2015, Traenkle et al. have described three CTNNB1-specific CBs (BC1, BC6, and BC9), whereas only the BC1-CB was shown to not interfere with the transcription of WNT-target genes upon treatment with CHIR and LiCl. This interference could be explained by the epitopes of BC6 and BC9 within the armadillo domain of CTNNB1, which is known to interact with a high number of other proteins (Hulsken, 1994; Behrens, 1998; Yang et al, 2002; Akiyama et al, 2004; Essers et al, 2005; Valenta et al, 2012). In contrast to BC6 and BC9, the BC1 epitope is located at the N-terminus of CTNNB1, thus it could be speculated that binding of the BC1 to this epitope does not sterically hinder important endogenous interacting proteins. Besides the identification of the epitope, the affinity of intrabodies in general seems to be important for generating functional molecular probes for live-cell imaging, wherein transient binding affinity molecules are highly desirable (Cassimeris et al, 2013). Whereas the affinity of a binding molecule can be determined easily *in situ* by various methods like surface plasmon resonance (Liedberg et al, 1983), the intracellular affinity might differ substantially. Firstly, the cellular milieu contains various factors, which are absent in the *in situ* assessment of the affinity. Secondly, the epitope of the POI recognized by the affinity binder might be masked by interacting proteins and vice versa. Addressing these factors, fluorescence recovery after photobleaching (FRAP) provides a method to analyze the intracellular binding kinetics and has been applied to study the interaction of an intrabody with the cognate antigen (Maier et al, 2015; Jullien et al, 2016). In this dissertation, the influence of the BC1-CB and the turnover-accelerated Ub-R-BC1-CB was analyzed by comparative analysis of CTNNB1 in parental cells and respective stable CB expressing cell lines. The CHIR-induced elevation of CTNNB1, as well as CTNNB1 recovery after CHIR removal, was highly similar in parental and stable CB expressing cell lines (**Figure 39, Figure 41, Figure 42**). Furthermore, the expression of the WNT target genes MYC, AXIN2 and CCND1 after CHIR treatment showed also no significant differences between parental U2OS and U2OS_Ub-R-BC1-CB cells (**Figure 43**). In summary, it is essential to exclude a possible effect of the CB

on its cognate antigen to obtain a nanoprobe suitable for live-cell imaging. FRAP analysis provides a suitable approach to analyze the intracellular affinity. Furthermore, comparative specific functional studies must be tailored onto the characteristics of the corresponding antigen, such as gene expression analysis of WNT target genes for CTNNB1 or analysis of the cell invasion after EMT induction between parental A549 and A549_VB6 cells (Maier et al, 2015).

6.2 Quantification of endogenous proteins by AMCBS

This study demonstrates that relative changes in the amount of a specific protein can be determined by simply following the CB fluorescence, an observation termed antigen-mediated CB stabilization (AMCBS). After illustrating this phenomenon for four different CBs (BC1-CB, αCA-CB, CCC-CB, VB6-CB) it can be hypothesized that this observation could be transferred to a wider range of CBs. Recently, two other studies presented similar conclusions of CBs being stabilized in the presence of their cognate antigens in mammalian cells, thereby strengthening the hypothesis of AMCBS as a more general characteristic of CBs (Blanco-Toribio et al, 2010; Tang et al, 2016).

Moreover, in the field of recombinant protein production using *E. coli*, a stabilizing effect of GST on a GST-specific V_HH fused to a SNAP-tag was described (Bossi et al, 2010). In addition, this study further illustrates that the antigen-induced stabilizing effect might be irrespective of the reporter moiety fused to the V_HH domain. Regarding the application in mammalian cells, reporter systems like luciferase fused to the NB moiety could provide an interesting expansion of the system, since bioluminescence might exhibit a lower detection limit, thus especially low abundant proteins could benefit from NB-luciferase fusions (Troy et al, 2004). However, by using a luciferase-based reporter the capability for real-time assessment of the antigen would be restricted and it has to be considered that luciferase comprises a MW of ~60 kDa, resulting in a NB-luciferase fusion of ~75 kDa. Consequently, this increase in MW could exhibit a steric hindrance in epitope accessibility, blockage of interacting factors or reduced nuclear import of the molecular probe (Marfori et al, 2011).

The question whether the antigen-mediated stabilization is an exclusive feature for V_HHs and V_HS or can be transferred to other protein-based intrabodies (e.g. scFvs, affibodies, DARPins) was not addressed in this work. But an analogous antigen-stabilizing observation was described for a scFv-based molecular probe (Sibler et al, 2005), indicating that this phenomenon is applicable for other kinds of affinity binder.

Interestingly, the aforementioned study as well as in the study of (Tang et al, 2016), a stabilization of the CB or scFV-based reporter was only observed after reducing the molecular probe ground level through introduction of destabilizing framework mutations or addition of a PEST sequence. In contrast, the CBs tested in this study already displayed an antigen-mediated stabilization in an unmodified condition. This might be explained by the fact that the initial observations of this effect have been obtained in context of a stable monoclonal BC1-CB expressing cell line (Traenkle et al, 2015), where a clone with a low-to-moderate basal CB expression was selected. Moreover, the additional experiments using unmodified CBs (αCA-CB, CCC-CB and VB6-CB) to illustrate the AMCBS phenomenon have also been performed using stable monoclonal cell lines. However, in transiently co-transfected HeLa cells the stabilizing effect of ectopically expressed CTNNB1 on the BC1-CB was evident, although the 1.7-fold increase in CB fluorescence was moderate.

In conclusion, different studies (Tang et al, 2016; Sibler et al, 2005; Bossi et al, 2010; Blanco-Toribio et al, 2010) reported an antigen stabilizing effect on an intrabody, thereby strengthening the presented results within this dissertation. A detailed explanation of this effect was neither provided in the aforementioned studies nor was the mechanism deciphered in this work, but the generated results allow room for speculations about the underlying mechanism.

Applied as an intracellular molecular probe, the CB expression itself is driven by a constitutive promoter and in antigen absence the CBs are constantly degraded leading to a steady-state level of CB molecules per cell. Antigen exposure increased the CB fluorescence, which represents the number of CB molecules within the cell. Since the CB expression is not altered, the remaining variable lies within the CB degradation rate. The results obtained in this study strongly suggest that CBs are degraded via the UPS, which is in agreement with the results reported by (Tang et al, 2016). In general, for proteasomal degradation specific E3 ubiquitin ligases recognize a target protein. Subsequently, this leads to an ubiquitinylation of nearby lysine residues, thereby priming the molecule for a degradation and finally the proteasome requires unstructured initiation regions in order to degrade to ubiquitinylated protein (Varshavsky, 2011). Based on this mechanism, it can be assumed that antigen binding might interfere with two critical steps of proteasome targeting: the accessibility of E3 ubiquitin ligases and the unstructured initiation sites. The principle of short-living proteins being stabilized via an interaction with another protein is well accepted (Campanero & Flemington, 1997; Johnson et al, 1998), thus this observation could also

provide an explanation for the AMCBS phenomenon. Additionally, the formation of an CB-antigen complex leads to an increase in MW of the CB and it is demonstrated that smaller target proteins are degraded more efficient than larger proteins or protein complexes (Hortin & Murthy, 2002). However, the molecular mechanisms leading to this effect can be manifold. It can be hypothesized that binding of a CB to the cognate antigen could compete with binding of E3 ubiquitin ligases or the CB-antigen interaction might mask the ubiquitinylation site of the CB. Moreover, the paratope forming CDRs of the nanobody moiety could function as initiation sites for proteasome degradation, since these areas can be defined as unstructured regions. As a consequence of antigen binding, these sites are masked and no longer accessible as initiation site. Despite this direct influence on the UPS-based degradation, the enhancement in molecular weight upon antigen-CB complex formation might further contribute to the stabilization by reducing the mobility of the complex. Since complex formation leads to a reduced diffusion (Verkman, 2003; Sibler et al, 2005), resulting in a decreased stochastic probability of a CB getting in close proximity to a proteasome.

Consequently, these presented mechanisms in context with the obtained results lead to the assumption that the intracellular affinity of the CB might be a key determinant of the AMCBS phenomenon. This hypothesis is further supported by the observation that the stabilization factor after antigen increase was irrespective of the absolute number of CBs within the cell. By exchanging the promoter for ectopic Ub-R-BC1-CB expression in HeLa cells, the absolute number of CB molecules differed within the cells, which is illustrated by the different fluorescence intensities in antigen absence. Interestingly, after ectopic CTNNB1 expression the obtained stabilization factors were nearly similar (~9-fold, **Figure 47**) for all constructs. However, the intracellular affinity is hard to provide, since the intracellular environment provides a complex dynamic black box containing a wide range of variables.

One restriction of this quantification method is provided by the fact that no general statement regarding the sensitivity of an AMCBS-based quantification approach can be provided. A clear statement about the minimal change in antigen concentration that can be portrayed by changes in CB fluorescence intensity cannot be made. The sensitivity might be mainly determined by the intracellular affinity of the CB, thus each CB would require a separate analysis of the sensitivity. Moreover, the sensitivity to monitor an increase in antigen concentration might differ in the accuracy in monitoring an antigen decrease. The accuracy

regarding an increase is mainly defined by CB expression and maturation, whereas the turnover of the CB might be the key determinant to monitor an antigen decrease.

In summary, this approach provides an easy readout since a fluorescence microscope is the only equipment required and the subsequent analysis can be easily performed with open-source software such as ImageJ. In general, it would be also possible to consider a readout system relying on a conventional plate reader, thereby simplifying the analysis and reducing the amount of data. But it has to be considered that some data regarding e.g. cell viability or CB distribution cannot be analyzed by using a plate reader.

The evidence from this work in context of the discussed studies implies that by following the CB fluorescence signal a conclusive prediction about the antigen abundance can be provided. However, the detailed elucidation of the underlying mechanism resulting in an antigen-mediated CB stabilization remains to be answered in the future.

6.3 Optimization of the chromobody technology

6.3.1 Generation of turnover-accelerated CBs to determine changes in antigen concentration more precisely

The initial observations of a CB signal intensity correlating with the protein amount of the cognate antigen were obtained after a substantial change in antigen concentration was induced in a longer time frame (e.g. 24 h after ectopic antigen expression or 72 h post siRNA-mediated antigen knockdown). To accurately monitor rapid and/or small changes in antigen concentration a low basal amount of unbound CB is beneficial. Notably, this is a general issue for intracellular reporter systems applied in live-cell imaging approaches. It is expected that the molecular probe exclusively stains its cognate antigen but freely diffusible affinity binder might prevent the specific detection of the co-localization. As the number of molecular probes for live-cell imaging is constantly growing, several approaches addressing this problem have been described until now.

One straightforward approach to ensure a low intrabody ground level is the usage of a weaker promoter for the expression, since a classical viral-driven expression (e.g. CMV) leads to a high level of the ectopically expressed protein. Recently, the SV40 early and human β-actin promoter have been applied to express different scFV-based intrabodies for live-cell imaging (Freund et al, 2014; Rinaldi et al, 2013). Another system to reduce the amount of unbound intrabody was provided by fusing a zinc finger DNA-binding domain with a KRAB

transcriptional repressor to an intrabody. Additionally, a zinc finger DNA binding domain was inserted upstream the CMV promoter of the molecular probe, thereby generating a negative feedback mechanism blocking the transcription of the intrabody by unbound molecules (Gross et al, 2013). Although both approaches improved the visualization quality of the respective antigens by the molecular probe, these approaches would not improve the quantification of rapid and strong increases in antigen concentration since the expression level of the intrabodies might be too low and their expression delayed. Thus, a reduction on CB protein level rather than on the expression level is preferable.

In this dissertation three approaches to reduce the amount of unbound CB on protein level have been tested: (i) the introduction of destabilizing framework mutations (ii) the addition of a C-terminal PEST sequence and (iii) generation of CB comprising a turnover accelerating N-terminus.

To reduce the amount of unbound intracellular NBs, recently distinct point mutations within CB framework regions were described, resulting in subsequent destabilization of the NBs (Tang et al, 2016). Upon antigen exposure, the destabilized NBs get conditionally stabilized and thus can be applied to detect or manipulate antigens in living cells. By transferring the point mutations S70R and S113F to the BC1-CB slightly reduced CB ground level and improved stabilization factors could be detected after antigen exposure. However, analysis the $BC1^{C70Y}$-TagGFP2 mutant showed that the introduction of the mutation abolished binding to CTNNB1. To circumvent the generation of non-functional binding molecules due to introduced framework mutations, the next approach was a C-terminal addition of a PEST domain in order to rapidly degrade the modified protein (Rechsteiner & Rogers, 1996), which is a widely applied approach to reduce intrabody and reporter level in general (Li et al, 1998; Leclerc et al, 2000; Sibler et al, 2005). The addition of the PEST sequence to the αCA-CB and BC1-CB resulted in a substantial decrease in CB fluorescence but for the BC1-CB this reduction was accompanied by accelerated cell death after transient transfection of the plasmid encoding for BC1-TagGFP2-PEST. The reasons for the onset of accelerated cell death was not further addressed but it can be speculated that the accelerated CB degradation might affected endogenous CTNNB1 due to the strength of the PEST sequence. Recently, nanobody-PEST fusions have been applied to acitvely reduce the endogenous protein amount of α-synuclein, an important protein in Parkinson disease (Joshi et al, 2012; Chatterjee et al, 2018). This example illustrates that addition of the PEST sequence to a NB or CB can result in an enhanced degradation of the cognate antigen.

Finally, in this dissertation the concept of the N-end rule, a key determinant of a protein's half-life, was applied to reduce the amount of unbound CBs. To identify N-terminal residues conferring a faster CB turnover, the ubiquitin fusion technique was implemented. After generation and testing of BC1-CB constructs containing every amino acid, the N-terminal amino acids Phe, Ala and Arg were identified, which is in line with other studies that analyzed the impact of the N-terminus on protein half-lives. Notably, Ala exclusively enhanced the turnover of BC1-CB constructs, irrespective of the fused fluorescent moiety, whereas no enhancement in turnover was observed for the Ala containing variants of α-CA-CB or VB6-CB. A further advantage of applying the ubiquitin fusion technique to transiently expressed CBs, was a less CB aggregation compared to the unmodified version. In addition, differences in turnover velocities were also detected for the different fluorescent moieties analyzed in this study (TagGFP2, eGFP, TagRFP and mCherry). In both cases, this effect can be explained by differences in number and positioning of lysine residues accessible for ubiquitinylation by E3 ligases. In this dissertation the development of a widely applicable strategy to reduce CB ground level was focused, whereby Arg was identified as most turnover accelerating amino acid. An enhanced degradation rate for Arg was observed for different CBs (BC1, VB6 and αCA), different FPs (TagGFP2, eGFP, TagRFP and mCherry) and in different cell systems (HeLa, U2OS and A549), leading to the assumption that it might be generally applicable for the generation of turnover-accelerated CBs.

6.3.2 Further possible optimizations of CB-based molecular probes to quantify endogenous proteins

As this study focused on the optimization of the CB degradation to precisely quantify dynamic changes of endogenous antigens, also the CB expression could be addressed. For the quantification of a rapid and strong antigen increase, an excess in CB expression is advantageous to ensure a precise response of the CB. Consequently, CB expression limiting factors can be found within the expression rate and maturation time of the CB.

The CB expression in the generated cell lines was driven by a strong CMV or EF1α promoter. To further enhance the CB expression, mRNA stabilizing components could be integrated into CB vector design. The insertion of a woodchuck hepatitis virus post-translational regulatory element (WPRE, ~600 bps) serves as an enhancer of gene expression in mammalian cells and could therefore easily be added (Brun et al, 2003; Klein et al, 2006). The molecular mechanisms of WPRE functionality are not fully understood, but may involve

RNA processing and mRNA export (Loeb et al, 1999). To further increase the CB expression, C-terminally added polyadenylation could confer an enhanced CB mRNA stability (Hager et al, 2008).

In this dissertation, four different FPs have been tested regarding their degradation rate when expressed as CB construct. But not only the degradation velocity might be different, also the maturation time of FPs vary ranging from only a few minutes (e.g. mGFPmut2) to several hours (mScarlet or mRuby3) (reviewed in (Balleza et al, 2018)). In addition, when aiming for an application as molecular probe in live-cell imaging, attention regarding the photostability of the FP should be paid (Crivat & Taraska, 2012). Exemplarily mGFPmut3 is reported to be the fastest maturing FP in the green category but its low photostability makes it a poor choice for time-lapse microscopy (Balleza et al, 2018).

By applying FPs in scientific research, various proteins have been analyzed in cell biology. As GFP was fused to a broad range of POIs, it was noted that some compounds such as salicylic acid can interfere with the fluorescent signals of FPs *in vivo* (Jonge et al, 2017). To exclude a possible interference, it is therefore essential to have reliable controls when aiming for a chromobody-based readout in applications like drug discovery. For example a cell line stably expressing a corresponding FP, to exclude undesired side effects of the compound on the FP, could be used.

Taken together, besides optimizing the CB degradation the FP maturation as well CB expression could be addressed to ensure an accurate antigen representation by the CB, whereas these modification might mainly influence the ability of illustrating rapid and strong antigen increases.

6.4 Site-directed integration of turnover-accelerated CBs by engineering the AAVS1 locus

To further optimize the stably CB expressing cell lines regarding the maintenance in long term cell culture, a new protocol utilizing CRISPR/Cas9-mediated gene editing was established. The standard method to generate stably CB expressing cell lines was transfection of a CMV-driven CB expression plasmid containing a specific selection marker followed by selection with appropriate antibiotics. However, this method neither allows a prediction of the CB integration site nor the number of integrated copies can be foreseen. Additionally, it has been demonstrated for different transgenes and cell lines that a CMV

promoter is prone to silencing via DNA methylation (Balleza et al, 2018). A similar effect was observed in this dissertation, wherein the CB expression changed towards a more heterogeneous and weaker phenotype over several passages. Comparative analysis revealed that usage of the EF1-α promoter results in a strong CB expression and is furthermore reported being suitable for long term culture (Norrman et al, 2010; Qin et al, 2010; Damdindorj et al, 2012). Moreover, CTNNB1-mediated BC1-CB stabilization was also evident for EF1-α-driven expression.

Overcoming the drawback of CB random integration, the application of CRISPR/Cas9 gene editing technology attained a robust and targeted transgenesis of the CB into AAVS1 safe harbor locus of DLD-1, HCT116 and HeLa cells. As in this study the CB integration within the monoclonal cell lines was exclusively analyzed by PCR genotyping, no information regarding a heterozygous or homozygous AAVS1 integration, or possible off-target integrations can be provided. Analysis of homo- or heterozygosity could be performed by junction PCR using primers binding outside the homology arms or by Southern blot (Koch et al, 2018). Notably, PCR-based genotyping of HeLa_AAVS1_ACT-CB cell clones revealed for one clone no AAVS1 site-specific integration. For further validation, the analysis of possible nuclease-based off-target effects should be performed, which are frequent side effects of the CRISPR/Cas9 approach (Fu et al, 2013). *In silico* analyses allow the prediction of preferred gRNA targeting sites, which could be pre-selected and analyzed via genomic PCR-based genotyping. However, for an unbiased and comprehensive analysis whole genome sequencing might be accomplished to detect off-target mutations (Zischewski et al, 2017). The implementation of Cas9 nuclease mutant variants (nickases) such as Cas9-D10A or Cas9n could further reduce off-target activity by 50- to 1,500-fold (Mali et al, 2013; Ran et al, 2013), but this would require a re-design of AAVS1-specific gRNAs. Furthermore, it is also worth mentioning that the established protocol is restricted to the human AAVS1 locus, as in mice the ROSA26 locus might be used as safe harbor for genomic engineering (Sadelain et al, 2012).

In summary, the implemented protocol provides a straight-forward strategy to generate stably CB-expressing human cell lines with targeted insertion of the CB transgene. However, prior application of the cell lines, further validations regarding homo- or heterozygous AAVS1 integration or off-target effects should be performed. In addition it must be noted that some cell lines might require optimization of the transfection protocol, selection

procedure or isolation and expansion conditions. Lastly, the stability in long-term cell culture needs to be assessed for each generated cell line in terms of homogenous CB expression.

6.5 Conclusions and future perspective

In this dissertation the utilization of CBs to quantify dynamic changes in endogenous protein concentration by a mechanism termed antigen-mediated CB stabilization (AMCBS) was demonstrated. Moreover, the enhancement of CB turnover achieved by implementing the N-end rule led to increased accuracy of AMCBS-based antigen quantification and simultaneously reducing CB aggregation post transient expression. Lastly, the method for generating cell lines stably expressing turnover-accelerated cell lines was optimized by establishing CRISPR/Cas9 gene editing protocol, which enables targeted transgenesis of the CB into a host cell genome.

As the number of available chromobodies is constantly growing, the employment of CBs for antigen quantification will provide a substantial benefit for live-cell imaging in the future. Consequently, the main limitation of this approach lies within the availability of functional CB molecular probes specifically targeting a protein of interest. However, continuous improvement in nanobody and chromobody screening techniques will further push the identification of new functional intracellular binder.

AMCBS-based antigen quantification becomes extremely exciting thinking of CBs targeting the post-translational modification, specific conformation changes or splice variants of a specific protein, as proteins in these specific circumstances cannot be addressed by other methods (e.g. GFP fusion) in living cells. Thus, the availability of turnover-accelerated affinity binder would provide an unprecedented opportunity to study signaling in living cells, thereby facilitating the gain of in-depth knowledge in cellular physiology.

Besides an application in basic research, AMCBS-based protein quantification might also be utilized in the field of applied sciences. As demonstrated in chapter 5.4.3, turnover-accelerated CBs can be employed to monitor drug action and kinetics. Based on these first results, the idea of turnover-accelerated CB embedded in phenotypic screens of pharmacological compounds is not very far away.

7 REFERENCES

Aberle H, Bauer A, Stappert J, Kispert A & Kemler R (1997) beta-catenin is a target for the ubiquitin-proteasome pathway. *The EMBO journal* **16:** 3797–3804

Ahmed D, Eide PW, Eilertsen IA, Danielsen SA, Eknæs M, Hektoen M, Lind GE & Lothe RA (2013) Epigenetic and genetic features of 24 colon cancer cell lines. *Oncogenesis* **2:** e71-

Akhtar W, Jong J de, Pindyurin AV, Pagie L, Meuleman W, Ridder J de, Berns A, Wessels LFA, van Lohuizen M & van Steensel B (2013) Chromatin position effects assayed by thousands of reporters integrated in parallel. *Cell* **154:** 914–927

Akiyama H, Lyons JP, Mori-Akiyama Y, Yang X, Zhang R, Zhang Z, Deng JM, Taketo MM, Nakamura T, Behringer RR, McCrea PD & Crombrugghe B de (2004) Interactions between Sox9 and beta-catenin control chondrocyte differentiation. *Genes & development* **18:** 1072–1087

Ashour J, Schmidt FI, Hanke L, Cragnolini J, Cavallari M, Altenburg A, Brewer R, Ingram J, Shoemaker C & Ploegh HL (2015) Intracellular expression of camelid single-domain antibodies specific for influenza virus nucleoprotein uncovers distinct features of its nuclear localization. *Journal of virology* **89:** 2792–2800

Autour A, C. Y. Jeng, Sunny, D. Cawte A, Abdolahzadeh A, Galli A, Panchapakesan, Shanker S. S., Rueda D, Ryckelynck M & Unrau PJ (2018) Fluorogenic RNA Mango aptamers for imaging small non-coding RNAs in mammalian cells. *Nat Commun* **9:** 642

Bachmair A, Finley D & Varshavsky A (1986) In vivo half-life of a protein is a function of its amino-terminal residue. *Science (New York, N.Y.)* **234:** 179–186

Baker M (2015) Reproducibility crisis: Blame it on the antibodies. *Nature* **521:** 274–276

Balleza E, Kim JM & Cluzel P (2018) Systematic characterization of maturation time of fluorescent proteins in living cells. *Nat Methods* **15:** 47–51

Bantscheff M, Schirle M, Sweetman G, Rick J & Kuster B (2007) Quantitative mass spectrometry in proteomics: a critical review. *Analytical and bioanalytical chemistry* **389:** 1017–1031

Behrens J (1998) Functional Interaction of an Axin Homolog, Conductin, with -Catenin, APC, and GSK3. *Science* **280:** 596–599

Behrens J, Kries JP von, Kühl M, Bruhn L, Wedlich D, Grosschedl R & Birchmeier W (1996) Functional interaction of beta-catenin with the transcription factor LEF-1. *Nature* **382:** 638–642

Berglund L, Björling E, Oksvold P, Fagerberg L, Asplund A, Al-Khalili Szigyarto C, Persson A, Ottosson J, Wernérus H, Nilsson P, Lundberg E, Sivertsson Å, Navani S, Wester K, Kampf C, Hober S, Pontén F & Uhlén M (2008) A Genecentric Human Protein Atlas for Expression Profiles Based on Antibodies. *Mol Cell Proteomics* **7:** 2019–2027

Bird RE, Hardman KD, Jacobson JW, Johnson S, Kaufman BM, Lee SM, Lee T, Pope SH, Riordan GS & Whitlow M (1988) Single-chain antigen-binding proteins. *Science (New York, N.Y.)* **242:** 423–426

Blanco-Toribio A, Muyldermans S, Frankel G & Fernández LÁ (2010) Direct injection of functional single-domain antibodies from E. coli into human cells. *PloS one* **5:** e15227

Bossi S, Ferranti B, Martinelli C, Capasso P & Marco A de (2010) Antibody-mediated purification of co-expressed antigen-antibody complexes. *Protein expression and purification* **72:** 55–58

Bradbury A & Plückthun A (2015) Reproducibility: Standardize antibodies used in research. *Nature* **518:** 27–29

Brauchle M, Hansen S, Caussinus E, Lenard A, Ochoa-Espinosa A, Scholz O, Sprecher SG, Pluckthun A & Affolter M (2014) Protein interference applications in cellular and developmental biology using DARPins that recognize GFP and mCherry. *Biology Open* **3:** 1252–1261

Bray F, Ferlay J, Soerjomataram I, Siegel RL, Torre LA & Jemal A (2018) Global cancer statistics 2018: GLOBOCAN estimates of incidence and mortality worldwide for 36 cancers in 185 countries. *CA: A Cancer Journal for Clinicians* **49:** 509

Brun S, Faucon-Biguet N & Mallet J (2003) Optimization of transgene expression at the posttranscriptional level in neural cells: implications for gene therapy. *Molecular therapy : the journal of the American Society of Gene Therapy* **7:** 782–789

Buchfellner A, Yurlova L, Nüske S, Scholz AM, Bogner J, Ruf B, Zolghadr K, Drexler SE, Drexler GA, Girst S, Greubel C, Reindl J, Siebenwirth C, Romer T, Friedl AA & Rothbauer U (2016) A New Nanobody-Based Biosensor to Study Endogenous PARP1 In Vitro and in Live Human Cells. *PloS one* **11:** e0151041

Buckley AM, Petersen J, Roe AJ, Douce GR & Christie JM (2015) LOV-based reporters for fluorescence imaging. *Current Opinion in Chemical Biology* **27:** 39–45

Burgess A, Lorca T & Castro A (2012) Quantitative live imaging of endogenous DNA replication in mammalian cells. *PloS one* **7:** e45726

Campanero MR & Flemington EK (1997) Regulation of E2F through ubiquitin-proteasome-dependent degradation: Stabilization by the pRB tumor suppressor protein. *Proceedings of the National Academy of Sciences* **94:** 2221–2226

Cassimeris L, Guglielmi L, Denis V, Larroque C & Martineau P (2013) Specific in vivo labeling of tyrosinated α-tubulin and measurement of microtubule dynamics using a GFP tagged, cytoplasmically expressed recombinant antibody. *PloS one* **8:** e59812

Cattaneo A & Biocca S (1999) The selection of intracellular antibodies. *Trends in biotechnology* **17:** 115–121

Chatterjee D, Bhatt M, Butler D, Genst E de, Dobson CM, Messer A & Kordower JH (2018) Proteasome-targeted nanobodies alleviate pathology and functional decline in an α-synuclein-based Parkinson's disease model. *NPJ Parkinson's disease* **4:** 25

Choe L, D'Ascenzo M, Relkin NR, Pappin D, Ross P, Williamson B, Guertin S, Pribil P & Lee KH (2007) 8-Plex Quantitation of changes in cerebrospinal fluid protein expression in subjects undergoing intravenous immunoglobulin treatment for Alzheimer's disease. *Proteomics* **7:** 3651–3660

Clevers H & Nusse R (2012) Wnt/β-Catenin Signaling and Disease. *Cell* **149:** 1192–1205

Cong F, Schweizer L, Chamorro M & Varmus H (2003) Requirement for a nuclear function of beta-catenin in Wnt signaling. *Molecular and cellular biology* **23:** 8462–8470

Cooper GM (2000) *The cell: A molecular approach.* American Society for Microbiology, Washington

Cornish-Bowden A (2013) The origins of enzyme kinetics. *FEBS Letters* **587:** 2725–2730

Crivat G & Taraska JW (2012) Imaging proteins inside cells with fluorescent tags. *Trends in biotechnology* **30:** 8–16

Damdindorj L, Karnan S, Ota A, Hossain E, Konishi Y, Hosokawa Y & Konishi H (2014) A comparative analysis of constitutive promoters located in adeno-associated viral vectors. *PloS one* **9:** e106472

Damdindorj L, Karnan S, Ota A, Takahashi M, Konishi Y, Hossain E, Hosokawa Y & Konishi H (2012) Assessment of the long-term transcriptional activity of a 550-bp-long human β-actin promoter region. *Plasmid* **68:** 195–200

Dantuma NP, Lindsten K, Glas R, Jellne M & Masucci MG (2000) Short-lived green fluorescent proteins for quantifying ubiquitin/proteasome-dependent proteolysis in living cells. *Nature biotechnology* **18:** 538–543

Desmyter A, Transue TR, Ghahroudi MA, Dao Thi M-H, Poortmans F, Hamers R, Muyldermans S & Wyns L (1996) Crystal structure of a camel single-domain VH antibody fragment in complex with lysozyme. *Nat Struct Mol Biol* **3:** 803–811

Dunn MR, Jimenez RM & Chaput JC (2017) Analysis of aptamer discovery and technology. *Nat. rev. chem.* **1:** 76

Emami KH, Nguyen C, Ma H, Kim DH, Jeong KW, Eguchi M, Moon RT, Teo J-L, Oh SW, Kim HY, Moon SH, Ha JR & Kahn M (2004) A small molecule inhibitor of -catenin/CREB-binding protein transcription. *Proceedings of the National Academy of Sciences* **101:** 12682–12687

Essers MAG, Vries-Smits LMM de, Barker N, Polderman PE, Burgering BMT & Korswagen HC (2005) Functional interaction between beta-catenin and FOXO in oxidative stress signaling. *Science (New York, N.Y.)* **308:** 1181–1184

Flajnik MF, Deschacht N & Muyldermans S (2011) A case of convergence: why did a simple alternative to canonical antibodies arise in sharks and camels? *PLoS biology* **9:** e1001120

Freund G, Desplancq D, Stoessel A, Weinsanto R, Sibler A-P, Robin G, Martineau P, Didier P, Wagner J & Weiss E (2014) Generation of an intrabody-based reagent suitable for

imaging endogenous proliferating cell nuclear antigen in living cancer cells. *Journal of molecular recognition : JMR* **27:** 549–558

Fu Y, Foden JA, Khayter C, Maeder ML, Reyon D, Joung JK & Sander JD (2013) High-frequency off-target mutagenesis induced by CRISPR-Cas nucleases in human cells. *Nature biotechnology* **31:** 822–826

Genst E de, Silence K, Decanniere K, Conrath K, Loris R, Kinne J, Muyldermans S & Wyns L (2006) Molecular basis for the preferential cleft recognition by dromedary heavy-chain antibodies. *Proceedings of the National Academy of Sciences* **103:** 4586–4591

Gibson DG, Young L, Chuang R-Y, Venter JC, Hutchison CA & Smith HO (2009) Enzymatic assembly of DNA molecules up to several hundred kilobases. *Nat Methods* **6:** 343–345

Glockshuber R, Schmidt T & Plueckthun A (1992) The disulfide bonds in antibody variable domains: effects on stability, folding in vitro, and functional expression in Escherichia coli. *Biochemistry* **31:** 1270–1279

Gonsalves FC, Klein K, Carson BB, Katz S, Ekas LA, Evans S, Nagourney R, Cardozo T, Brown, A. M. C. & DasGupta R (2011) An RNAi-based chemical genetic screen identifies three small-molecule inhibitors of the Wnt/wingless signaling pathway. *Proceedings of the National Academy of Sciences* **108:** 5954–5963

Goujon M, McWilliam H, Li W, Valentin F, Squizzato S, Paern J & Lopez R (2010) A new bioinformatics analysis tools framework at EMBL-EBI. *Nucleic Acids Research* **38:** W695-W699

Gross GG, Junge JA, Mora RJ, Kwon H-B, Olson CA, Takahashi TT, Liman ER, Ellis-Davies GCR, McGee AW, Sabatini BL, Roberts RW & Arnold DB (2013) Recombinant Probes for Visualizing Endogenous Synaptic Proteins in Living Neurons. *Neuron* **78:** 971–985

Gygi SP, Rist B, Gerber SA, Turecek F, Gelb MH & Aebersold R (1999) Quantitative analysis of complex protein mixtures using isotope-coded affinity tags. *Nat Biotechnol* **17:** 994–999

Hager S, Frame FM, Collins AT, Burns JE & Maitland NJ (2008) An internal polyadenylation signal substantially increases expression levels of lentivirus-delivered transgenes but has the potential to reduce viral titer in a promoter-dependent manner. *Human gene therapy* **19:** 840–850

Halff EF, Versteeg M, Brondijk, T Harma C & Huizinga EG (2014) When less becomes more: optimization of protein expression in HEK293-EBNA1 cells using plasmid titration - a case study for NLRs. *Protein expression and purification* **99:** 27–34

Hamers-Casterman C, Atarhouch T, Muyldermans S, Robinson G, Hamers C, Songa EB, Bendahman N & Hamers R (1993) Naturally occurring antibodies devoid of light chains. *Nature* **363:** 446–448

Handeli S & Simon JA (2008) A small-molecule inhibitor of Tcf/beta-catenin signaling down-regulates PPARgamma and PPARdelta activities. *Molecular cancer therapeutics* **7:** 521–529

Hassanzadeh-Ghassabeh G, Devoogdt N, Pauw P de, Vincke C & Muyldermans S (2013) Nanobodies and their potential applications. *Nanomedicine (London, England)* **8:** 1013–1026

He TC, Sparks AB, Rago C, Hermeking H, Zawel L, da Costa LT, Morin PJ, Vogelstein B & Kinzler KW (1998) Identification of c-MYC as a target of the APC pathway. *Science (New York, N.Y.)* **281:** 1509–1512

Helma J, Schmidthals K, Lux V, Nüske S, Scholz AM, Kräusslich H-G, Rothbauer U & Leonhardt H (2012) Direct and dynamic detection of HIV-1 in living cells. *PloS one* **7:** e50026

Hortin GL & Murthy J (2002) Substrate size selectivity of 20S proteasomes: analysis with variable-sized synthetic substrates. *Journal of Protein Chemistry* **21:** 333–337

Hsu C-C, Li H-P, Hung Y-H, Leu Y-W, Wu W-H, Wang F-S, Lee K-D, Chang P-J, Wu C-S, Lu Y-J, Huang TH-M, Chang Y-S & Hsiao S-H (2010) Targeted methylation of CMV and E1A viral promoters. *Biochemical and biophysical research communications* **402:** 228–234

Huang S-MA, Mishina YM, Liu S, Cheung A, Stegmeier F, Michaud GA, Charlat O, Wiellette E, Zhang Y, Wiessner S, Hild M, Shi X, Wilson CJ, Mickanin C, Myer V, Fazal A, Tomlinson R, Serluca F, Shao W & Cheng H et al (2009) Tankyrase inhibition stabilizes axin and antagonizes Wnt signalling. *Nature* **461:** 614–620

Hulsken J (1994) E-cadherin and APC compete for the interaction with beta-catenin and the cytoskeleton. *The Journal of Cell Biology* **127:** 2061–2069

Irannejad R, Tomshine JC, Tomshine JR, Chevalier M, Mahoney JP, Steyaert J, Rasmussen SGF, Sunahara RK, El-Samad H, Huang B & Zastrow M von (2013) Conformational biosensors reveal GPCR signalling from endosomes. *Nature* **495:** 534–538

Ivanchenko S, Godinez WJ, Lampe M, Kräusslich H-G, Eils R, Rohr K, Bräuchle C, Müller B & Lamb DC (2009) Dynamics of HIV-1 assembly and release. *PLoS pathogens* **5:** e1000652

Janeway (2005) *Immunobiology: the immune system in health and disease: janeway2005immunobiology*. Garland Science New York

Jho E-h, Zhang T, Domon C, Joo C-K, Freund J-N & Costantini F (2002) Wnt/beta-catenin/Tcf signaling induces the transcription of Axin2, a negative regulator of the signaling pathway. *Molecular and cellular biology* **22:** 1172–1183

Johnson PR, Swanson R, Rakhilina L & Hochstrasser M (1998) Degradation Signal Masking by Heterodimerization of MATα2 and MATa1 Blocks Their Mutual Destruction by the Ubiquitin-Proteasome Pathway. *Cell* **94:** 217–227

Jonge J de, Hofius D & Hennig L (2017) Salicylic acid interferes with GFP fluorescence in vivo. *Journal of experimental botany* **68:** 1689–1696

Joshi SN, Butler DC & Messer A (2012) Fusion to a highly charged proteasomal retargeting sequence increases soluble cytoplasmic expression and efficacy of diverse anti-synuclein intrabodies. *mAbs* **4:** 686–693

Jullien D, Vignard J, Fedor Y, Béry N, Olichon A, Crozatier M, Erard M, Cassard H, Ducommun B, Salles B & Mirey G (2016) Chromatibody, a novel non-invasive molecular tool to explore and manipulate chromatin in living cells. *Journal of cell science* **129:** 2673–2683

Kabat EA, Te Wu T, Foeller C, Perry HM & Gottesman KS (1992) *Sequences of proteins of immunological interest.* DIANE publishing

Kafri P, Hasenson SE, Kanter I, Sheinberger J, Kinor N, Yunger S & Shav-Tal Y (2016) Quantifying β-catenin subcellular dynamics and cyclin D1 mRNA transcription during Wnt signaling in single living cells. *eLife* **5:** 3797

Kaiser PD, Maier J, Traenkle B, Emele F & Rothbauer U (2014) Recent progress in generating intracellular functional antibody fragments to target and trace cellular components in living cells. *Biochimica et biophysica acta* **1844:** 1933–1942

Khong Nguyen V, Hamers R, Wyns L & Muyldermans S (1999) Loss of splice consensus signal is responsible for the removal of the entire CH1 domain of the functional camel IGG2A heavy-chain antibodies11This work was supported by the VLIR, VIB and FGWO. *Molecular immunology* **36:** 515–524

Kimelman D & Xu W (2006) beta-catenin destruction complex: insights and questions from a structural perspective. *Oncogene* **25:** 7482–7491

Klein R, Ruttkowski B, Knapp E, Salmons B, Günzburg WH & Hohenadl C (2006) WPRE-mediated enhancement of gene expression is promoter and cell line specific. *Gene* **372:** 153–161

Knorre DG, Kudryashova NV & Godovikova TS (2009) Chemical and Functional Aspects of Posttranslational Modification of Proteins. *Acta Naturae* **1:** 29–51

Koch B, Nijmeijer B, Kueblbeck M, Cai Y, Walther N & Ellenberg J (2018) Generation and validation of homozygous fluorescent knock-in cells using CRISPR-Cas9 genome editing. *Nature protocols* **13:** 1465–1487

Köhler G & Milstein C (1975) Continuous cultures of fused cells secreting antibody of predefined specificity. *Nature* **256:** 495–497

Koide A, Wojcik J, Gilbreth RN, Hoey RJ & Koide S (2012) Teaching an old scaffold new tricks: monobodies constructed using alternative surfaces of the FN3 scaffold. *Journal of molecular biology* **415:** 393–405

Korinek V (1997) Constitutive Transcriptional Activation by a beta -Catenin-Tcf Complex in APC-/- Colon Carcinoma. *Science* **275:** 1784–1787

Kotin RM, Linden RM & Berns KI (1992) Characterization of a preferred site on human chromosome 19q for integration of adeno-associated virus DNA by non-homologous recombination. *The EMBO journal* **11:** 5071–5078

Krishnan M, Park JM, Cao F, Wang D, Paulmurugan R, Tseng JR, Gonzalgo ML, Gambhir SS & Wu JC (2006) Effects of epigenetic modulation on reporter gene expression: implications for stem cell imaging. *FASEB journal : official publication of the Federation of American Societies for Experimental Biology* **20:** 106–108

Lampe M, Briggs JAG, Endress T, Glass B, Riegelsberger S, Kräusslich H-G, Lamb DC, Bräuchle C & Müller B (2007) Double-labelled HIV-1 particles for study of virus-cell interaction. *Virology* **360:** 92–104

Leclerc GM, Boockfor FR, Faught WJ & Frawley LS (2000) Development of a destabilized firefly luciferase enzyme for measurement of gene expression. *BioTechniques* **29:** 590-1, 594-6, 598 passim

Li X, Duan X, Yang K, Zhang W, Zhang C, Fu L, Ren Z, Wang C, Wu J, Lu R, Ye Y, He M, Nie C, Yang N, Wang J, Yang H, Liu X, Tan W & Fugmann SD (2016) Comparative Analysis of Immune Repertoires between Bactrian Camel's Conventional and Heavy-Chain Antibodies. *PLoS ONE* **11:** e0161801

Li X, Zhao X, Fang Y, Jiang X, Duong T, Fan C, Huang C-C & Kain SR (1998) Generation of Destabilized Green Fluorescent Protein as a Transcription Reporter. *J. Biol. Chem.* **273:** 34970–34975

Liedberg B, Nylander C & Lunström I (1983) Surface plasmon resonance for gas detection and biosensing. *Sensors and Actuators* **4:** 299–304

Lindemann C, Thomanek N, Hundt F, Lerari T, Meyer HE, Wolters D & Marcus K (2017) Strategies in relative and absolute quantitative mass spectrometry based proteomics. *Biological chemistry* **398:** 687–699

Lo C-A, Kays I, Emran F, Lin T-J, Cvetkovska V & Chen BE (2015) Quantification of Protein Levels in Single Living Cells. *Cell Reports* **13:** 2634–2644

Loeb JE, Cordier WS, Harris ME, Weitzman MD & Hope TJ (1999) Enhanced expression of transgenes from adeno-associated virus vectors with the woodchuck hepatitis virus

posttranscriptional regulatory element: implications for gene therapy. *Human gene therapy* **10:** 2295–2305

Löfblom J, Feldwisch J, Tolmachev V, Carlsson J, Ståhl S & Frejd FY (2010) Affibody molecules: Engineered proteins for therapeutic, diagnostic and biotechnological applications. *FEBS Letters* **584:** 2670–2680

Lu R, Markowetz F, Unwin RD, Leek JT, Airoldi EM, MacArthur BD, Lachmann A, Rozov R, Ma'ayan A, Boyer LA, Troyanskaya OG, Whetton AD & Lemischka IR (2009) Systems-level dynamic analyses of fate change in murine embryonic stem cells. *Nature* **462:** 358–362

Luo Y, Liu C, Cerbini T, San H, Lin Y, Chen G, Rao MS & Zou J (2014) Stable enhanced green fluorescent protein expression after differentiation and transplantation of reporter human induced pluripotent stem cells generated by AAVS1 transcription activator-like effector nucleases. *Stem cells translational medicine* **3:** 821–835

Lyakhov I, Zielinski R, Kuban M, Kramer-Marek G, Fisher R, Chertov O, Bindu L & Capala J (2010) HER2- and EGFR-Specific Affiprobes: Novel Recombinant Optical Probes for Cell Imaging. *ChemBioChem* **11:** 345–350

Maier J, Traenkle B & Rothbauer U (2015) Real-time analysis of epithelial-mesenchymal transition using fluorescent single-domain antibodies. *Scientific reports* **5:** 13402

Mali P, Yang L, Esvelt KM, Aach J, Guell M, DiCarlo JE, Norville JE & Church GM (2013) RNA-guided human genome engineering via Cas9. *Science (New York, N.Y.)* **339:** 823–826

Mandic A, Strebinger D, Regali C, Phillips NE & Suter DM (2017) A novel method for quantitative measurements of gene expression in single living cells. *Methods* **120:** 65–75

Marfori M, Mynott A, Ellis JJ, Mehdi AM, Saunders NFW, Curmi PM, Forwood JK, Bodén M & Kobe B (2011) Molecular basis for specificity of nuclear import and prediction of nuclear localization. *Biochimica et biophysica acta* **1813:** 1562–1577

Mattiazzi Usaj M, Styles EB, Verster AJ, Friesen H, Boone C & Andrews BJ (2016) High-Content Screening for Quantitative Cell Biology. *Trends in Cell Biology* **26:** 598–611

Maynard J & Georgiou G (2000) Antibody engineering. *Annual review of biomedical engineering* **2:** 339–376

McDaniel LD & Schultz RA (1993) Elevation of sister chromatid exchange frequency in transformed human fibroblasts following exposure to widely used aminoglycosides. *Environ. Mol. Mutagen.* **21:** 67–72

Mendez MG, Kojima S-I & Goldman RD (2010) Vimentin induces changes in cell shape, motility, and adhesion during the epithelial to mesenchymal transition. *FASEB journal : official publication of the Federation of American Societies for Experimental Biology* **24:** 1838–1851

Meyer T de, Muyldermans S & Depicker A (2014) Nanobody-based products as research and diagnostic tools. *Trends in biotechnology* **32:** 263–270

Michaelis L, Menten ML, Johnson KA & Goody RS (2011) The original Michaelis constant: translation of the 1913 Michaelis-Menten paper. *Biochemistry* **50:** 8264–8269

Miyaoka Y, Berman JR, Cooper SB, Mayerl SJ, Chan AH, Zhang B, Karlin-Neumann GA & Conklin BR (2016) Systematic quantification of HDR and NHEJ reveals effects of locus, nuclease, and cell type on genome-editing. *Scientific reports* **6:** 23549

Mojica, F J M, Díez-Villaseñor C, García-Martínez J & Almendros C (2009) Short motif sequences determine the targets of the prokaryotic CRISPR defence system. *Microbiology (Reading, England)* **155:** 733–740

Morgan DO (op. 2007) *The Cell cycle: Principles of control.* New Science Press; Sinauer Associates, London, Sunderland, MA

Moriya H (2015) Quantitative nature of overexpression experiments. *Molecular biology of the cell* **26:** 3932–3939

Mukherjee A & Schroeder CM (2015) Flavin-based fluorescent proteins: emerging paradigms in biological imaging. *Current Opinion in Biotechnology* **31:** 16–23

Muyldermans S (2001) Single domain camel antibodies: current status. *Journal of biotechnology* **74:** 277–302

Muyldermans S, Cambillau C & Wyns L (2001) Recognition of antigens by single-domain antibody fragments: the superfluous luxury of paired domains. *Trends in Biochemical Sciences* **26:** 230–235

Norrman K, Fischer Y, Bonnamy B, Wolfhagen Sand F, Ravassard P & Semb H (2010) Quantitative comparison of constitutive promoters in human ES cells. *PloS one* **5:** e12413

Oceguera-Yanez F, Kim S-I, Matsumoto T, Tan GW, Xiang L, Hatani T, Kondo T, Ikeya M, Yoshida Y, Inoue H & Woltjen K (2016) Engineering the AAVS1 locus for consistent and scalable transgene expression in human iPSCs and their differentiated derivatives. *Methods* **101:** 43–55

Ong S-E, Blagoev B, Kratchmarova I, Kristensen DB, Steen H, Pandey A & Mann M (2002) Stable Isotope Labeling by Amino Acids in Cell Culture, SILAC, as a Simple and Accurate Approach to Expression Proteomics. *Mol Cell Proteomics* **1:** 376–386

Ong S-E & Mann M (2006) A practical recipe for stable isotope labeling by amino acids in cell culture (SILAC). *Nature protocols* **1:** 2650–2660

Orford K, Crockett C, Jensen JP, Weissman AM & Byers SW (1997) Serine phosphorylation-regulated ubiquitination and degradation of beta-catenin. *J. Biol. Chem.* **272:** 24735–24738

Panza P, Maier J, Schmees C, Rothbauer U & Söllner C (2015) Live imaging of endogenous protein dynamics in zebrafish using chromobodies. *Development (Cambridge, England)* **142:** 1879–1884

Paredes V, Park JS, Jeong Y, Yoon J & Baek K (2013) Unstable expression of recombinant antibody during long-term culture of CHO cells is accompanied by histone H3 hypoacetylation. *Biotechnology letters* **35:** 987–993

Plückthun A (2015) Designed Ankyrin Repeat Proteins (DARPins): Binding Proteins for Research, Diagnostics, and Therapy. *Annu. Rev. Pharmacol. Toxicol.* **55:** 489–511

Qin JY, Zhang L, Clift KL, Hulur I, Xiang AP, Ren B-Z, Lahn BT & Hansen IA (2010) Systematic Comparison of Constitutive Promoters and the Doxycycline-Inducible Promoter. *PloS one* **5:** e10611

Ran FA, Hsu PD, Lin C-Y, Gootenberg JS, Konermann S, Trevino AE, Scott DA, Inoue A, Matoba S, Zhang Y & Zhang F (2013) Double nicking by RNA-guided CRISPR Cas9 for enhanced genome editing specificity. *Cell* **154:** 1380–1389

Rechsteiner M & Rogers SW (1996) PEST sequences and regulation by proteolysis. *Trends in Biochemical Sciences* **21:** 267–271

Riedl J, Crevenna AH, Kessenbrock K, Yu JH, Neukirchen D, Bista M, Bradke F, Jenne D, Holak TA, Werb Z, Sixt M & Wedlich-Soldner R (2008) Lifeact: a versatile marker to visualize F-actin. *Nat Methods* **5:** 605–607

Riedl J, Flynn KC, Raducanu A, Gärtner F, Beck G, Bösl M, Bradke F, Massberg S, Aszodi A, Sixt M & Wedlich-Söldner R (2010) Lifeact mice for studying F-actin dynamics. *Nat Meth* **7:** 168–169

Rinaldi A-S, Freund G, Desplancq D, Sibler A-P, Baltzinger M, Rochel N, Mély Y, Didier P & Weiss E (2013) The use of fluorescent intrabodies to detect endogenous gankyrin in living cancer cells. *Experimental Cell Research* **319:** 838–849

Rodolosse A, Barbat A, Chantret I, Lacasa M, Brot-Laroche E, Zweibaum A & Rousset M (1998) Selecting agent hygromycin B alters expression of glucose-regulated genes in transfected Caco-2 cells. *The American journal of physiology* **274:** G931-8

Rogers S, Wells R & Rechsteiner M (1986) Amino acid sequences common to rapidly degraded proteins: the PEST hypothesis. *Science (New York, N.Y.)* **234:** 364–368

Romao E, Morales-Yanez F, Hu Y, Crauwels M, Pauw P de, Hassanzadeh GG, Devoogdt N, Ackaert C, Vincke C & Muyldermans S (2016) Identification of Useful Nanobodies by Phage Display of Immune Single Domain Libraries Derived from Camelid Heavy Chain Antibodies. *Current pharmaceutical design* **22:** 6500–6518

Rothbauer U, Zolghadr K, Muyldermans S, Schepers A, Cardoso MC & Leonhardt H (2008) A versatile nanotrap for biochemical and functional studies with fluorescent fusion proteins. *Molecular & cellular proteomics : MCP* **7:** 282–289

Rothbauer U, Zolghadr K, Tillib S, Nowak D, Schermelleh L, Gahl A, Backmann N, Conrath K, Muyldermans S, Cardoso MC & Leonhardt H (2006) Targeting and tracing antigens in live cells with fluorescent nanobodies. *Nat Meth* **3:** 887–889

Rudikoff S & Pumphrey JG (1986) Functional antibody lacking a variable-region disulfide bridge. *Proceedings of the National Academy of Sciences* **83:** 7875–7878

Sabidó E, Selevsek N & Aebersold R (2012) Mass spectrometry-based proteomics for systems biology. *Current Opinion in Biotechnology* **23:** 591–597

Sadelain M, Papapetrou EP & Bushman FD (2012) Safe harbours for the integration of new DNA in the human genome. *Nat Rev Cancer* **12:** 51–58

Satelli A & Li S (2011) Vimentin in cancer and its potential as a molecular target for cancer therapy. *Cellular and molecular life sciences : CMLS* **68:** 3033–3046

Sato S-I, Yatsuzuka K, Katsuda Y & Uesugi M (2018) Method for Imaging Live-Cell RNA Using an RNA Aptamer and a Fluorescent Probe. *Methods in molecular biology (Clifton, N.J.)* **1649:** 305–318

Sato Y, Kujirai T, Arai R, Asakawa H, Ohtsuki C, Horikoshi N, Yamagata K, Ueda J, Nagase T, Haraguchi T, Hiraoka Y, Kimura A, Kurumizaka H & Kimura H (2016) A Genetically Encoded Probe for Live-Cell Imaging of H4K20 Monomethylation. *Journal of molecular biology* **428:** 3885–3902

Sato Y, Mukai M, Ueda J, Muraki M, Stasevich TJ, Horikoshi N, Kujirai T, Kita H, Kimura T, Hira S, Okada Y, Hayashi-Takanaka Y, Obuse C, Kurumizaka H, Kawahara A, Yamagata K, Nozaki N & Kimura H (2013) Genetically encoded system to track histone modification in vivo. *Scientific reports* **3:** 2436

Schnell U, Dijk F, Sjollema KA & Giepmans, Ben N G (2012) Immunolabeling artifacts and the need for live-cell imaging. *Nat Methods* **9:** 152–158

Schorpp K, Rothenaigner I, Maier J, Traenkle B, Rothbauer U & Hadian K (2016) A Multiplexed High-Content Screening Approach Using the Chromobody Technology to Identify Cell Cycle Modulators in Living Cells. *Journal of biomolecular screening* **21:** 965–977

Schumacher D, Helma J, Schneider AFL, Leonhardt H & Hackenberger CPR (2018) Nanobodies: Chemical Functionalization Strategies and Intracellular Applications. *Angewandte Chemie (International ed. in English)* **57:** 2314–2333

Schwanhäusser B, Busse D, Li N, Dittmar G, Schuchhardt J, Wolf J, Chen W & Selbach M (2011) Global quantification of mammalian gene expression control. *Nature* **473:** 337–342

Secker K-A (2016) *Experimental studies of antigen-induced chromobody stabilization for image-based protein quantification in living cells.* Masterthesis, Pharmaceutical Sciences and Technologies, University of Tuebingen

Seglen PO & Reith A (1976) Ammonia inhibition of protein degradation in isolated rat hepatocytes. *Experimental Cell Research* **100:** 276–280

Sekine K, Takebe T & Taniguchi H (2014) Fluorescent labeling and visualization of human induced pluripotent stem cells with the use of transcription activator-like effector nucleases. *Transplantation proceedings* **46:** 1205–1207

Shtutman M, Zhurinsky J, Simcha I, Albanese C, D'Amico M, Pestell R & Ben-Ze'ev A (1999) The cyclin D1 gene is a target of the beta-catenin/LEF-1 pathway. *Proceedings of the National Academy of Sciences* **96:** 5522–5527

Sibler A-P, Courtête J, Muller CD, Zeder-Lutz G & Weiss E (2005) Extended half-life upon binding of destabilized intrabodies allows specific detection of antigen in mammalian cells. *The FEBS journal* **272:** 2878–2891

Sievers F, Wilm A, Dineen D, Gibson TJ, Karplus K, Li W, Lopez R, McWilliam H, Remmert M, Soding J, Thompson JD & Higgins DG (2011) Fast, scalable generation of high-quality protein multiple sequence alignments using Clustal Omega. *Molecular Systems Biology* **7:** 539

Skube SB, Chaverri JM & Goodson HV (2010) Effect of GFP tags on the localization of EB1 and EB1 fragments in vivo. *Cytoskeleton (Hoboken, N.J.)* **67:** 1–12

Smith JR, Maguire S, Davis LA, Alexander M, Yang F, Chandran S, ffrench-Constant C & Pedersen RA (2008) Robust, Persistent Transgene Expression in Human Embryonic Stem Cells Is Achieved with AAVS1-Targeted Integration. *Stem Cells* **26:** 496–504

Snapp EL (2009) Fluorescent proteins: a cell biologist's user guide. *Trends in Cell Biology* **19:** 649–655

Spencer GJ, Utting JC, Etheridge SL, Arnett TR & Genever PG (2006) Wnt signalling in osteoblasts regulates expression of the receptor activator of NFkappaB ligand and inhibits osteoclastogenesis in vitro. *Journal of cell science* **119:** 1283–1296

Stadler C, Rexhepaj E, Singan VR, Murphy RF, Pepperkok R, Uhlén M, Simpson JC & Lundberg E (2013) Immunofluorescence and fluorescent-protein tagging show high correlation for protein localization in mammalian cells. *Nat Methods* **10:** 315–323

Stadler C, Skogs M, Brismar H, Uhlén M & Lundberg E (2010) A single fixation protocol for proteome-wide immunofluorescence localization studies. *Journal of Proteomics* **73:** 1067–1078

Steeland S, Vandenbroucke RE & Libert C (2016) Nanobodies as therapeutics: big opportunities for small antibodies. *Drug discovery today* **21:** 1076–1113

Stoltenburg R, Reinemann C & Strehlitz B (2007) SELEX—A (r)evolutionary method to generate high-affinity nucleic acid ligands. *Biomolecular Engineering* **24:** 381–403

Strzalka W & Ziemienowicz A (2011) Proliferating cell nuclear antigen (PCNA): a key factor in DNA replication and cell cycle regulation. *Annals of botany* **107:** 1127–1140

Tanaka T & Rabbitts TH (2008) Functional intracellular antibody fragments do not require invariant intra-domain disulfide bonds. *Journal of molecular biology* **376:** 749–757

Tang JC, Drokhlyansky E, Etemad B, Rudolph S, Guo B, Wang S, Ellis EG, Li JZ & Cepko CL (2016) Detection and manipulation of live antigen-expressing cells using conditionally stable nanobodies. *eLife* **5**

The Cancer Genome Atlas Network (2012) Comprehensive molecular characterization of human colon and rectal cancer. *Nature* **487:** 330–337

Thorn K (2017) Genetically encoded fluorescent tags. *Molecular biology of the cell* **28:** 848–857

Toulany M, Maier J, Iida M, Rebholz S, Holler M, Grottke A, Jüker M, Wheeler DL, Rothbauer U & Rodemann HP (2017) Akt1 and Akt3 but not Akt2 through interaction with DNA-PKcs stimulate proliferation and post-irradiation cell survival of K-RAS-mutated cancer cells. *Cell death discovery* **3:** 17072

Traenkle B, Emele F, Anton R, Poetz O, Haeussler RS, Maier J, Kaiser PD, Scholz AM, Nueske S, Buchfellner A, Romer T & Rothbauer U (2015) Monitoring interactions and dynamics of endogenous beta-catenin with intracellular nanobodies in living cells. *Molecular & cellular proteomics : MCP* **14:** 707–723

Traenkle B & Rothbauer U (2017) Under the Microscope: Single-Domain Antibodies for Live-Cell Imaging and Super-Resolution Microscopy. *Frontiers in Immunology* **8**

Troy T, Jekic-McMullen D, Sambucetti L & Rice B (2004) Quantitative Comparison of the Sensitivity of Detection of Fluorescent and Bioluminescent Reporters in Animal Models. *Mol Imaging* **3:** 153535002004031

Valenta T, Hausmann G & Basler K (2012) The many faces and functions of β-catenin. *The EMBO journal* **31:** 2714–2736

Valera A, Perales JC, Hatzoglou M & Bosch F (1994) Expression of the neomycin-resistance (neo) gene induces alterations in gene expression and metabolism. *Human gene therapy* **5:** 449–456

van Audenhove I & Gettemans J (2016) Nanobodies as Versatile Tools to Understand, Diagnose, Visualize and Treat Cancer. *EBioMedicine* **8:** 40–48

van der Linden R, Geus B de, Stok W, Bos W, van Wassenaar D, Verrips T & Frenken L (2000) Induction of immune responses and molecular cloning of the heavy chain antibody repertoire of Lama glama. *Journal of immunological methods* **240:** 185–195

van der Linden RH, Frenken LG, Geus B de, Harmsen MM, Ruuls RC, Stok W, Ron L de, Wilson S, Davis P & Verrips CT (1999) Comparison of physical chemical properties of llama VHH antibody fragments and mouse monoclonal antibodies. *Biochimica et biophysica acta* **1431:** 37–46

Varley ZK, Pizzarelli R, Antonelli R, Stancheva SH, Kneussel M, Cherubini E & Zacchi P (2011) Gephyrin regulates GABAergic and glutamatergic synaptic transmission in hippocampal cell cultures. *The Journal of biological chemistry* **286:** 20942–20951

Varshavsky A (2005) Ubiquitin fusion technique and related methods. *Methods in enzymology* **399:** 777–799

Varshavsky A (2011) The N-end rule pathway and regulation by proteolysis. *Protein science : a publication of the Protein Society* **20:** 1298–1345

Vavouri T, Semple JI, Garcia-Verdugo R & Lehner B (2009) Intrinsic Protein Disorder and Interaction Promiscuity Are Widely Associated with Dosage Sensitivity. *Cell* **138:** 198–208

Verkman AS (2003) [28] Diffusion in cells measured by fluorescence recovery after photobleaching. In *Biophotonics*, Marriott G (ed) pp. 635–648. Amsterdam [u.a.]: Acad. Press

Vernet E, Lundberg E, Friedman M, Rigamonti N, Klausing S, Nygren P-Å & Gräslund T (2009) Affibody-mediated retention of the epidermal growth factor receptor in the secretory compartments leads to inhibition of phosphorylation in the kinase domain. *New Biotechnology* **25:** 417–423

Vigano MA, Bieli D, Schaefer JV, Jakob RP, Matsuda S, Maier T, Plückthun A & Affolter M (2018) DARPins recognize mTFP1 as novel reagents for in vitro and in vivo protein manipulations. *Biology Open* **7:** bio036749

Vincke C & Muyldermans S (2012) Introduction to heavy chain antibodies and derived Nanobodies. *Methods in molecular biology (Clifton, N.J.)* **911:** 15–26

Virant D, Traenkle B, Maier J, Kaiser PD, Bodenhöfer M, Schmees C, Vojnovic I, Pisak-Lukáts B, Endesfelder U & Rothbauer U (2018) A peptide tag-specific nanobody enables high-quality labeling for dSTORM imaging. *Nature communications* **9:** 930

Voskuil JLA (2014) Commercial antibodies and their validation. *F1000Res* **3:** 232

Vu KB, Ghahroudi MA, Wyns L & Muyldermans S (1997) Comparison of llama VH sequences from conventional and heavy chain antibodies. *Molecular immunology* **34:** 1121–1131

Wang S, Xiao Y, Zhang DD & Wong PK (2018) A gapmer aptamer nanobiosensor for real-time monitoring of transcription and translation in single cells. *Biomaterials* **156:** 56–64

White BD, Chien AJ & Dawson DW (2012) Dysregulation of Wnt/β-Catenin Signaling in Gastrointestinal Cancers. *Gastroenterology* **142:** 219–232

Wiese S, Reidegeld KA, Meyer HE & Warscheid B (2007) Protein labeling by iTRAQ: a new tool for quantitative mass spectrometry in proteome research. *Proteomics* **7:** 340–350

Worley CK, Ling R & Callis J (1998) Engineering in vivo instability of firefly luciferase and Escherichia coli beta-glucuronidase in higher plants using recognition elements from the ubiquitin pathway. *Plant molecular biology* **37:** 337–347

Wurm FM (2004) Production of recombinant protein therapeutics in cultivated mammalian cells. *Nat Biotechnol* **22:** 1393–1398

Xia W, Bringmann P, McClary J, Jones PP, Manzana W, Zhu Y, Wang S, Liu Y, Harvey S, Madlansacay MR, McLean K, Rosser MP, MacRobbie J, Olsen CL & Cobb RR (2006) High levels of protein expression using different mammalian CMV promoters in several cell lines. *Protein expression and purification* **45:** 115–124

Yang F, Li X, Sharma M, Sasaki CY, Longo DL, Lim B & Sun Z (2002) Linking beta-catenin to androgen-signaling pathway. *J. Biol. Chem.* **277:** 11336–11344

Yang Y, Mariati, Chusainow J & Yap, Miranda G S (2010) DNA methylation contributes to loss in productivity of monoclonal antibody-producing CHO cell lines. *Journal of biotechnology* **147:** 180–185

Yao H, Ashihara E & Maekawa T (2011) Targeting the Wnt/β-catenin signaling pathway in human cancers. *Expert opinion on therapeutic targets* **15:** 873–887

Yu H, Kago G, Yellman CM & Matouschek A (2016) Ubiquitin-like domains can target to the proteasome but proteolysis requires a disordered region. *The EMBO journal* **35:** 1522–1536

Zhang J-P, Li X-L, Li G-H, Chen W, Arakaki C, Botimer GD, Baylink D, Zhang L, Wen W, Fu Y-W, Xu J, Chun N, Yuan W, Cheng T & Zhang X-B (2017) Efficient precise knockin with a double cut HDR donor after CRISPR/Cas9-mediated double-stranded DNA cleavage. *Genome biology* **18:** 35

Zhang P-W, Haidet-Phillips AM, Pham JT, Lee Y, Huo Y, Tienari PJ, Maragakis NJ, Sattler R & Rothstein JD (2016) Generation of GFAP::GFP astrocyte reporter lines from human adult fibroblast-derived iPS cells using zinc-finger nuclease technology. *Glia* **64:** 63–75

Zischewski J, Fischer R & Bortesi L (2017) Detection of on-target and off-target mutations generated by CRISPR/Cas9 and other sequence-specific nucleases. *Biotechnology advances* **35:** 95–104

Zolghadr K, Gregor J, Leonhardt H & Rothbauer U (2012) Case Study on Live Cell Apoptosis-Assay Using Lamin-Chromobody Cell-Lines for High-Content Analysis. In

Single Domain Antibodies, Saerens D, Muyldermans S (eds) pp. 569–575. Totowa, NJ: Humana Press

Zolghadr K, Mortusewicz O, Rothbauer U, Kleinhans R, Goehler H, Wanker EE, Cardoso MC & Leonhardt H (2008) A fluorescent two-hybrid assay for direct visualization of protein interactions in living cells. *Molecular & cellular proteomics : MCP* **7:** 2279–2287

8 ANNEX

8.1 Publications

Parts of this thesis are published in:

Bettina-Maria Keller, Julia Maier, Kathy-Ann Secker, Stefanie-Maria Egetemaier, Yana Parfyonova, Ulrich Rothbauer and Bjoern Traenkle. Chromobodies to quantify changes of endogenous protein concentration in living cells. Molecular & Cellular Proteomics, 2018 Sep 18, doi: 10.1074/mcp.TIR118.000914.

Bettina-Maria Keller, Julia Maier, Melissa Weldle, Soeren Segan, Bjoern Traenkle, Ulrich Rothbauer. A strategy to optimize the generation of stable chromobody cell lines for visualization and quantification of endogenous proteins in living cells. Antibodies, 2019 Jan 07, doi: 10.3390/antib8010010.

Review article:

Bettina-Maria Keller, Julia Maier, Sören Segan, Björn Tränkle, Ulrich Rothbauer. Nano- und Chromobodies für high-content und super-resolution imaging. Biospektrum (2018) 24: 274. doi: 10.1007/s12268-018-0919-4.

8.2 Danksagung

An erster Stelle möchte ich mich bei meinem Doktorvater Professor Dr. Ulrich Rothbauer bedanken. Vielen Dank lieber Uli für deine erstklassige Betreuung und Unterstützung. Ob im Labor, bei der Analyse von Daten, der Besprechung der Ergebnisse und auch beim Schreiben - vielen Dank für deine Mühe und die Zeit, die du dir stets genommen hast.

Ebenfalls danken möchte ich Herrn Professor Dr. Stefan Laufer für die Begutachtung dieser Arbeit.

Ein großes Dankeschön geht an dieser Stelle an Dr. Björn Tränkle. Bevor ich nochmal ein ganzes Kapitel schreiben müsste, mache ich es ganz einfach: Danke dir, lieber Björn, für alles!

Auch bedanken möchte ich mich bei den besten Kollegen Dr. Julia Maier, Dr. Philipp Kaiser und Sören Segan – vielen Dank für euer stets offenes Ohr und eure Unterstützung. Ebenfalls danke ich den Studenten, die am AMCBS Projekt mitgewirkt haben: Kathy-Ann Secker, Melissa Weldle, Yana Parfyonova und Stefanie-Maria Egetemaier. Aber auch den Kollegen und Studenten, die unsere Arbeitsgruppe während meiner Zeit am NMI bereichert haben, möchte ich danken: Funmi, Markus, Magdalene, Marc, Kaja und Jessi. Danke euch allen für die schöne Zeit, mit euch zu arbeiten hat unglaublich Spaß gemacht.

Ein riesiges Danke geht an dieser Stelle an meine ehemaligen Kommilitonen Michael Ghosh, Maren Steinke und Andre Schwarz, denn ohne eine erfolgreiche Studienzeit wäre eine Promotion nicht möglich gewesen. Danke für die unglaublich tolle und witzige Studienzeit - aber auch für eure Unterstützung in den zahllosen Praktika und beim Lernen.

Besonders danken möchte ich auch meinen Eltern und dem Rest meiner Familie. Mein größter Dank geht an meine Großeltern Anna-Maria und Josef Pfeiffer, ihnen beiden widme ich diese Arbeit in unendlicher Dankbarkeit für Ihre Liebe, Zuneigung und Erziehung.

Zuletzt will ich mich bei dir bedanken, Frank Lämmle. In schwierigen Zeiten hattest du immer die richtigen Worte parat, hast mich auf den Boden der Tatsachen zurück geholt, mich aufgeheitert und mit neuer Motivation versorgt. Danke für deine konstruktive Herangehensweise, deine Geduld, dein Verständnis und deinen Rückhalt.